ARL-TR-8822 ● SEP 2019

DEVCOM ARMY RESEARCH LABORATORY

Reducing Low Cost Competent Munition (LCCM) Thermal Battery Volumes by Factors of 2 to 3 and Extending LCCM Thermal Lifetimes by Factors of 10 to 20 or More: Part 1

by Frank C Krieger

NOTICES

Disclaimers

The findings in this report are not to be construed as an official Department of the Army position unless so designated by other authorized documents.

Citation of manufacturer's or trade names does not constitute an official endorsement or approval of the use thereof.

Destroy this report when it is no longer needed. Do not return it to the originator.

ARL-TR-8822 ● SEP 2019

Reducing Low Cost Competent Munition (LCCM) Thermal Battery Volumes by Factors of 2 to 3 and Extending LCCM Thermal Lifetimes by Factors of 10 to 20 or More: Part 1

by Frank C Krieger
Sensors and Electron Devices Directorate, CCDC Army Research Laboratory

REPORT DOCUMENTATION PAGE

Form Approved
OMB No. 0704-0188

1. REPORT DATE *(DD-MM-YYYY)*	**2. REPORT TYPE**	**3. DATES COVERED (From - To)**
September 2019	Technical Report	1 July 2016–27 September 2019

4. TITLE AND SUBTITLE

Reducing Low Cost Competent Munition (LCCM) Thermal Battery Volumes by Factors of 2 to 3 and Extending LCCM Thermal Lifetimes by Factors of 10 to 20 or More: Part 1

5a. CONTRACT NUMBER

5b. GRANT NUMBER

5c. PROGRAM ELEMENT NUMBER

6. AUTHOR(S)

Frank C Krieger

5d. PROJECT NUMBER

5e. TASK NUMBER

5f. WORK UNIT NUMBER

7. PERFORMING ORGANIZATION NAME(S) AND ADDRESS(ES)

CCDC Army Research Laboratory
ATTN: FCDD-RLS-DP
2800 Powder Mill Road, Adelphi, MD 20783-1138

8. PERFORMING ORGANIZATION REPORT NUMBER

ARL-TR-8822

9. SPONSORING/MONITORING AGENCY NAME(S) AND ADDRESS(ES)

10. SPONSOR/MONITOR'S ACRONYM(S)

11. SPONSOR/MONITOR'S REPORT NUMBER(S)

12. DISTRIBUTION/AVAILABILITY STATEMENT

Approved for public release; distribution is unlimited.

13. SUPPLEMENTARY NOTES

14. ABSTRACT

Munitions thermal battery electrochemical cells typically operate at temperatures of 400 to 600 °C and their lifetimes are typically limited by a lack of temperature control. Possible methods of removal of high thermal conductivity H_2 gas from their operating atmospheres that could prolong their lifetimes by factors ranging from 1.5 to 3 are discussed and demonstrated in this Part 1 report. A recently conceived temperature control method that should be applicable to most munitions thermal batteries might easily prolong their present thermal lifetimes by factors of 10 to 20 or more. That new temperature control method is under investigation and will be discussed in a subsequent Part 2 report.

15. SUBJECT TERMS

thermal battery, heat transfer, thermal conductivity, gas control, mathematical modeling, chemical processing, materials selection

16. SECURITY CLASSIFICATION OF:			**17. LIMITATION OF ABSTRACT**	**18. NUMBER OF PAGES**	**19a. NAME OF RESPONSIBLE PERSON**
a. REPORT	**b. ABSTRACT**	**c. THIS PAGE**			Frank C Krieger
Unclassified	Unclassified	Unclassified	UU	109	**19b. TELEPHONE NUMBER (Include area code)** (301) 394-3115

Contents

List of Figures

List of Tables

Acknowledgments

The author would like to acknowledge Mr Bruce Geil for his sustained support and insightful suggestions that contributed to the present report. His suggestions can be expected to facilitate future work on this project.

1. Introduction

Pressed pellet munitions thermal reserve batteries are important sources of power for traditional, smart, and nuclear munitions weaponry. Their capabilities are well known and they are expected to remain important power sources for munitions applications into the indefinite future. These batteries can deliver high currents, voltages, and operational reliabilities over wide ambient temperature ranges (typically –40 to +60 °C) under high mechanical stresses and have long shelf lives (10- to 20-year shelf life requirements are typical). Munitions thermal batteries are typically built in a "dry room" under a relative humidity of greater than or equal to 1% (–34.0 °C dew point) to avoid moisture contamination, dried under vacuum, hermetically sealed, and then sealed into a munition that will be used one time only many years later. They have been used in the 155-mm howitzer[1–3] with setback forces on the order of 15,000 times the standard force of gravity on the earth's surface (15,000 g's) and at spin rates of 275 revolutions per second (RPS). Pressed pellet munitions thermal reserve batteries are more commonly used in low spin (0 to 20 RPS) situations and are used in numerous Department of Defense (DOD) and Department of Energy (DOE) missile and nuclear applications. Operational reliability levels for pressed pellet thermal reserve batteries generally range from 99.9% at a 95% confidence level for munitions applications to 99.999% at a 98% confidence level for nuclear applications. Production costs for thermal batteries are generally considered to be moderate and the batteries are often used in applications where mission reliability is of crucial importance.

The US Army Combat Capabilities Development Command Army Research Laboratory (ARL) has done extensive laboratory experimentation, in-house development, and mathematical modeling in thermal batteries for many years[4,5,6] and has applied lessons learned from those past programs to the present study. Previously developed test fixtures and experimental procedures for the well documented Low Cost Competent Munition (LCCM)[3] thermal battery were modified as required for use in the present study. ARL has also done literature searches and laboratory experimentation on numerous molten salt electrochemical systems and chemical preprocessing methods that have been used in thermal batteries for ARL customers and by other laboratories.[7] Noteworthy capabilities, opportunities, characteristics, and challenges of munitions thermal reserve battery technology are summarized in Appendix A.

Pressed pellet munitions thermal reserve battery technology is presently regarded by many as a mature technology with little room for future improvement in the absence of major technical innovation.[8,9] Partly for this reason, partly because present production-type munitions thermal reserve batteries are believed adequate

to meet military requirements in the near future, and partly because the technology base is relatively small financially, thermal battery technology was recently deemphasized within the Army. The Army "Long-Range Precision Fires Modernization Priority", which can be expected to use many thermal reserve batteries remains, nevertheless, a top priority.

Mathematical modeling, when combined with a knowledge of thermal battery performance, chemical preprocessing, and thermal battery construction methods, clearly shows that most present munitions thermal reserve batteries are grossly overdesigned (larger than necessary) in order to meet heat transfer requirements. In the long term, mathematical models and laboratory experiments clearly show that presently required volumes for most thermal battery applications could be reduced by huge amounts because the thermal conductivity values of the thermal insulation packages could be greatly reduced simply by controlling the operating gas atmospheres within the porous thermal insulation packages. In the short term, even minimal advances in gas control and mathematical parametric optimization can be expected to be of significant help to the "Long Term Precision Fires" modernization priority.

The importance of the quantities and chemical compositions of internally evolved gases present during thermal battery operation has been recognized and gas characterization and control efforts have been reported since at least as early as 1960.[10,11] Early efforts on gas characterization during thermal battery operation focused on reducing the gross quantity of gas evolved during pyrotechnic ignition in order to avoid rupture of the hermetically sealed stainless steel (SS) external battery cases. Internal gas atmosphere control to control heat transfer in munitions thermal reserve batteries has been successful in numerous laboratory tests, but was never fully optimized in production. Instead, production-type thermal batteries have routinely been made larger than necessary (overdesigned for heat transfer) to the point where the required temperature maintenance of the cell stack during battery operation could be easily accomplished. The effects of the gas control problems on production battery lifetimes have been acknowledged and mitigated for specific applications by battery vendors when possible to do so by using simple methods such as choosing construction methods and materials known to evolve less gas during battery operation, controlling impurity levels, and minimizing water contamination during battery construction.

By combining operating atmosphere gas control with appropriate changes in battery construction and materials processing, mathematical modeling clearly shows that volumetric energy density values for many presently fielded thermal batteries could be increased by factors of 5 or more. It should be emphasized that such batteries would require gas control not available at present. In addition, the thin film anode,

cathode, and electrolyte components that would be required for very small thermal batteries remain untested or tested only in exploratory manners, but mathematically modeled examples that contain all the required pyrotechnic and electrochemical materials might become feasible when using future production techniques. With a moderate vacuum operating gas atmosphere (~50 μ Hg [microns of mercury] or 6.67 Pa [pascal]) and adequately thin-film anode, cathode, and electrolyte components, the mathematical models show that small (~0.20 inches in diameter by ~0.25 inches tall), low current (1.5 mA) thermal batteries delivering 5.4 to 7.2 V could last 566 s with a nominal volumetric thermal battery energy density value of 0.090 Wh/l.[12]

Operating thermal battery chemical complexity combined with the high operating temperatures of the highly reactive electrochemical cell stack components (typically 400 to 600 °C) and the long required thermal battery shelf lives makes any simple, rapidly implemented, and demonstrably reliable removal of H_2 gas from thermal battery operating atmospheres difficult. A sustained initial effort by workers ranging from materials scientists to production line engineers would be required for the initial testing and development of both the precursor materials and the operating thermal batteries in order to reliably obtain the smallest sizes and longest lifetimes. Once the proper procedures become established and understood, however, the added cost required to implement and maintain the required technology should become nominal added costs and efforts that would be easily acceptable for most thermal battery applications. Proof of the effectiveness of any proposed technological method to operate reliably both before and after a 20-year shelf life period must be demonstrated.

Because gas control in operating thermal batteries shows great potential for battery miniaturization but has proven difficult to implement simply and reliably in the past, the purpose of the present report is to summarize previous efforts and to identify promising approaches for future work on gas control that might be required to make future munitions thermal reserve batteries significantly smaller than at present. The first experiments done for this report in 2017 (HPST1 through HPST4) showed that H_2 gas evolved from heat paper pyrotechnic powders containing significant amounts of lead dioxide (PbO_2) could not be removed effectively using zirconium/barium chromate ($Zr/BaCrO_4$) pyrotechnic powders and results from those experiments are not included in this report. Data from the last four gas control experiments done in 2017 (HPST5 through HPST8) are analyzed and compared with similar tests from gas control experiments done in 2012 to help illustrate and analyze the present successes and challenges of operating atmosphere gas control experimentation. HPST8 was the most successful H_2 gas removal test done during 2017. For HPST8 the evolved gas was confined within the hermetically sealed

reusable test fixture (RTF) using a bellows valve (BVRTF) for nominally 188 s after pyrotechnic ignition to facilitate chemical reactions between the evolved gas and the pyrotechnic ash.

After the HPST8 test, the experimental process was reconsidered. The HPST9 experiment was then constructed similar to the HPST8 experiment except that proportionately more $BaCrO_4$ was added to the heat paper and 26.05 STP cc of oxygen gas (O_2) at a measured pressure of 759.2 Torr was confined within the RTF during pyrotechnic ignition. For HPST9, BVRTF remained hermetically sealed for 208 s after heat paper ignition, after which BVRTF was opened to the evacuated gas handling system (GHS) with the bellows valve to sample bottle 1 (BVSB1) open. BVSB1 was then closed approximately 270 s after the scan started to collect the evolved gas sample. Analysis of the SB1 gas sample showed that the HPST9 experiment was successful in removing all measurable traces of H_2 gas from the sealed RTF atmosphere (no visible gas chromatograph [GC] H_2 peak observed). This had never been accomplished previously. These results with their implications are reported and discussed in this report and compared with the tests that were done in FY 2012. The FY 2012 accomplishments in H_2 gas control are reported in the references and discussed briefly in this report.

The GHS and the experimental methodology were both systematically improved during the experiments HPST1 through HPST9. The measured GHS volumes and gas pressures for the individual tests HPST5 through HPST8 are shown in this report for possible use in future analyses. Pressure-time data points at nominal 0.1-s intervals for the entire duration of the experiments HPST5 through HPST9 are in progress for possible future analysis on request.

A primary initial goal of the work discussed in this report is to experimentally demonstrate reliable H_2 gas evolution reduction to essentially zero by using simple methods that could be quickly applied to presently fielded production-type munitions thermal batteries. One simple method investigated in this report is to initiate 28/72-wt% $Zr/BaCrO_4$ pyrotechnic powder-based heat paper mixed with added $BaCrO_4$ in the hermetically sealed GHS to remove the H_2 gas evolved on ignition as completely as possible while simultaneously removing the resulting water vapor through chemical interaction with the heat paper ash components. Heat paper that uses 22/78-wt% $Zr/BaCrO_4$ has also been used in the past and has been shown to produce markedly less H_2 gas than the more commonly used heat paper made from 28/72-wt% $Zr/BaCrO_4$.[10] $Zr/BaCrO_4$ powder mixtures with higher ratios of $BaCrO_4$ have been shown experimentally to remove both H_2 and H_2O from the surrounding gas atmospheres. The optimal weight ratio of heat paper to $BaCrO_4$ for the removal of ambient hydrogen (H_2) gas and the possibility of reacting some ambient H_2 gas with O_2 evolved during pyrotechnic ignition are two areas of

immediate interest. Because the ash that removes the H_2 and H_2O gases is not formed until the battery is initiated, there is no need to protect the gas-removing agent during the approximately 20-year storage life of the battery. The ability to remove H_2 gas completely from the atmosphere of an operating thermal battery could be extremely helpful for the Long-Range Precision Fires Modernization Priority.

Comprehensive mathematical models for munitions thermal reserve battery heat transfer and electrochemical optimization are available, in use, and constantly being improved at present.[13–16] The effectiveness of H_2 gas control in extending munitions thermal reserve battery lifetimes under ad hoc circumstances has been demonstrated experimentally many times in recent years[3,17–21] and has been reported to and discussed with all of the major munitions thermal reserve battery vendors in the United States. The calibration and use of a GC customized for thermal battery gas composition analysis at ARL using standard samples gas has been analyzed and discussed previously.[22]

This report was primarily written to summarize some of the applications and characteristics of presently used munitions thermal reserve batteries and to demonstrate how operating gas atmosphere control in future thermal batteries could be used to reduce the presently required volumes of those batteries by huge amounts. Analyses of mathematical models and experimental results consistently show the huge improvements (much smaller sizes and much longer lifetimes) that could be achieved for most munitions thermal reserve battery energy densities by the control of operating gas atmospheres in present thermal batteries.

2. Heat Transfer in Thermal Batteries: Microporous Thermal Insulators and Gas Control

Because space is at a premium for most conventional and nuclear munitions applications, high volumetric battery energy density values are almost always desirable. Because of the high operating temperatures of thermal cells and the limited space for thermal insulation in munitions, heat transfer is usually the major limitation to reducing munitions thermal reserve battery sizes and increasing volumetric energy density values. Total elimination of H_2 gas from munitions thermal reserve battery operating gas atmospheres could lower present porous thermal insulation package thermal conductivity values by nominal factors ranging from 1.5 to 3 even when starting with the best (microporous) thermal insulators as a baseline.[23,24] Because munitions thermal reserve battery cell stack electrochemical capacities are often larger than necessary to provide additional mass and heat while the stack cools, the simple removal of H_2 gas from a thermal

battery with no other changes could often produce a significant immediate increase in battery lifetime for many munitions reserve thermal batteries presently used in field applications.

Microporous thermal insulation particle sizes for munitions thermal batteries are nominally less than 0.1 micro–meter (μ–m) diameter and are chosen for use with air at room temperature and 1 atmosphere (atm) pressure (760 Torr). Microporous thermal insulators are superior because 1) they use opacification agents such as particulate metal oxides to reduce radiant heat transfer, and 2) the bulk insulation particle pore structures are small enough to interfere with the mean free paths of the enclosed gas molecules, which can substantially reduce the bulk insulation thermal conductivity values to values even below those of the given enclosed gas. The mean free path of any particular gas can be calculated from the effective gas molecular diameter and from the temperature and pressure of the gas. Calculated mean free paths of air and H_2 gases at 25 °C and 10^5 Pa (0.986923 std-atm pressure), for example, have been reported as 0.0691 and 0.126 μ–m, respectively.[25] In addition to possessing low thermal conductivity values, microporous insulators can be used as load-bearing materials for thermal battery electrochemical cell stacks, even in LCCM–type artillery applications that typically require mechanical support under initial setback forces on the order of 15,000 g's.

For thermal insulators with larger particle sizes, the thermal conductivity values of the thermal insulation in working thermal batteries will often approximate the thermal conductivity values of the gas atmospheres enclosed in the porous thermal insulation structures. Thermal conductivity values for relevant gases are shown in Figs. 1 and 2.[26] When starting with many of these less expensive and larger particle size thermal insulators as a baseline, insulation thermal conductivity values could be reduced by a much larger nominal factor of about 6 by the removal of H_2 gas, as can be seen in Fig. 1. The thermal conductivity values of porous thermal insulators in operating thermal batteries with large particle sizes would be reduced from being similar to those of H_2 to being similar to those of air in Fig. 1, because approximately 95% of the remaining gases present during thermal battery operation (nitrogen [N_2], O_2, carbon monoxide [CO], methane [CH_4], and carbon dioxide [CO_2]) will collectively have thermal conductivity values similar to those of air. Opacification agents or other methods of reducing radiation heat transfer will be required for both large and small particle size thermal insulating materials.

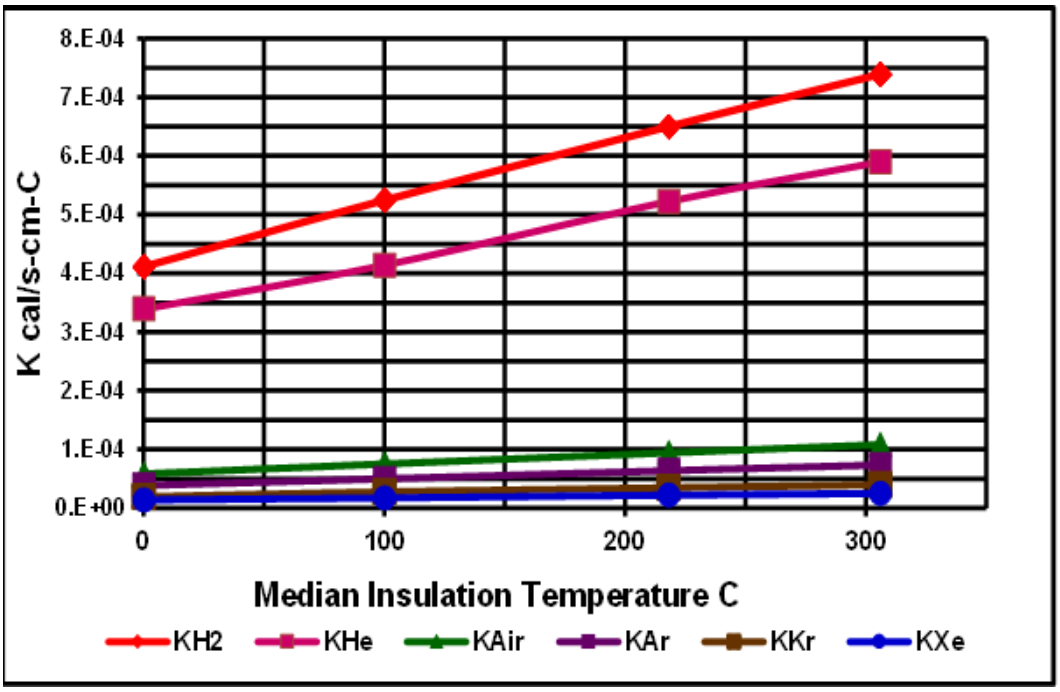

Fig. 1 Thermal conductivity values of selected gases—H_2 through xenon (Xe)

If H_2 gas could be removed, some of the less expensive thermal insulators would become nearly as effective as some of the best present microporous thermal insulators for many thermal battery applications when used with appropriate opacification agents. The optimized miniaturization of operating thermal batteries to the smallest possible sizes is complex, but the elimination of H_2 gas from the operating atmospheres is almost always a highly effective starting point. Some easily implemented method of totally eliminating the evolution of H_2 gas or at least reducing the amount of H_2 gas evolved to a reliably low level might produce sufficient thermal battery energy density improvements so that private thermal battery companies would feel financially compelled to expend the additional effort in battery construction and/or improved chemical processing techniques necessary to develop more fully miniaturized munitions thermal reserve battery designs.

Once thermal battery volumes have been minimized for thermal insulation with H_2 gas completely removed during operation, further significant reductions in thermal conductivity values could still be achieved using gas control methods. The extent of the additional improvement possible can be seen in Fig. 2 (the lower part of Fig. 1 with an expanded y-axis), which shows more clearly the large differences in thermal conductivity values for the four gases that appear to have similar thermal conductivity values in Fig. 1. As noted in the introduction, further improvement in thermal lifetimes even after the operating gas atmosphere has been completely

controlled remains possible by optimization of the thermal battery electrochemical-heat source stacks.

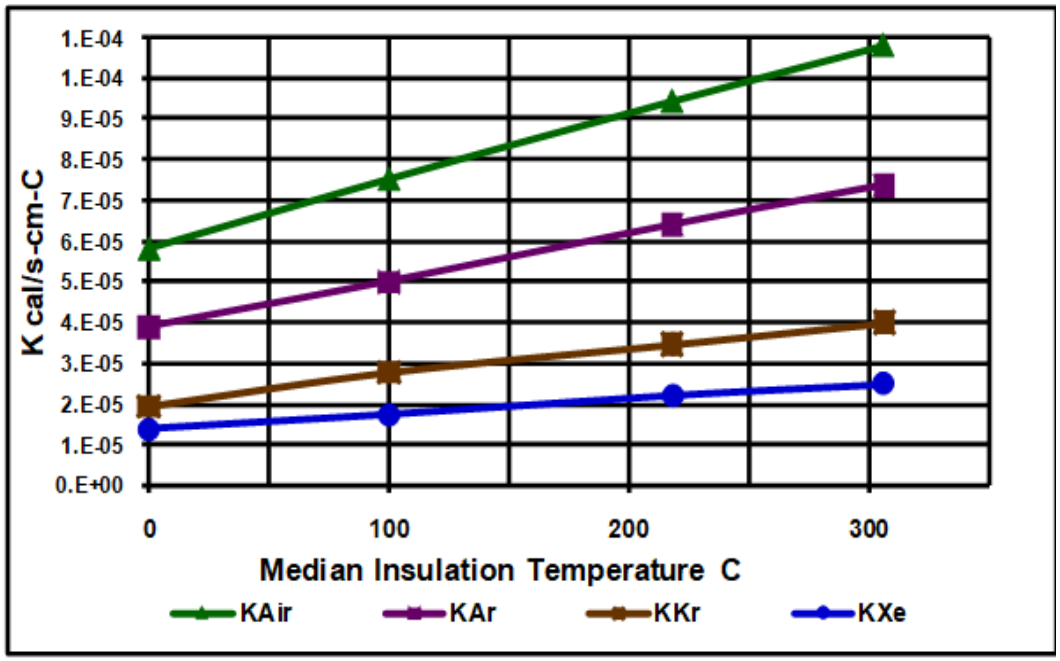

Fig. 2 Thermal conductivity values of selected gases—air through Xe (from Fig. 1)

Typical gas compositions of operating munitions thermal reserve batteries made both by vendors and at ARL start at 50 % to 80 % H_2 gas by volume on pyrotechnic ignition and gradually decline from the starting H_2 gas volume percentage by 20% to 40% by volume while showing a significant increase of CH_4 gas during a typical 2- to 5-min munitions thermal battery lifetime as shown in Appendix A (Fig. A–1). Thermal battery lifetimes have been experimentally improved at ARL and Sandia National Laboratories, and by commercial vendors simply by backfilling and hermetically sealing existing thermal batteries with low thermal conductivity value chemically inert gases such as argon, krypton, or Xe.[17-19]

Table 1 shows the experimental effect of letting the H_2 gas escape and burn off (which produced effectively complete H_2 gas removal by intentional case venting) during the operation of the pressed pellet LCCM (hermetically sealed) and MANLOS (vented) munitions thermal reserve batteries built at ARL. MANLOS and LCCM thermal batteries were much different in size (nominally 561.0 cc and 26.74 cc total internal case volumes respectively),[5,6] but both used similar, predominantly microporous, thermal insulation packages commonly used in the field so that their measured thermal conductivity values as shown in Table 1 would be nominally equal in the same internal operating gas atmosphere.

Table 1 Nominal measured operating thermal battery thermal insulation package global thermal conductivity values for ARL built thermal batteries during operation with (Sealed Case–LCCM) and without (Vented Case–MANLOS) H_2 gas in the operating atmosphere.

Experimental Global Thermal Conductivity Values of Predominantly Microporous Thermal Insulation Packages During Thermal Battery Operation With and Without H_2 Gas in Porous Thermal Insulation at the Nominal Thermal Insulation Package Median Temperature of ~ 300 °C During Battery Operation	
Battery	**Global Thermal Conductivity of Thermal Insulation Package x 10^4 cal/s-cm-°C**
LCCM Hermetically Sealed (H_2 Present)	**4.1**
MANLOS (Vented – H_2 Burned/Allowed to Escape	**1.3**

Note: Measured thermal conductivity value ratio for these two predominantly microporous battery thermal insulation packages during operation at the nominal median thermal insulation temperature of 300 °C during thermal battery operation is 4.1/1.3 = 3.15.

Significant improvements in thermal battery energy densities can often be achieved simply by using new thermal insulation materials as they become available. Non-microporous thermal insulators[27] have been used for many years as thermal cell stack side-wraps with the dual purpose of absorbing leaking molten salt electrolyte from operating thermal cells and simultaneously providing limited side-wrap thermal insulation. These insulators are much more effective at absorbing molten salt electrolyte leaks from the thermal cell outer diameters to prevent ionic short circuits than are presently used microporous thermal insulators and they do not react chemically with lithium (Li)/aluminum (Al) and Li/silicon (Si) anodes significantly at thermal battery operating temperatures as do the microporous thermal insulators.

Non-microporous thermal insulation is an often acceptable and relatively inexpensive thermal insulation used as a major component of the thermal insulation packages of many presently fielded munitions thermal batteries. Recently developed non-microporous thermal insulators have been shown to perform acceptably while maintaining physical contact with the Li/Al and Li/Si anodes of operating thermal batteries and simultaneously providing longer thermal battery lifetimes than traditionally used non-microporous thermal insulators.[27–31]

3. Experimental

Previously established gas collection, gas quantity, and gas composition test methods were used.[3,18–20] Gas quantities were determined from the measured gas pressures during the tests and from GHS volumes previously measured using the ideal gas law in conjunction with calculations of physical volumes and water weight

methods. Rounding errors and interim parametric experimental uncertainties for the calculations were ignored during the calculations and their effects were then explained later in the text as necessary to facilitate mathematical procedures involving operations such as subtracting two large numbers to obtain a critically important smaller number.

SS sample bottles with the manufacturer's stated internal volume of 10 cc ± 10% served as the primary standards for determining all gas volumes. For the 2012 tests the internal volumes of the sample bottles plus SS attachments were originally assumed to be equal to 10 cc. The manufacturer's stated accuracy of the Dual Capacitance Manometer (DCM) used for gas pressure readings was 0.5% of the reading. A drawing of a GHS used in 2012 is shown in Appendix B. All 2017 through 2019 gas volumes for the HPST5 through HPST9 tests were ultimately measured at room temperature using the DCM measured gas pressure with the ideal gas law using a single designated but representative 10-cc internal volume SS reference sample bottle. Identical sample bottle types and SS attachments to the bellows valves attached to those sample bottles (Fig. 3) were used for the 2012 and the 2017 through 2019 gas evolution tests.

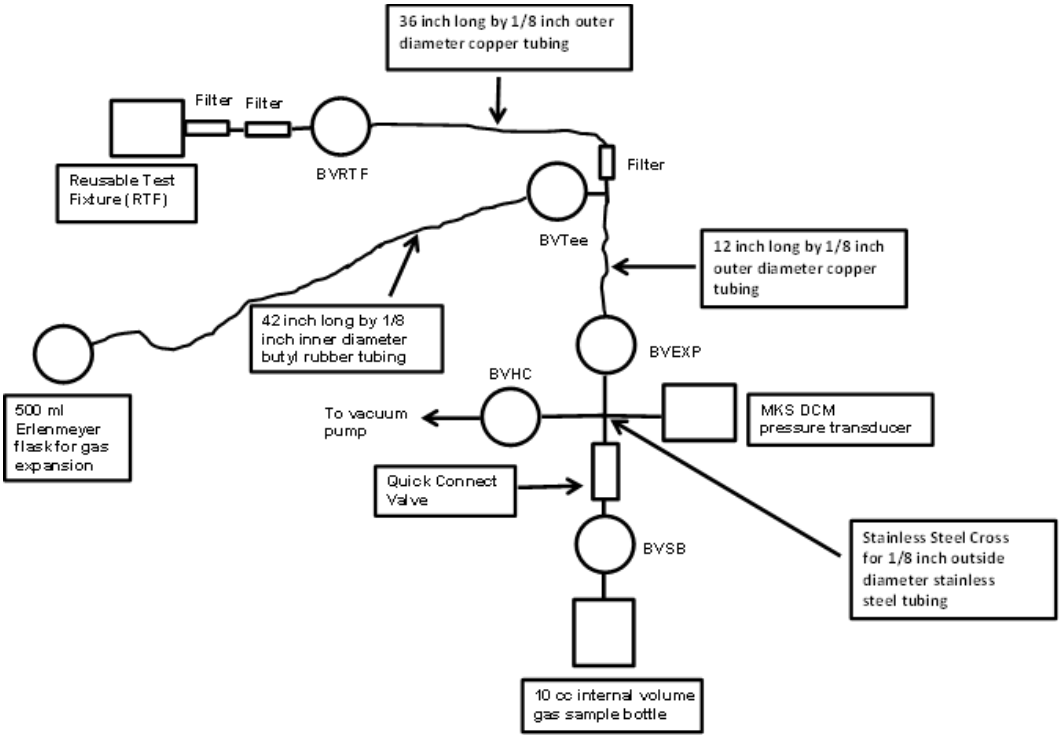

Fig. 3 Gas evolution testing and collection manifold for HPST8 (Not to scale)

Notes: Internal Volumes (cc): RTF physical cylinder bottom 24.88; empty RTF +SS tubing up to closed BVRTF = 26.93 by ideal gas law (gas-ash reaction volume can be completely confined within the RTF + tubing up to closed BVRTF); GHS + RTF + SB = 54.44; Erlenmeyer flask + butyl tube = 590.0. Total volume of 10 cc SB plus tubing to closed BVSB=12.95 ± 5%.

For the 2017 through 2019 tests HPST5 through HPST9, the representative and designated sample bottle plus SS tubing to the closed BVSB was first used to measure successively larger portions of the GHS volume. All 2017 GHS volumes were ultimately confirmed by a combination of physically measured volumes along with the weight of the water in the water-filled 500-cc Erlenmeyer flask shown in Fig. 3. By these methods the total volume of the designated sample bottle plus SS tubing to the BVSB was determined to be 12.95 cc to an estimated accuracy of ±5% and that sample bottle then became the primary reference for both the 2012 and the 2017 gas quantities.

The previously reported gas quantity values for the 2012 tests[19] were then multiplied by a nominal correction factor of 1.295 and those corrected 2012 gas quantities are used in calculations throughout this report. This gas quantity correction is the only required correction to any of the values reported in the 2012 gas analyses. All gas volumes for this report were ultimately measured to an estimated accuracy of ±5%.

The 2017 GHS configurations used to measure gas quantities in this report were sequentially developed starting from the 2012 GHS in order to produce a smaller, more versatile GHS that could produce higher, more easily measured gas test pressures and/or use smaller quantities of pyrotechnic powders. Higher gas pressures help the evolved H_2 gas to react more readily with the Zr/$BaCrO_4$ LCCM flight test heat paper (LCCMFTHP) pyrotechnic powder ash and the added $BaCrO_4$. Detailed drawings of the 2017 RTF and the RTF SS insets that can be used to reduce the effective volume of the RTF in order to increase the test gas pressures are shown in Appendix C. The GHS used to measure the gas quantities for both the HPST8 and HPST9 experiments is shown in Fig. 3.

The 2017 experiments were originally planned to be a series of experiments using LCCM-type thermal cells in LCCM-type thermal battery stacks so that thermal cell heat generation rates and battery stack heat losses could be easily measured as has been done many times previously.[3] The individual experiments were therefore designated HPSTn with n designating the number of the experiment. The first HPSTn experiments using only heat paper were expected to be finished quickly. Those results were expected to confirm the 2012 gas evolution test results and to provide a check of the 2017 experimental test procedures. Eight gas evolution tests (HPST1 through HPST8) were done in 2017, and all eight tests used only heat paper or heat paper plus $BaCrO_4$. Although $BaCrO_4$ was shown to remove H_2 gas from the surrounding atmosphere successfully, none of the eight tests done in 2017 were as successful as the 2012 tests had been. Tests HPST1 through HPST4 used a heat paper that contained significant amounts of PbO_2, and little or no H_2 gas was

removed using added $BaCrO_4$ in those tests. Tests HPST5 through HPST8 in 2017 used the same LCCMFTHP (28/72-wt% Zr/$BaCrO_4$) as did the 2012 tests. The HPST5 through HPST8 tests removed evolved H_2 gas effectively but were not quite as successful as the 2012 tests.

For experiment HPST5, which used only LCCMFTHP as a baseline test, all of the gas insets shown in Appendix C were used and the internal volume of the RTF with insets was calculated at 4.59 cc. After experiment HPST5, the SS insets were not used in order to more easily prevent electrical short circuits between the RTF and the nichrome wire match. The bellows valve BVRTF was added to the GHS after the HPST7 experiment to confine the evolved gas inside the RTF close to the pyrotechnic powder ash and to further increase the gas pressure and gas-ash chemical reaction rates on initiation of the pyrotechnic powders starting with experiment HPST8. The internal empty (no SS insets added) RTF cylinder had a calculated physical volume of 24.88 cc (1.25 inch diameter by 1.237 inches deep) as shown in Appendix C and could be isolated from the rest of the GHS using bellows valve BVRTF starting with the HPST8 test. The total volume of the empty RTF plus attached SS tubing and internal BVRTF volume open to the RTF when BVRTF was closed using the DCM measured gas pressures and the ideal gas law was measured at 26.93 cc. The RTF inner case dimensions without the SS insets were similar to those of the internal case dimensions of the flight test LCCM thermal batteries successfully tested in the 155-mm howitzer at Yuma, Arizona, on 5 August 2008 (24.72 cc [1.2455 inch diameter by 1.2382 inches deep]).[3]

Evolved gas volumes were calculated from DCM-measured evolved gas pressures and the previously measured GHS volumes using Excel spreadsheets. Evolved gas chemical composition measurements were made on the gases collected in the sample bottles using a GC customized for thermal battery evolved gas analysis that used a porous layer open tubular (PLOT) gas capillary column with a thermal conductivity detector and an ultra-high purity (UHP) argon carrier gas. Gas samples were injected from the 10 cc SS sample bottles using a 6-port SS valve with a 50 µ-l SS sample loop. The chemical compositions were generally accurate to approximately ±10.0% of the percentage measured as described previously. For a gas composition percentage measured as 10% by volume of the total mixture to ±10% accuracy the true value of that particular gas composition percentage will generally fall somewhere between approximately 9% and 11% by volume of the total mixture.[19,20,22]

Representative measured gas leak rates from ambient room atmospheric pressure at approximately 25 °C into the evacuated GHS at a nominal pressure of 0.05 Torr (6.67 Pa) were 3.362E–05 std-atm-cc/s with BVRTF and BVTEE of Fig. 3 both open and 1.585E–07 std-atm-cc/s with BVRTF and BVTEE both closed (a leak rate

of 1 standard atmosphere cubic centimeter per second [std-atm-cc/s] equals a leak rate of one cubic centimeter of an ideal gas measured at one std-atm [0 °C and 760 Torr] per second). The GHS could not be as tightly sealed when BVTEE to the Erlenmeyer flask and BVRTF were both open. During a typical 30-min gas evolution test with BVRTF and BVTEE both open a calculated total of 30 × 60 × 3.362E–05 = 0.06052 std-atm-cc of ambient room temperature air would have leaked into the evacuated GHS at a nominal pressure of 0.05 Torr. With BVTEE and BVRTF both closed, the representative amount of ambient laboratory room air at 25 °C that leaked into the evacuated GHS in 30 min at a nominal pressure of 0.05 Torr would have been much less (30 × 60 × 1.585E-07 = 0.0002844 std-atm-cc).

A step-by-step test procedure checklist for the Standing Operating Procedure (SOP) for pyrotechnic powder gas evolution and collection in this report is shown in Appendix D along with supporting procedures for preparing and installing the silicone rubber gaskets (SRGs) used to seal the RTF, ignite the pyrotechnic powder, and make the nichrome wire match. That SOP addresses important safety issues encountered when working with thermal battery materials, including the importance of proper grounding to avoid inadvertent electrostatic ignition of the pyrotechnic materials, wearing of proper personal protective equipment (PPE), and proper hazardous materials (HAZMAT) handling, storage, and disposal methods.

4. Heat Paper Gas Evolution Experiments Done in 2012 and in 2017–2019

An experiment done in 2012 that used 2.412 g of LCCMFTHP as the only test component evolved a corrected volume of 13.87 std-atm-cc of total gas/g of LCCMFTHP when ignited and evolved no apparent water vapor.[19] Table 2 shows that when 2.4224 g of LCCMFTHP was mixed in gross layers with 1.0950 g of $BaCrO_4$ powder and ignited that a corrected volume of 0.5605 std-atm-cc of total gas/g of the LCCMFTHP was evolved excluding apparent water vapor so that 100 × (13.87 – 0.5605) / 13.87) = 95.96% of the total gas that would have been evolved based on the first experiment in Table 2 was removed. As noted in Section 3, the total amount of gas reported in 2012 used the manufacturer's stated sample bottle volume of 10 cc instead of the nominal 12.95-cc volume for the sample bottle plus associated tubing measured in 2017, but the percentage of total gas removed in 2012 remains unchanged at 95.96%. The small amount of H_2 gas remaining (less than 4.04%) in an H_2/air mixture would have a thermal conductivity very similar to that of air[19,26] so that this 2012 experiment could be counted as a success because it demonstrated that a gas could be produced that would have reduced the thermal conductivity values of microporous thermal insulation packages by factors of 1.5

to 3 by removing H_2 gas. The corrected evolved gas quantities for the 2012 tests are shown in Table 2 and the HPST5 through HPST9 gas quantities and gas compositions measured in 2017–2019 from the same LCCMFTHP are shown in Tables 3 and 4. Table 3 shows that for HPST8 a total of $100 \times (16.07 - 1.565) / 16.07 = 90.26$ % of the H_2 gas was removed based on the amount of H_2 gas that was evolved for HPST5. Internal GHS and RTF volumes used for specific tests as the GHS was systematically improved are shown in text below the respective tables.

All of the heat paper samples evaluated in the 2012 and 2017–2019 experiments analyzed in this report were taken from the same vendor-supplied batch and used 28/72-wt% Zr/$BaCrO_4$ pyrotechnic powder. Previous experiments dating from as early as 1960 have shown that 22/78-wt% Zr/$BaCrO_4$ pyrotechnic powder produces little gas.[10,11] More recent experiments have shown that 22/78-wt% Zr/$BaCrO_4$ pyrotechnic powder can also remove H_2 gas present from other sources, apparently by oxidizing H_2 gas to water.[19] Based on these previous results, a promising approach to study H_2 gas removal regardless of its original source would be to initiate either 28/72- or 22/78-wt% Zr/$BaCrO_4$ heat paper powder in a GHS with added $BaCrO_4$ powder and measure the amount of H_2 gas removed. Because 28/72-wt% Zr/$BaCrO_4$ is more readily available and more commonly used, that material was chosen for experimentation in this report. The HPST5 test used only 28/72-wt% Zr/$BaCrO_4$ pyrotechnic powder and served as a baseline test for H_2 gas evolution. The HPST6 and HPST7 tests used increasingly intimate mixing methods of the 28/72-wt% Zr/$BaCrO_4$ pyrotechnic powder with the extra $BaCrO_4$ powder. The HPST8 test, which was the most successful test done in 2017, used the HPST7 intimate powder mixing procedure and in addition used a BVRTF to hold the evolved gas within the RTF to permit enhanced interaction between the evolved gas and the pyrotechnic powder ash. The first HPST8 sample bottle was closed approximately 305 s after the start of the electronic scan (~295 s after pyrotechnic ignition) and the second HPST8 sample bottle was closed 1055 s after the start of the electronic scan. Experimental details for the 2017 tests are outlined in Tables 3 and 4 and discussed. Calculation details for GHS volumes and evolved gas quantities using experiments HPST8 and HPST9 as examples are shown and explained in Appendix E.

Table 2 Evolved (LCCMFTHP) 2012 gas quantities (corrected in 2017) and gas compositions (unchanged)

Total Gas Evolved/g of Heat Paper (Excluding Water Vapor) std-atm-cc/g				
	2.412 g Heat Paper		2.4224 g Heat Paper + 1.0950 g $BaCrO_4$	
	13.87		0.5605	
SB1 (SB2) Gas Volume Percentages				
	SB1	SB2	SB1	SB2
H_2	82.4	72.7	78.0	60.5
O_2	0.00	2.13	3.03	6.71
N_2	0.00	0.00	6.76	21.3
CO	16.2	23.4	12.3	11.5
CH_4	1.44	1.81	0.00	0.00
CO_2	0.00	0.00	0.00	0.00
Total	100.04	100.04	100.09	100.01
Apparent Total Water Vapor Volume after Gas Expansion std-atm-cc/g of Heat Paper				
	0.00		9.507 (2445.3 s After Ignition)	

Notes: All original[19] 2012 gas quantities and internal GHS volumes were multiplied by 1.294644 as described in Section 3 and Appendix E to obtain the corrected values shown for Table 2.
GHS+RTF-pyrotechnic ash volume (left column) = 80.24 cc.
GHS+RTF-pyrotechnic ash volume (right column) = 79.93 cc.
Gas expansion desiccator plus butyl tubing = 2874.68 cc.

Table 3 Evolved LCCMFTHP gas quantities and compositions measured in 2017 (experiments HPST5 and HPST8)

Total Measured Gas Evolved (std-atm-cc)/g of Heat Paper				
	HPST5		HPST8	
	0.9451 g Heat Paper No Additive – No BVRTF		1.134 g Heat Paper + 0.6509 g $BaCrO_4$ Intimate Mix – BVRTF Closed for 198.7 s After Scan Start	
	Pyrotechnic Ignition 11.197 s after Scan Start		Pyrotechnic Ignition (Manual Record Only) 10 s after Scan Start	
Total Volume of All Gases Evolved When SB1 and SB2 Were Closed (std-atm-cc/g of Heat Paper) and Closing Time After Initial Pressure Rise (s)				
SB1	20.79	41.8 s	6.229	106.2 s
SB2	20.42	794.8 s	5.923	856.2 s
SB1 (SB2) Gas Volume Percentages				
	SB1	SB2	SB1	SB2
H_2	77.28	56.92	25.13	26.12
O_2	0.11	1.35	19.81	3.28
N_2	0.47	8.15	2.76	13.36
CO	14.65	8.67	8.23	9.95
CH_4	5.95	15.16	1.65	1.78
CO_2	1.54	9.74	42.42	48.99
Total	100.00	99.99	100.00	103.48
Calculated Total Volume H_2 Gas Evolved When Indicated Sample Bottle Was Closed (std-atm-cc/g of Heat Paper) and Closing Time After Initial Pressure Rise (s)				
SB1	16.07	41.8 s	1.565	106.2 s
SB2	13.57	794.8 s	1.532	856.2 s
Apparent Liquid Water Expressed as Vapor (std-atm-cc) From Gas Expansion/g of Heat Paper Measured at End of Scan (seconds)				
0.4710 (1398.7 s After Ignition)			5.700 (1722.4 s After Ignition)	

Notes: HPST5 small GHS+RTF (with SS insets)-pyrotechnic ash volume = 15.20 cc.
HPST5 calculated pyrotechnic ash plus nickel ribbon volume = 0.2381 cc.
HPST5 small GHS = 10.85 cc – RTF (with SS insets) = 4.59 cc – large GHS = 111.59 cc.
Erlenmeyer flask+butyl tube volume = 590.0 cc by measurement and calculation.
HPST5 total volume for water expansion at 1398.7 s after ignition =15.20+111.59+590 = 716.79 cc.
HPST8 RTF+GHS+SB-ash volume = 26.93+14.56+12.95-.41 = 54.03 cc.
HPST8 empty RTF plus tubing to closed BVRTF volume = 26.93 cc – small GHS volume = 14.56 cc – Sample bottle plus SS tubing to SS BVSB volume = 12.95 cc ± 5%.
HPST8 calculated pyrotechnic ash volume plus nickel ribbon 0.4146 cc.
No large GHS.
Erlenmeyer flask+butyl tube volume = 590.0 cc by measurement and calculation (Appendix E).
HPST8 total volume for water expansion at 1921.4 s after ignition (sample bottle is closed) = 14.56+26.93–0.4146+590 = 631.08 cc.

Table 4 Evolved LCCMFTHP gas quantities and compositions measured in 2017 (experiments HPST6 and HPST7)

Total Measured Gas Evolved (std-atm-cc)/g of Heat Paper				
	HPST6		HPST7	
	1.1059 g Heat Paper + 0.4929 g $BaCrO_4$ in Discrete Chemical Layers – No BVRTF		1.1415 g Heat Paper + 0.4932 g $BaCrO_4$ Intimately Mixed – No BVRTF	
	Pyrotechnic Ignition 6.897 s after Scan Start		Pyrotechnic Ignition 5.897 s after Scan Start	
Total Volume of All Gases Evolved When SB1 and SB2 Were Closed (std-atm-cc/g of Heat Paper) and Closing Time After Initial Pressure Rise (s)				
SB1	6.132	50.1 s	7.610	61.1 s
SB2	5.366	923.1 s	7.179	1061.1 s
SB1 (SB2) Gas Volume Percentages				
	SB1	SB2	SB1	SB2
H_2	82.84	71.23	69.40	46.64
O_2	0.54	2.04	0.40	2.84
N_2	0.42	7.83	1.33	7.83
CO	12.98	13.92	16.32	15.76
CH_4	2.47	2.82	3.03	2.22
CO_2	0.75	2.16	9.53	19.18
Total	100.01	100.00	100.01	94.47
Calculated Total Volume H_2 Gas Evolved When Indicated Sample Bottle Was Closed (std-atm-cc/g of Heat Paper) and Closing Time After Initial Pressure Rise (s)				
SB1	5.080	50.1 s	5.281	61.1 s
SB2	4.013	923.1 s	3.784	1061.1 s
Apparent Liquid Water Expressed as Vapor (std-atm-cc) From Gas Expansion/g of Heat Paper Measured at End of Scan (seconds after ignition)				
2.281 (1572.8 s After Ignition)			4.403 (1854.7 s After Ignition)	

Notes: HPST6 small GHS+RTF volume (no insets)-pyrotechnic ash volume = 35.35 cc.
HPS6 Small GHS volume = 10.85 cc.
HPST6 calculated pyrotechnic ash volume = 0.3731 cc.
HPST6 large GHS volume = 111.59 cc.
Erlenmeyer flask+butyl tube volume = 590.0 cc by measurement and calculation.
HPST6 total volume for water expansion at 1572.8 s after ignition = 35.35+111.59+590 = 736.94 cc.
HPST7 small GHS+RTF volume (no insets)-pyrotechnic ash volume = 38.51 cc.
HPST7 RTF volume = 24.88 cc – small GHS volume = 14.01 cc.
HPST7 calculated pyrotechnic ash volume = 0.3813 cc.
No large GHS.
Erlenmeyer flask+butyl tube volume = 590.0 cc by measurement and calculation.
HPST7 total volume for water expansion at 1854.7 s after ignition = 24.88+14.01-.3813+590 = 628.51 cc.

The HPST9 experiment done in 2019 used a higher ratio of $BaCrO_4$ along with 26.05 std-atm-cc O_2 in the RTF with BVRTF closed for the first 208.0 s after pyrotechnic powder ignition. The HPST9 experimental results are shown in Table 5. Note that for HPST8 done in 2017 $100 \times (16.07 - 1.565) / 16.07 = 90.26\%$ of the evolved H_2 gas was removed and that for HPST9 done in 2019 100% of the measurable evolved H_2 gas was removed (no H_2 GC peak visible).

Table 5 Evolved LCCMFTHP gas quantities and compositions measured in 2019 (experiment HPST9)

Total Measured Gas Evolved (std-atm-cc)/g of Heat Paper		
HPST9		
1.134 g Heat Paper + 0.756 g $BaCrO_4$ Along With 26.05 cc STP O_2 Gas Initially Sealed Within RTF on Ignition – $BaCrO_4$ Powder and Heat Paper Were Intimately Mixed – RTF Remained Sealed for 208 s After Scan Start – RTF Was Then Opened for Gas Sample Collections		
Pyrotechnic Ignition (Manual Record Only) Occurred ~3 s After Scan Start		
Total Volume of All Gases Present When SB1 and SB2 Were Closed (std-atm-cc/g of Heat Paper) and SB Closing Time After Scan Start (s) – Some Laboratory Ambient Air Entered GHS When SB2 Was Added to Quick Connect Valve		
SB1	**13.55**	**270 s**
SB2	**15.95**	**1030 s**
SB1 (SB2) Gas Volume Percentages		
	SB1	**SB2**
H_2	**0.00**	**0.00**
O_2	**55.35***	**25.85***
N_2	**0***	**55.44***
CO	**0.00**	**0.00**
CH_4	**0.00**	**0.00**
CO_2	**44.65***	**18.71**
Total	**100.00**	**100.00**
Calculated Total Volume H_2 Gas Evolved When Indicated Sample Bottle Was Closed (std-atm-cc/g of Heat Paper) and Closing Time After Scan Start (s) – All H_2 was Removed from the Test Gas Atmosphere		
SB1	**0.00**	**270 s**
SB2	**0.00**	**1030 s**
Apparent Liquid Water Expressed as Vapor (std-atm-cc) From Gas Expansion/g of Heat Paper Measured at End of Scan (1928 s After Scan Start)		
0.7784 (1928 s After Scan Start)		
***The Proportion of O_2 to N_2 by this GC Measurement is Uncertain But This Uncertainty Will Not Affect Thermal Insulation Thermal Conductivity Significantly Because The Total Amount of O_2 plus N_2 is Correct to Nominally ± 10% and Thermal Conductivity Values of O_2 and N_2 are Similar**		

Notes: HPST9 RTF+GHS+SB-ash volume = 26.93+14.56+12.95-.44 = 54.00 cc.
HPST8 and HPST9 used the same GHS and RTF – The only internal GHS plus RTF volumetric difference was that the solid HPST8 pyrotechnic ash volume was estimated at 0.4146 cc while the HPST9 pyrotechnic ash volume was estimated at 0.4380 cc because additional $BaCrO_4$ was used in HPST9 (see tables E-1 and E-3 in Appendix E).

The pressure-time curves for the HPST5 through HPST9 experiment gas collections are shown in Figs. 4 through 8. While analyzing the HPST5 through HPST9 pressure-time curves shown in Figs. 4 through 8 it is helpful to remember that the measured evolved gas quantities other than water vapor will be saturated with water vapor at the experimental temperature so long as liquid water is present in the system (see Appendix E for examples of the calculated water vapor amounts in evolved gas samples).

Figures 7 and 8 for HPST8 and HPST9 include the times after the start of the electronic scan before BVRTF was opened and the gas pressure in the GHS started to increase. Pyrotechnic initiation for HPST8 and HPST9 as recorded manually occurred nominally 10 s and nominally 3 s respectively after the start of the electronic scan. Before BVRTF was opened the measured gas pressure in the GHS remained at zero (nominally 50 μ Hg or 6.67 Pa) for both experiments. A summary analysis of the HPST5-HPST9 experiments and of the similar experiments done in 2012 is shown in Table 6.

Table 6 Summary analysis of HPST5 to HPST9 and 2012 gas evolution experiments

H_2 Gas Removed by Added $BaCrO_4$ During 2017 Measured at Time SB1 Was Closed and Mass Ratio of Added $BaCrO_4$ to LCCMFTHP Heat Paper				
Experiment Designation/Time After Scan Start That SB1 Was Manually Closed (s)		Total H_2 Evolved Gas Present When SB1 Was Closed (std-atm-cc)/g of Heat Paper	H_2 Removed by Added $BaCrO_4$ When SB1 Was Closed Based on HPST5 Gas Evolution (std-atm-cc)/g of $BaCrO_4$	Mass Ratio of Added $BaCrO_4$ to Heat Paper
Expt.	s			
HPST5	56	16.07	0	0
HPST6	57	5.080	24.65	0.4457
HPST7	67	5.281	24.97	0.4321
HPST8	305	1.565	25.27	0.5740
HPST9	270	0	*	0.6667
*Unknown – O_2 gas originally present reacted with the evolved gases and some of the original O_2 gas remained at the end of the HPST9 experiment				
H_2 Gas Removed from EXPT 2 by Added $BaCrO_4$ During 2012 Based on EXPT1 Gas Evolution[19] – Total EXPT1 Gas Measured at 82.4 Volume % H_2				
EXPT 1		11.43	0	0
EXPT 2		0.4372	24.25	0.4520
Note that the H_2 gas evolution rate of the LCCMFTHP heat paper increased by 40.59% by these numbers from 2012 to 2017				

Events on all five scans HPST5 through HPST9 that caused pressure changes can be verified to within nominally 0.1 s using the electronic time-pressure recordings from the initial measured pressure rises. Manually recorded times such as closing the sample bottles that did not cause immediate pressure changes are generally believed correct within about ±2 s. For HPST5 through HPST7, the RTF was open to the GHS (no BVRTF present) and the initial pressure rise occurred at the moment of ignition of the pyrotechnic. BVRTF was then added to the GHS for HPST8. For HPST8, the manually recorded pyrotechnic powder ignition occurred approximately 10 s after the start of the electronic scan. SB1 was closed

approximately 305 s after the electronic scan start and 106.201 s after BVRTF was opened. The HPST8 evolved gas was initially held within the RTF (BVRTF closed) for 198.7 s after the scan start before opening BVRTF to produce the first pressure rise for HPST8 and the HPST9 evolved gas was initially held within the RTF (BVRTF closed) for 208.0 s after the scan start before opening BVRTF to produce the first pressure rise for HPST9.

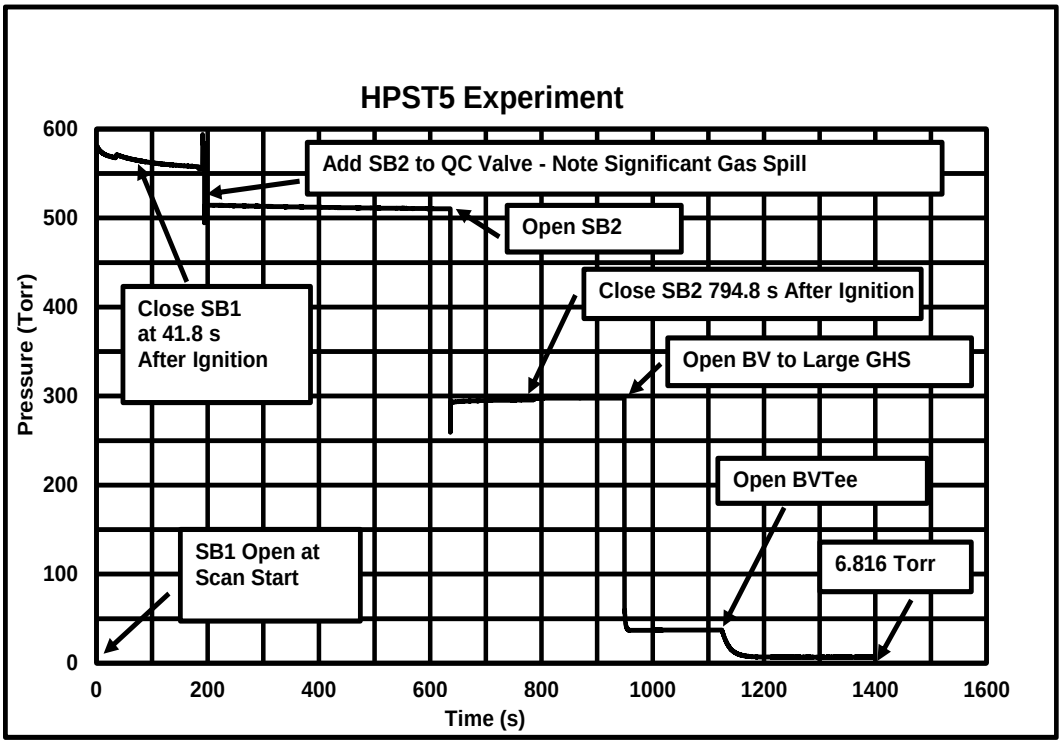

Fig. 4 HPST5 pressure-time curve

Notes: See Table 3 for internal volumes of HPST5 GHS components.
Temperature of GHS during HPST5 experiment was 24.2 °C.
Note that the total gas pressures measured for HPST5, which used no added $BaCrO_4$, are significantly higher than the gas pressures measured in any of the experiments HPST6 through HPST8.
Gas pressure when SB1 was closed was measured at 569.913 Torr.
Gas pressure when SB2 was closed was measured at 297.6168 Torr.

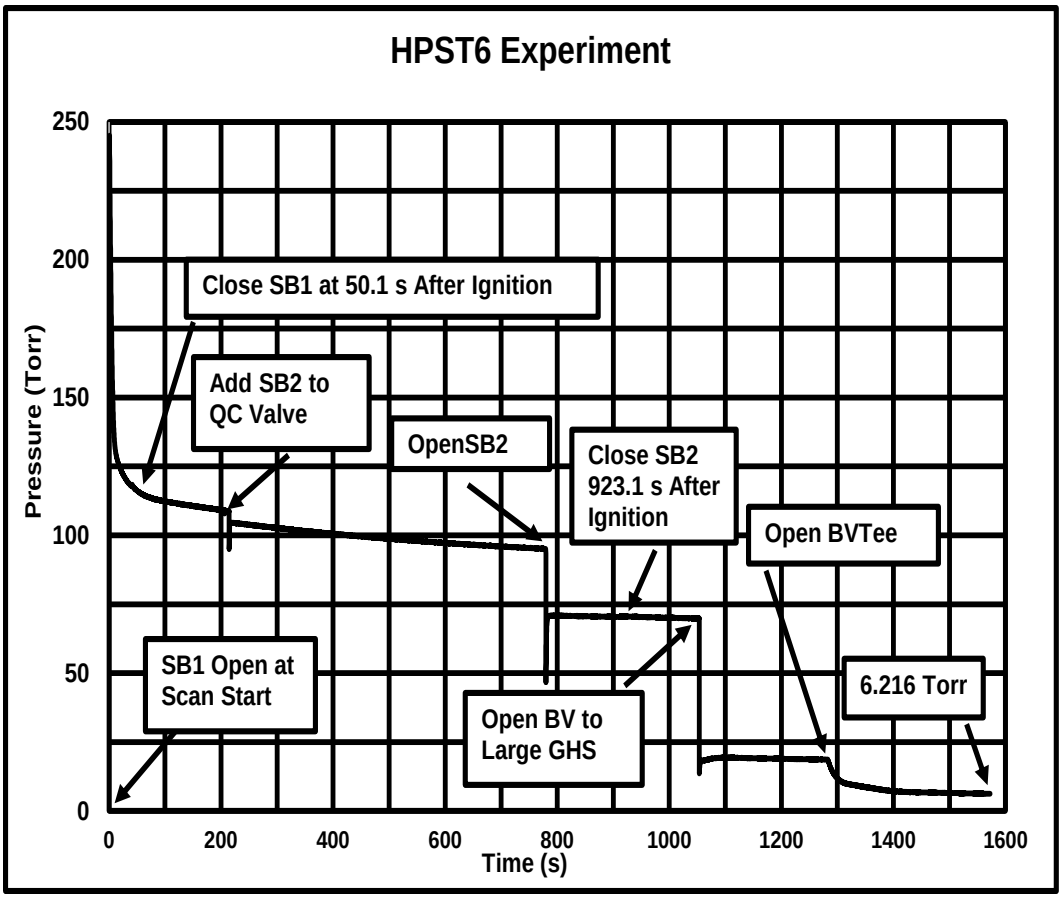

Fig. 5 HPST6 pressure-time curve

Notes: See Table 4 for internal volumes of HPST6 GHS components.
Temperature of GHS during HPST6 experiment was 24.3 °C.
Gas pressure when SB1 was closed was measured at 116.2234 Torr.
Gas pressure when SB2 was closed was measured at 70.5407 Torr.

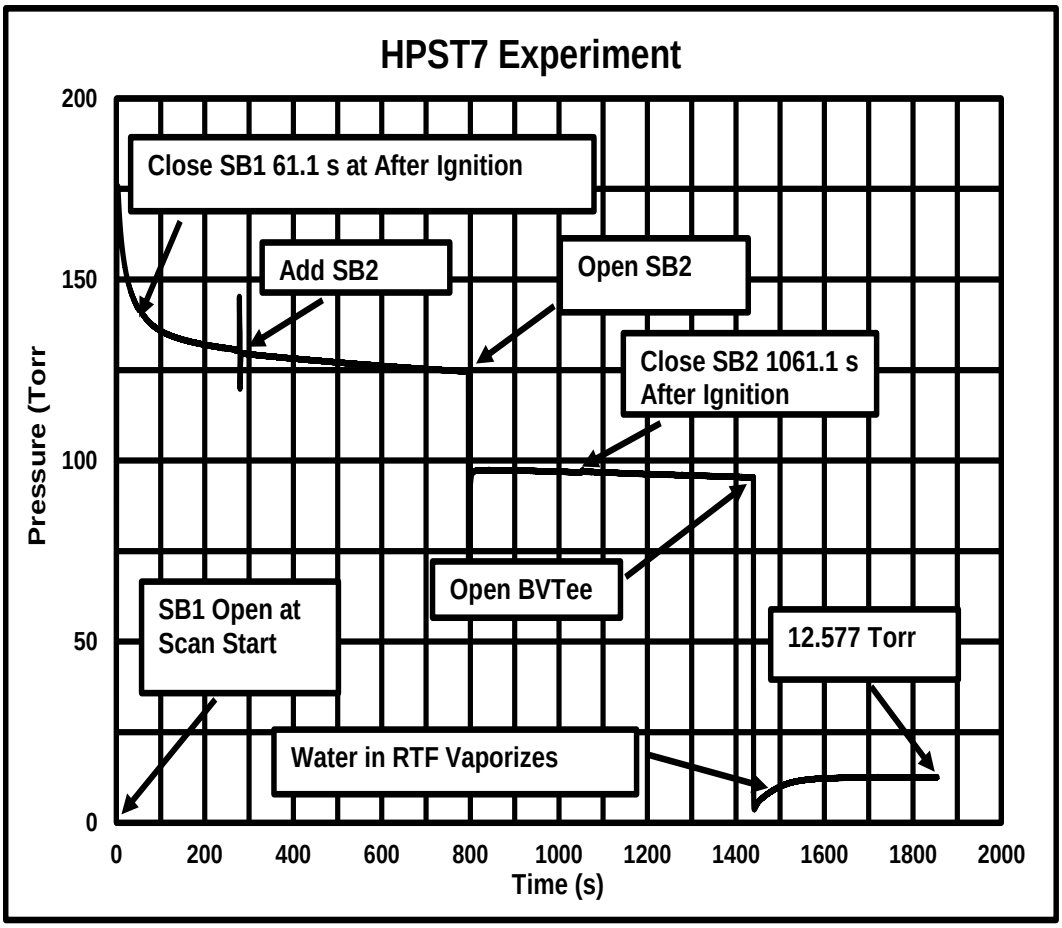

Fig. 6 HPST7 pressure-time curve

Notes: See Table 4 for internal volumes of HPST7 GHS components.
Temperature of GHS during HPST7 experiment was 25.2 °C.
Gas pressure when SB1 was closed was measured at 140.1417 Torr.
Gas pressure when SB2 was closed was measured at 96.9456 Torr.

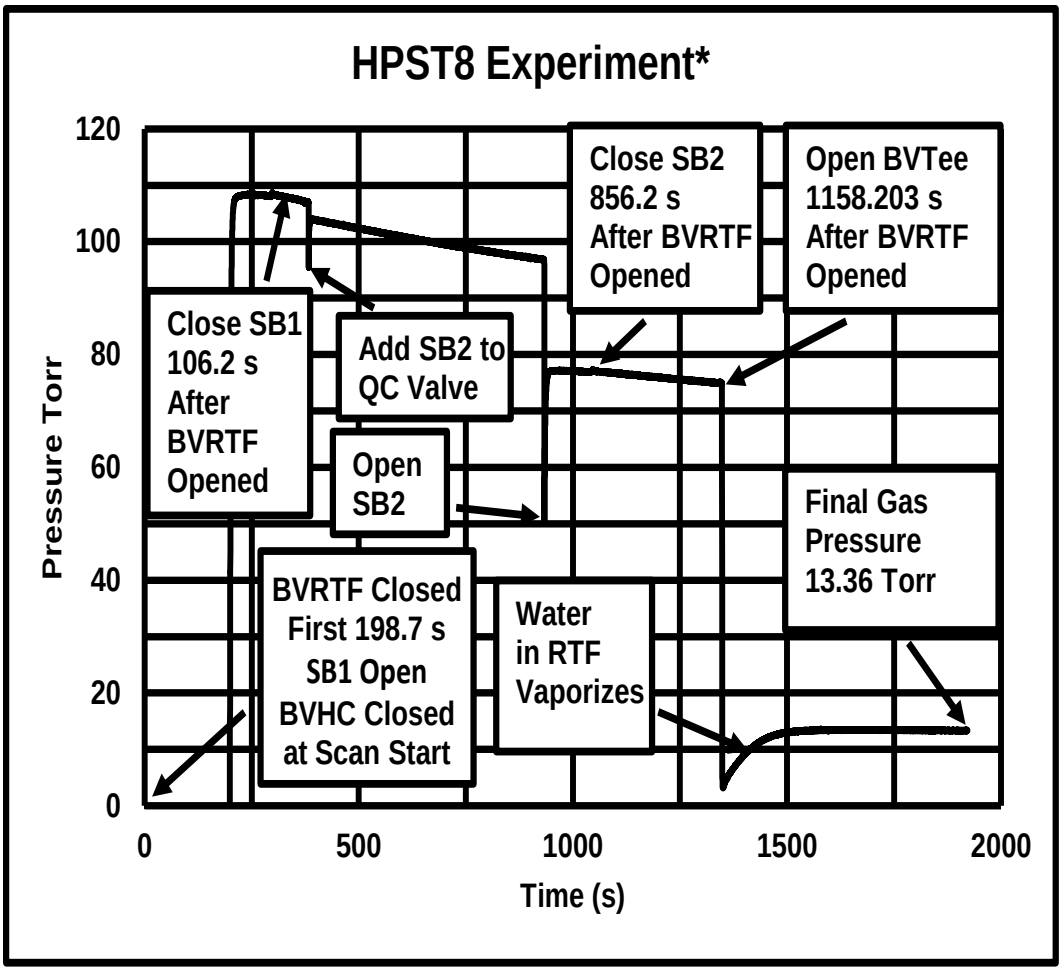

Fig. 7 HPST8 pressure-time curve

* Time zero is start of scan - Times can be measured within 0.1 s only if events cause pressure changes.

Notes: See Table 3 for internal volumes of HPST8 GHS components.
Temperature of GHS during HPST8 experiment was 24.5 °C.
The HPST8 electronic scan was stopped 1772.4 s after BVRTF was opened (initial pressure rise) and 1921.197 s after the scan was started (manually recorded ignition was ~10 s after the scan was started)
Note that the initial gas pressures measured for HPST8 when BVRTF was opened are significantly lower than the gas pressures measured when the heat paper was initiated in experiments HPST6 and HPST7.
Gas pressure when SB1 was closed was measured at 108.2795 Torr.
Gas pressure when SB2 was closed was measured at 77.0100 Torr.

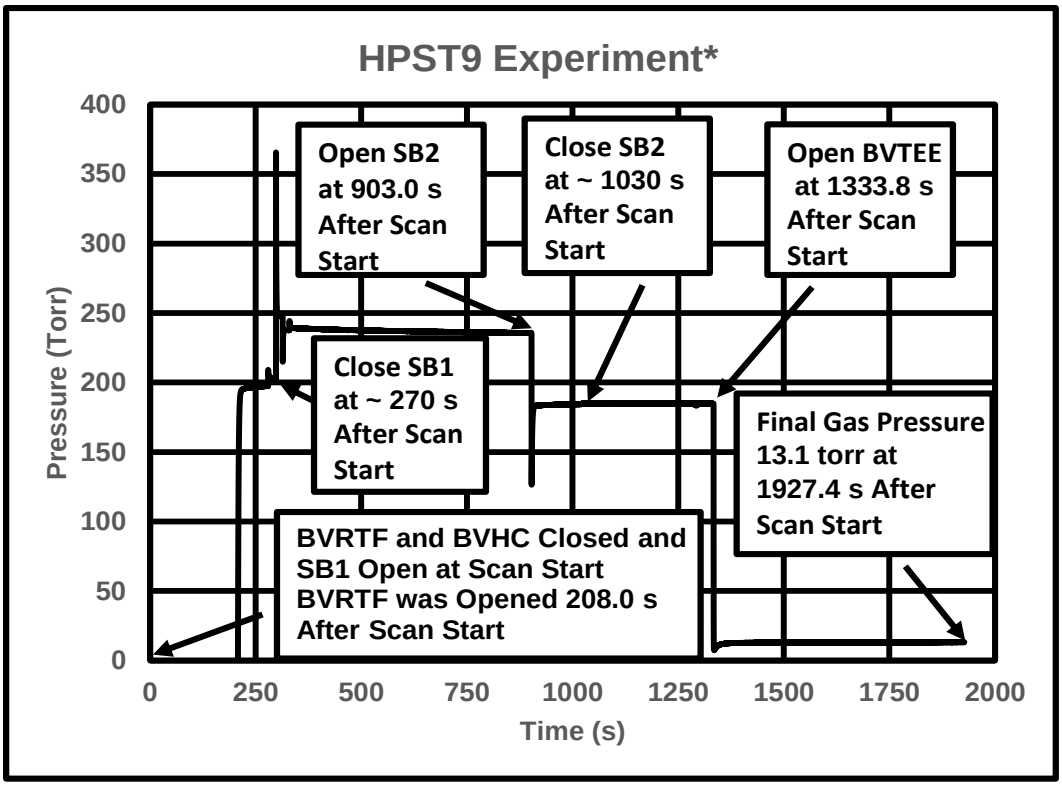

Fig. 8 HPST9 pressure-time curve

* Time zero is start of scan - Times can be measured within 0.1 s only if events cause pressure changes.
Notes: Gas pressure spiked at 365.6 Torr when SB2 was added 298.2 s after scan start.
See tables E-3 and E-4 for internal volumes of HPST9 GHS components.
Temperature of GHS during HPST9 experiment was 9.45 °C.
The HPST9 electronic scan was stopped 1719.4 s after BVRTF was opened (initial pressure rise) and 1927.4 s after the scan was started (manually recorded ignition was ~3 s after the scan was started).
Gas pressure when SB1 was closed was measured at 197.274 Torr.
Gas pressure when SB2 was closed was measured at 184.971 Torr.

Note that the total gas pressure never rises as high as the HPST5 values when excess $BaCrO_4$ is present for experiments HPST6 or HPST7. The HPST5, HPST6, and HPST7 experiments all measured the gas pressure directly during the initial pressure rise. The HPST7 powders were more thoroughly mixed than the HPST6 powders and the initial gas pressures for the HPST7 experiment were lower.

The HPST8 gas was manually released from the RTF by opening BVRTF to begin the pressure rise 198.7 s after the start of the electronic scan. For HPST8, the manually recorded pyrotechnic ignition occurred approximately 10 s after the start of the electronic scan. For HPST9, the gas was held in the RTF for 208.0 s after the start of the electronic scan and the manually recorded pyrotechnic powder ignition occurred approximately 3 s after the start of the electronic scan. Time zero for all curves shown in Figs. 8 and 9 was nominally 0.1 s before the first digitally recorded pressure rise.

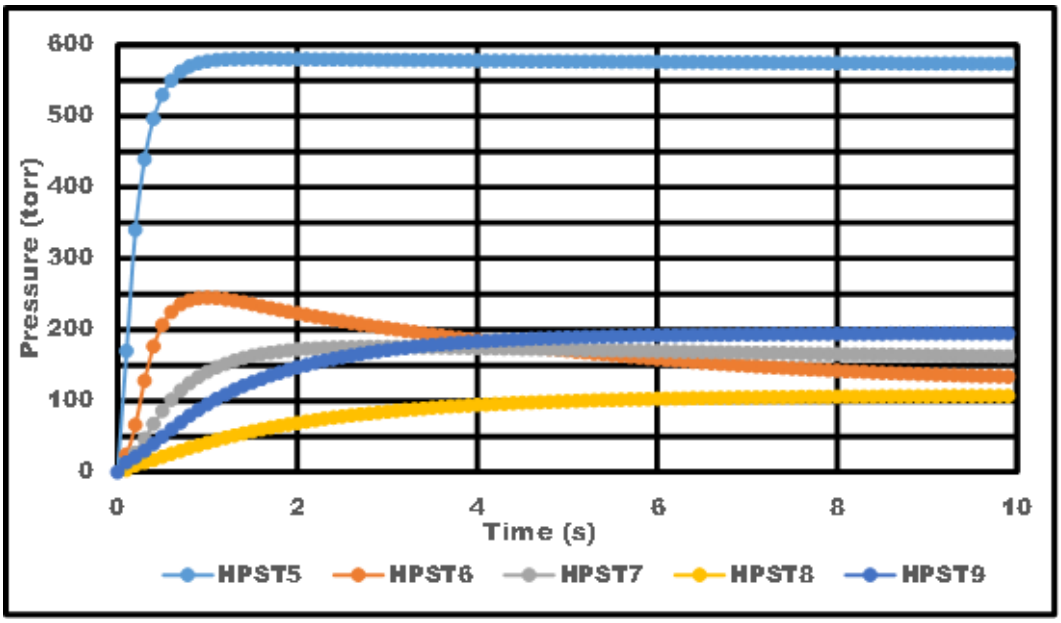

Fig. 9 First 10 s of pressure rise for experiments HPST5 through HPST9

The low gas pressure values for HPST6 and HPST7 of Figs. 9 and 10 definitely show that most or all of the gas reactions with the pyrotechnic ash for HPST6 and HPST7 occurred before approximately 2 s after pyrotechnic powder ignition. Nearly all of the evolved gas had either already reacted with the ignited pyrotechnic ash solid residue and/or other evolved gas components or else had not yet been evolved by the time the first data point was taken at nominally 0.1 s after the initial pressure rise resulting from pyrotechnic powder ignition. No extremely sudden spike of gas pressure was observed at the moment of pyrotechnic powder ignition for HPST5, HPST6, or HPST7, all of which were ignited with the DCM directly monitoring the gas pressure at the moment of ignition. Nor is there evidence of any sudden or large gas pressure increase later (after 10 s) in any of the HPST5 through HPST9 experiments that would indicate the occurrence of unexpected gas evolution reactions (Figs. 4–8).

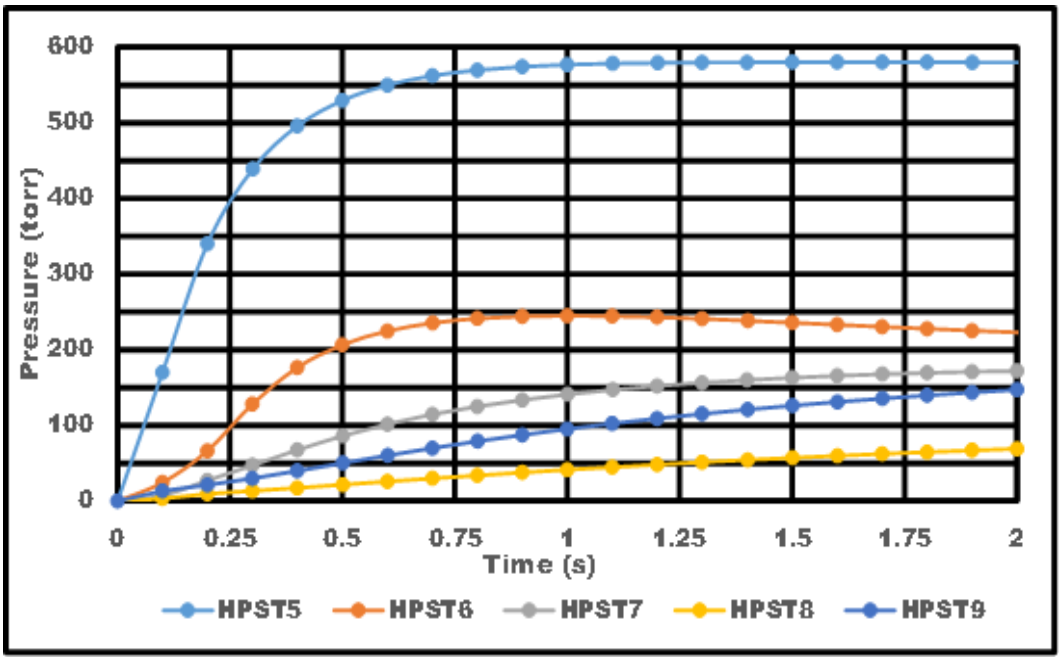

Fig. 10 First second of pressure rise for experiments HPST5 through HPST9

5. Postmortem Photographs for 2017 and 2019

A postmortem photograph of the HPST6 experiment, which used only three discrete chemical layers (heat paper/$BaCrO_4$/heat paper) for mixing, is shown in Fig. 11. The heat paper for tests HPST7 through HPST9 was first torn into small pieces and then intimately mixed with the $BaCrO_4$ powder. The HPST7 postmortem photograph with its uniform black color (Fig. 12) suggests an enhanced reaction of the $BaCrO_4$ with the Zr/$BaCrO_4$ pyrotechnic heat paper ash but the actual amounts of H_2 gas evolved by HPST6 and HPST7 were nearly identical as shown in Table 4. The postmortem ash of HPST8 visually appeared nearly identical to that of HPST7 and postmortem ash of HPST8 was not photographed. However, the HPST8 ash in the hermetically sealed RTF removed considerably more H_2 gas, as shown in Tables 3 and 4.

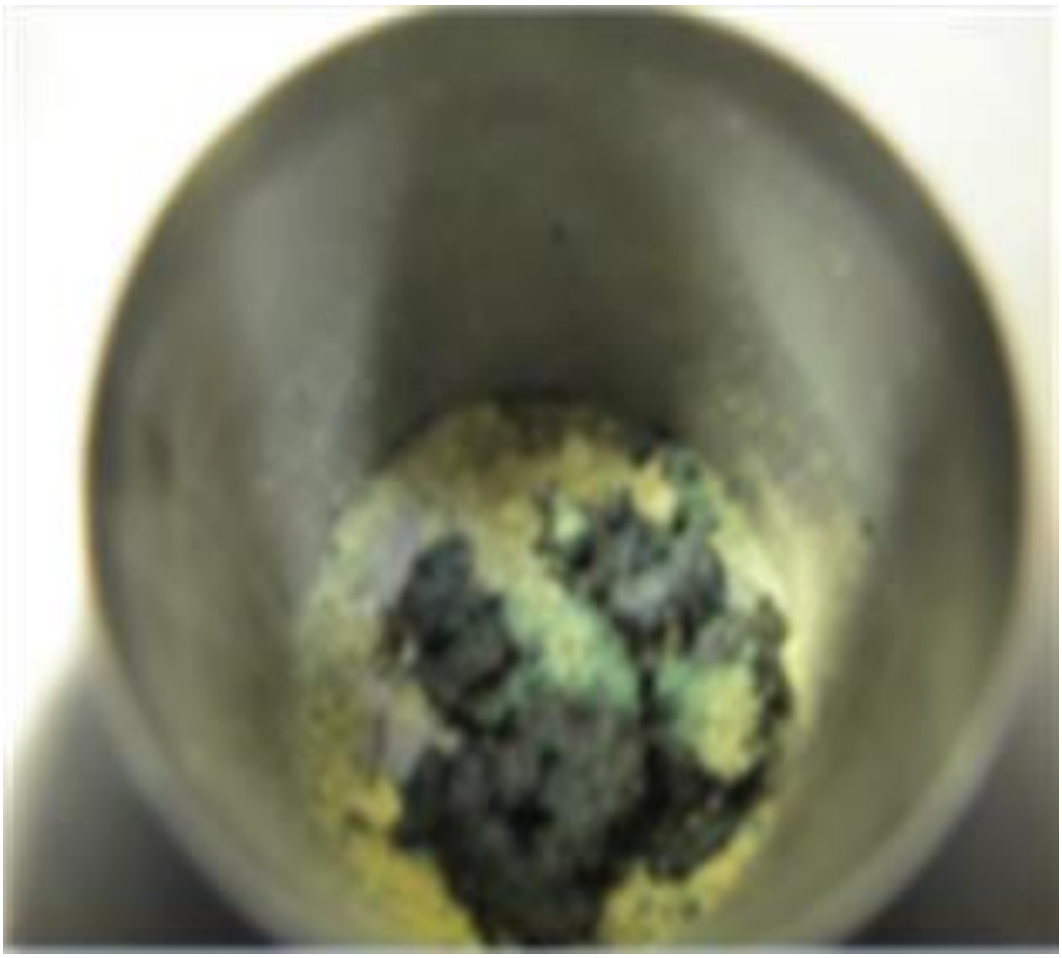

Fig. 11 HPST6 postmortem ash photograph

Yellow $BaCrO_4$ and LCCMFTHP were mixed using only three separate layers (heat paper/$BaCrO_4$/heat paper) for the HPST6 test.

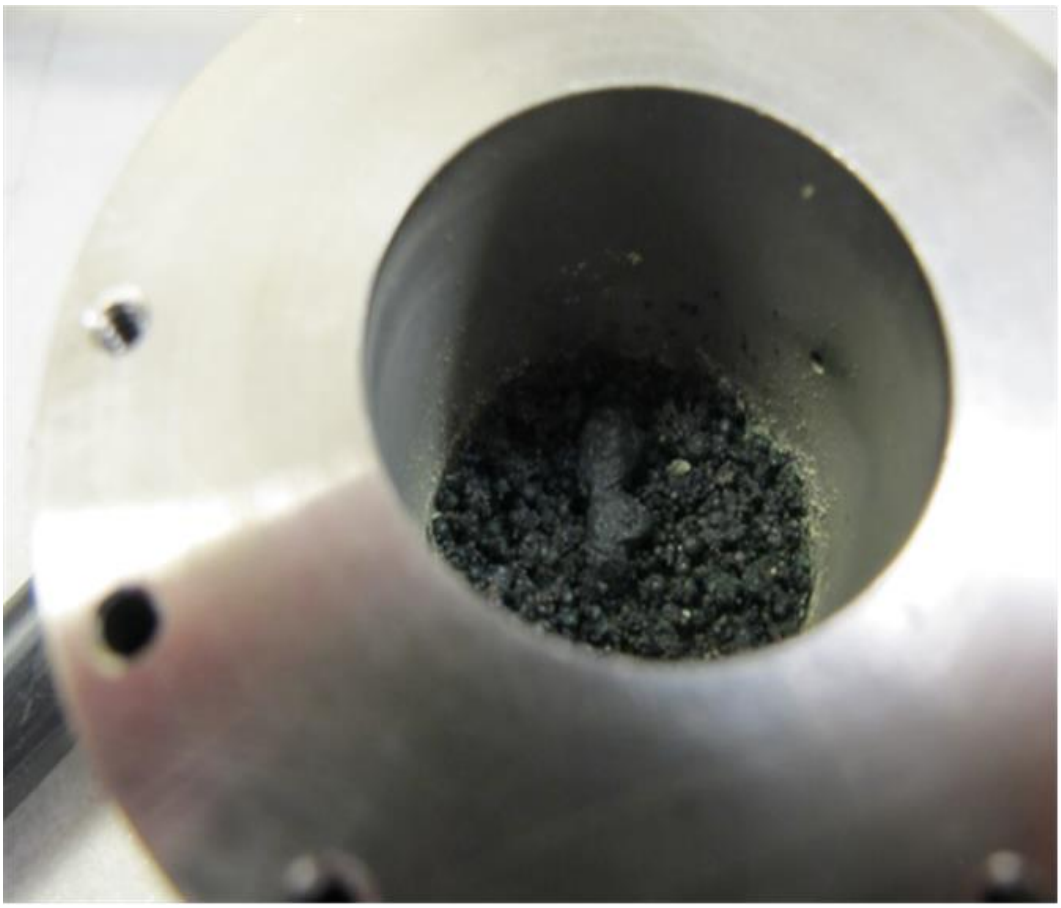

Fig. 12 HPST7 postmortem ash photograph

Yellow $BaCrO_4$ and small torn LCCMFTHP pieces were intimately mixed for the HPST7 through HPST9 tests. The HPST8 test was constructed as identically as possible to the HPST7 test, except that a bellows valve (BVRTF) was added to confine the evolved gas inside the RTF for the HPST8 test.

Fig. 13 HPST9 postmortem ash photograph

Experiment HPST9 was essentially a repeat of experiment HPST8 except that a greater weight fraction of $BaCrO_4$ was used (see Table 6) and 26.05 std-atm-cc of O_2 at a measured pressure of 759.2 Torr was present in the hermetically sealed RTF when the HPST9 heat paper was ignited. A detailed SOP of the HPST9 experimental procedure with a step-by-step checklist procedure is shown in Appendix D.

The white area to the right of the large glazed ash nodule on the right of Fig. 13 is the RTF SS bottom. The RTF SS bottom was almost uniformly covered with postmortem ash in experiments HPST7 and HPST8. Significant amounts of yellow $BaCrO_4$ visible both in the bulk of the ash mixture and on the RTF side walls in HPST9 (Fig. 14) show much greater agitation of the heat paper/$BaCrO_4$ mixture from pyrotechnic powder ignition when O_2 was present during ignition than occurred in the HPST7 and HPST8 tests (Fig. 12). The hermetically sealed HPST5 through HPST9 experimental pyrotechnics were all initiated with a moderate vacuum of approximately 6.67 Pa (50 μ Hg) inside the hermetically sealed GHS.

Fig. 14 HPST9 RTF and header postmortem

6. Gas Chromatography Results

Figure 15 shows a GC calibration done in 2019 using standardized gas samples that contained all six of the gases previously shown to be present in significant quantities during thermal battery operation (H_2, O_2, N_2, CO, CH_4, and CO_2). The O_2 and N_2 chromatographic peaks were difficult to separate using the PLOT capillary column. An expanded detail of the $O_2 + N_2$ chromatographic peak directly below is shown in Fig. 16.

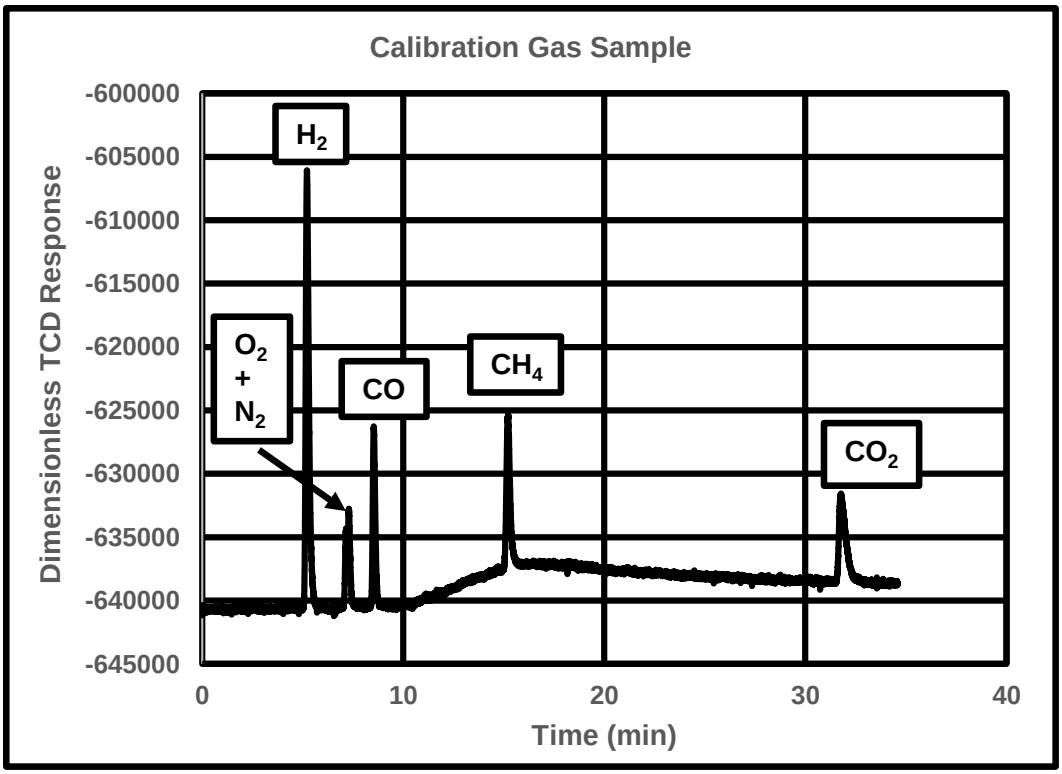

Fig. 15 GC calibration curve (667.8 Torr total gas pressure measured at GC)

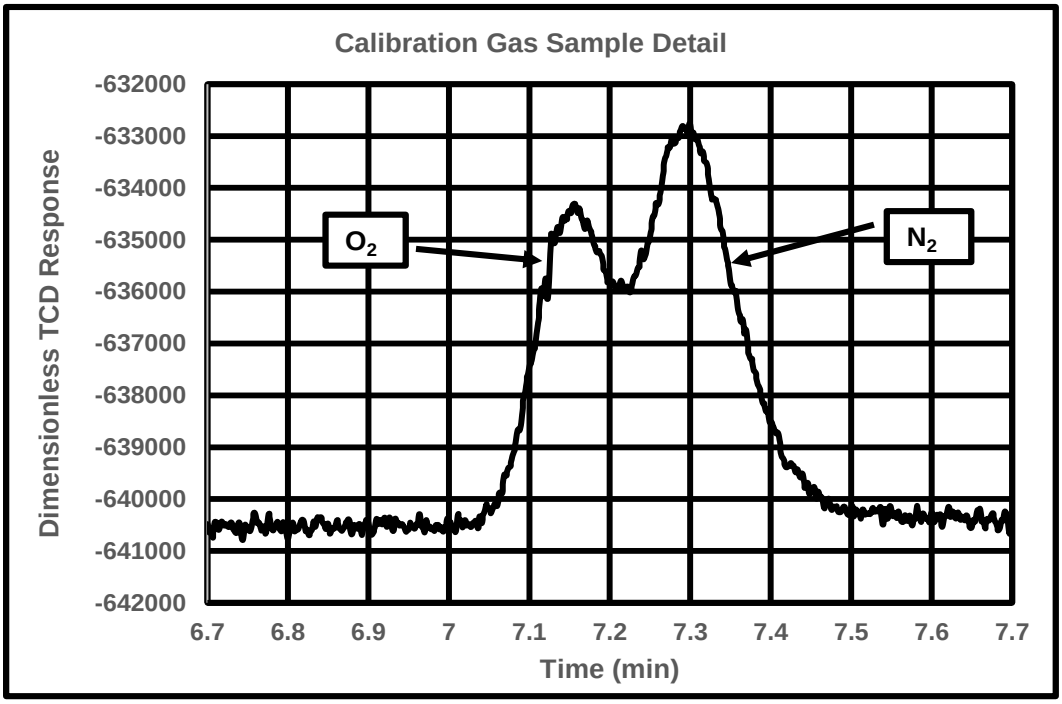

Fig. 16 GC calibration curve detail (667.8 Torr total gas pressure measured at GC)

This is the O_2 + N_2 chromatographic peak of Fig. 15 with an expanded y-axis. The GC analysis of the standardized gas samples showed the O_2 peak occurring at 7.156 min and the N_2 peak occurring at 7.299 min.

Figure 17 is the chromatogram for the first sample bottle (SB1) taken by closing BVRTF 106.2 s after BVRTF was opened in the HPST8 experiment (Fig. 7). This chromatogram is typical for the HPST5 through HPST8 series. All of the calibration gases are present although in reduced amounts compared with those of the gas calibration standard, mostly because of the reduced gas pressure of the first HPST8 sample bottle (64.3 Torr at the GC) compared with that of the calibration gas (667.8 Torr at the GC). The large H_2 peak obtained from the small percentage (25.13) of H_2 actually present in HPST8 even at the reduced gas pressure shows the large affinity of H_2 gas for the PLOT capillary column. The other gases show small peaks because they have lower affinity for the capillary column, but the summed quantities of those other gases is 74.87% of the total gas quantity for HPST8 as shown in Table 3.

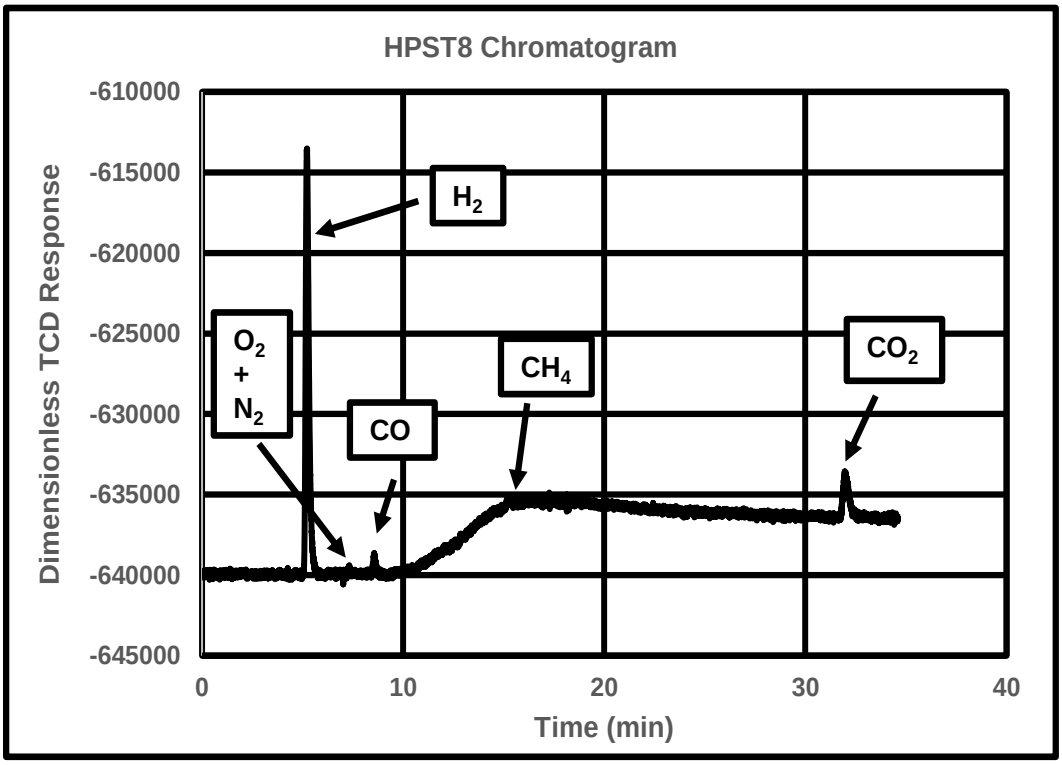

Fig. 17 HPST8 (SB1) GC curve (64.3 Torr total gas pressure measured at GC)

Figure 18 is the chromatogram for the second sample bottle (SB2) taken by closing SB2 856.2 s after BVRTF was opened in the HPST8 experiment (Fig. 7). All of the gases found in SB1 are still present in SB2 and are present at similar quantities except that the O_2/N_2 percentage ratio has changed from 19.81/2.76 in SB1 to 3.28/13.36 in SB2 (Table 3).

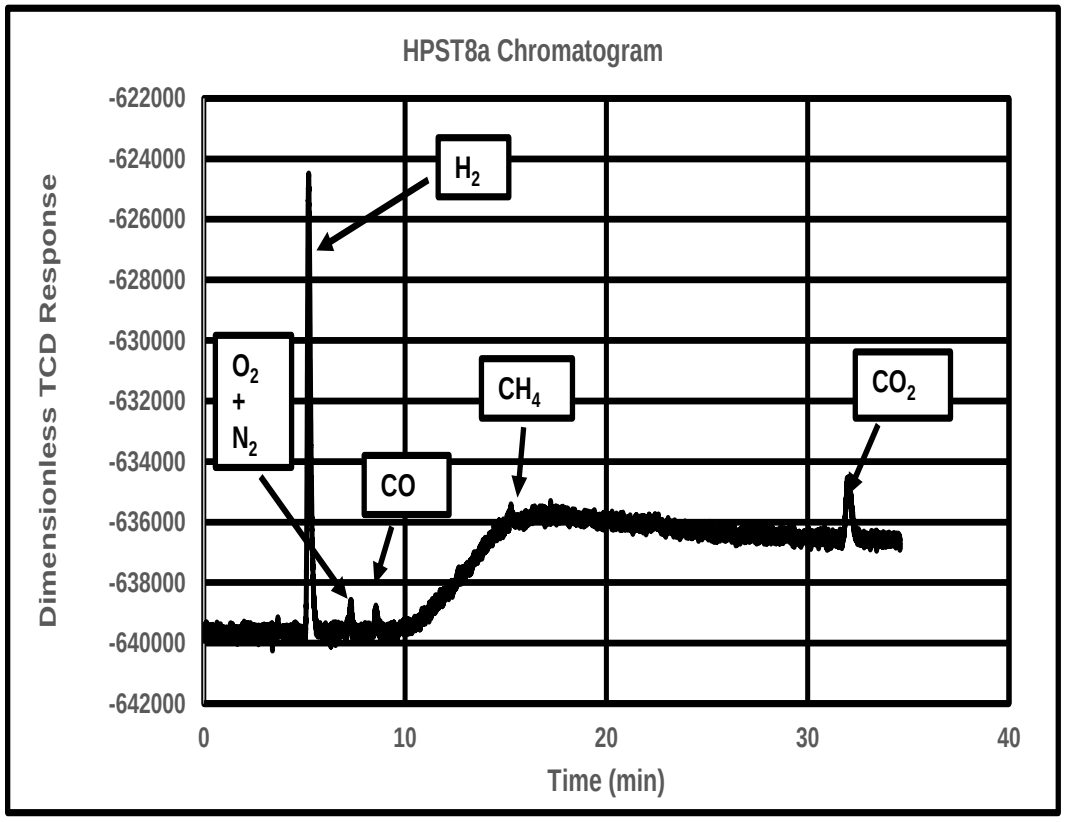

Fig. 18 HPST8a (SB2) GC curve (45.5 Torr total gas pressure measured at GC)

Figure 19 is an expanded chromatographic detail for the second sample bottle (SB2) taken in the HPST8 experiment (Fig. 7; Fig. 18). According to Table 3, this sample bottle contains 5.923 × 0.1981 = 1.173 std-atm-cc O_2 and 5.923 × 0.0276 = 0.1635 std-atm-cc N_2. The N_2 peak is distinct here even with only a small amount of N_2 present.

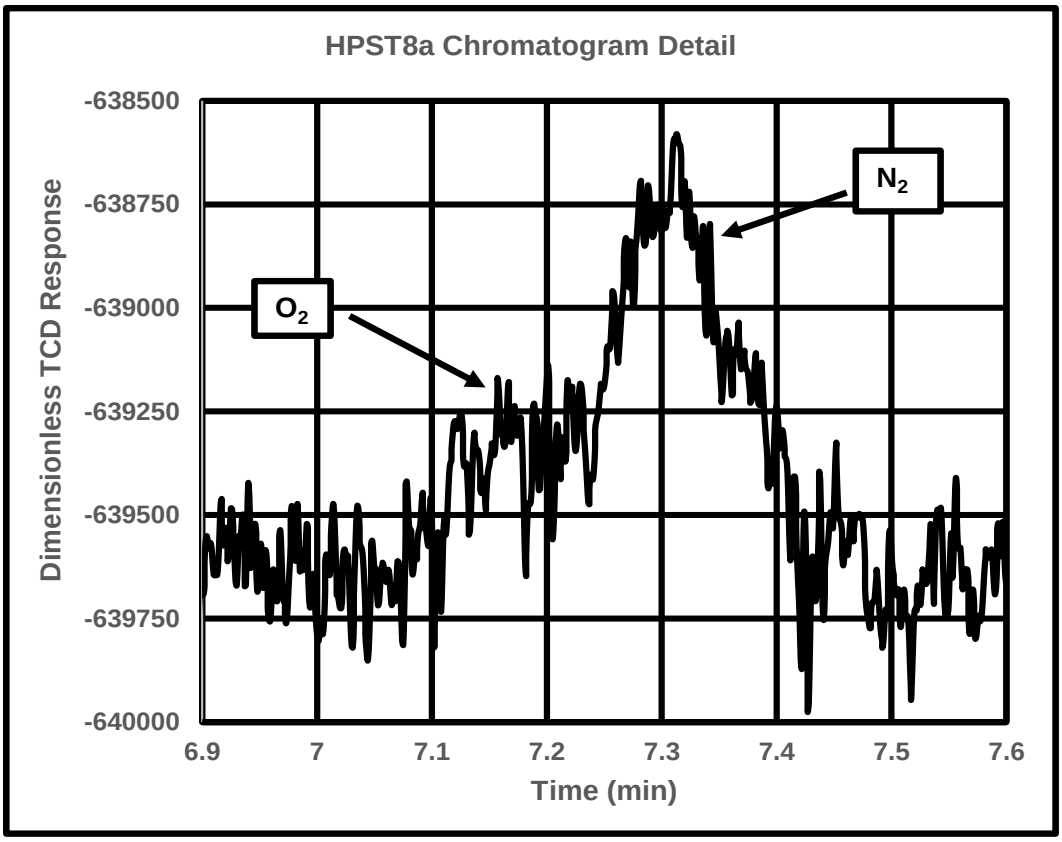

Fig. 19 HPST8a (SB2) GC curve detail (45.5 Torr total gas pressure measured at GC)

This expanded y-axis plot from Fig. 18 illustrates the O_2/N_2 chromatographic peak in greater detail and shows more clearly the GC baseline noise, which largely accounts for the ragged visible appearance of the chromatographic curve. Accuracy of the chromatographic gas percentage measurements has been observed to decrease significantly for gases at pressures below about 50 Torr.

Figure 20 is the chromatogram for the first sample bottle taken (SB1) closed at 270 ± 2 s after the scan start (manually recorded time) in the HPST9 experiment (Fig. 8). This first sample bottle HPST9 shows no visible H_2 peak and the apparent complete removal of all calibration and HPST8 gases shown in Figs. 15 and 17 except for CO_2, O_2, and possibly N_2. This is highly encouraging and has never been accomplished in any previous ARL gas evolution experiments. The complete absence of CH_4 and CO in the HPST9 chromatograms suggests that they have both been converted to CO_2.

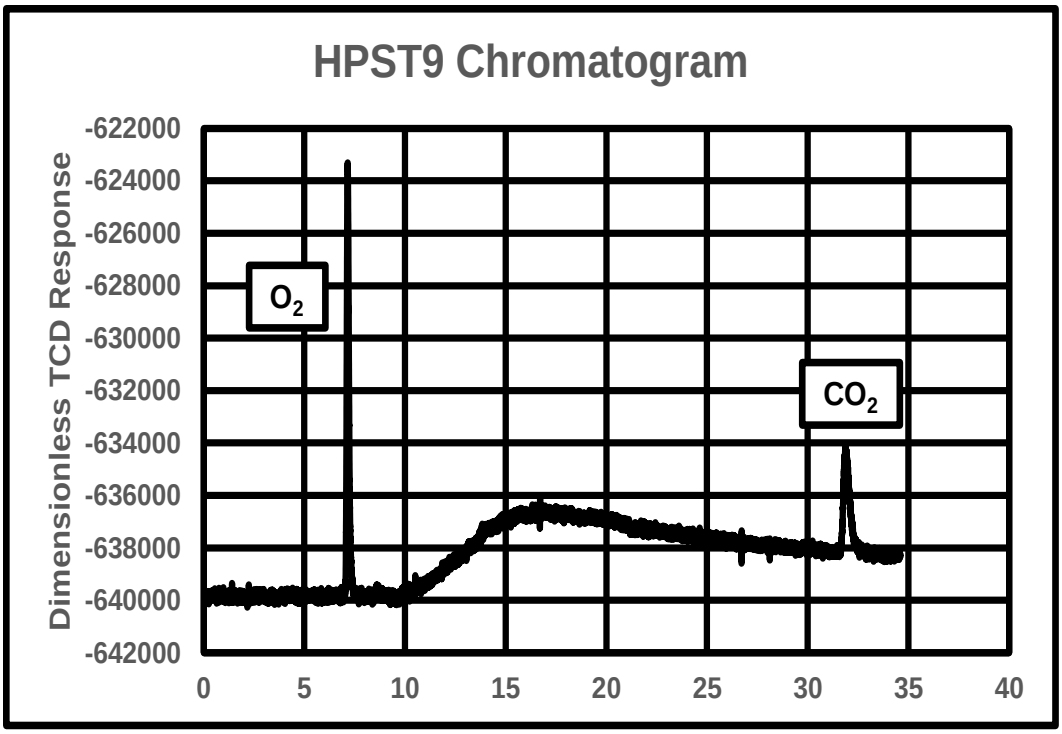

Fig. 20 HPST9 (SB1) GC curve (111.3 Torr total gas pressure measured at GC)

Figure 21 is a chromatographic detail of the first (SB1) HPST9 sample bottle. Note the absence of a separate N_2 chromatographic peak. N_2 may still be present, but no air had been spilled into the system when this first sample bottle was closed. If only O_2 is present under this curve a total of $13.55 \times 0.5535 = 7.500$ std-atm-cc of O_2 would be present according to the values reported in Table 5. Note that if approximately 0.1635 std-atm-cc of N_2 were present here as in the HPST8a detail of Fig. 19, as might be expected, then the expected N_2 peak at nominally 7.3 min with a nominal TCD response of –638625 would approximately reach the right-hand tail of the curve shown in Fig. 20.

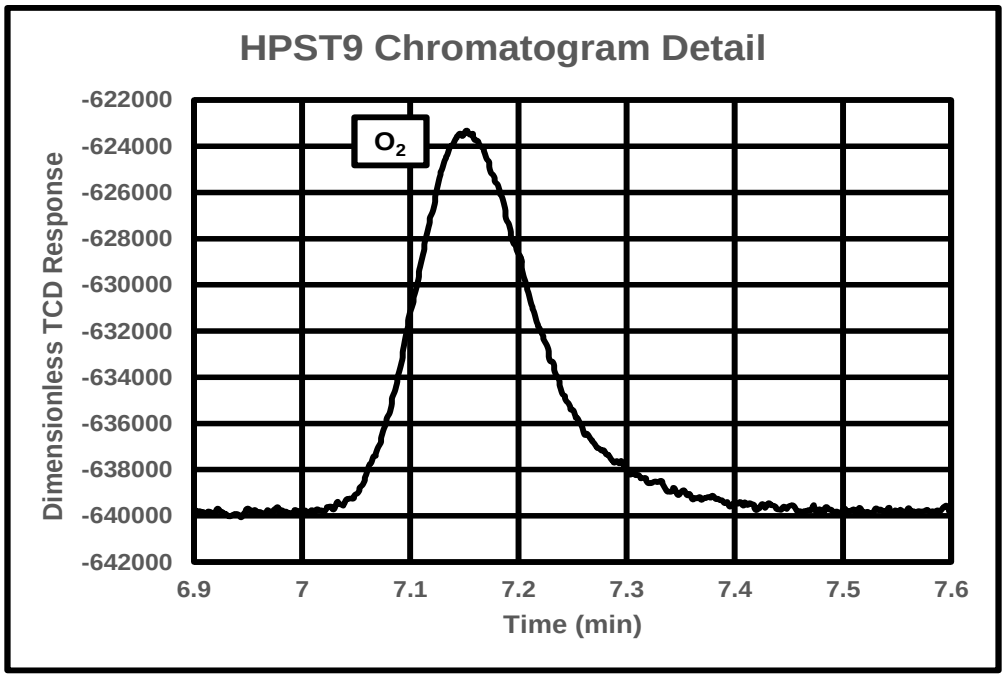

Fig. 21 HPST9 (SB1) GC curve detail (111.3 Torr total gas pressure measured at GC)

Figure 22 is the chromatogram for the second HPST9 sample bottle (SB2) closed at 1030 ± 2 s after the scan start (manually recorded time, Figs. 8 and 20). All of the gases found in SB1 are still present in SB2, but approximately 2.40 std-atm-cc of laboratory ambient air leaked into the GHS when SB2 was added (Tables 5 and E-3).

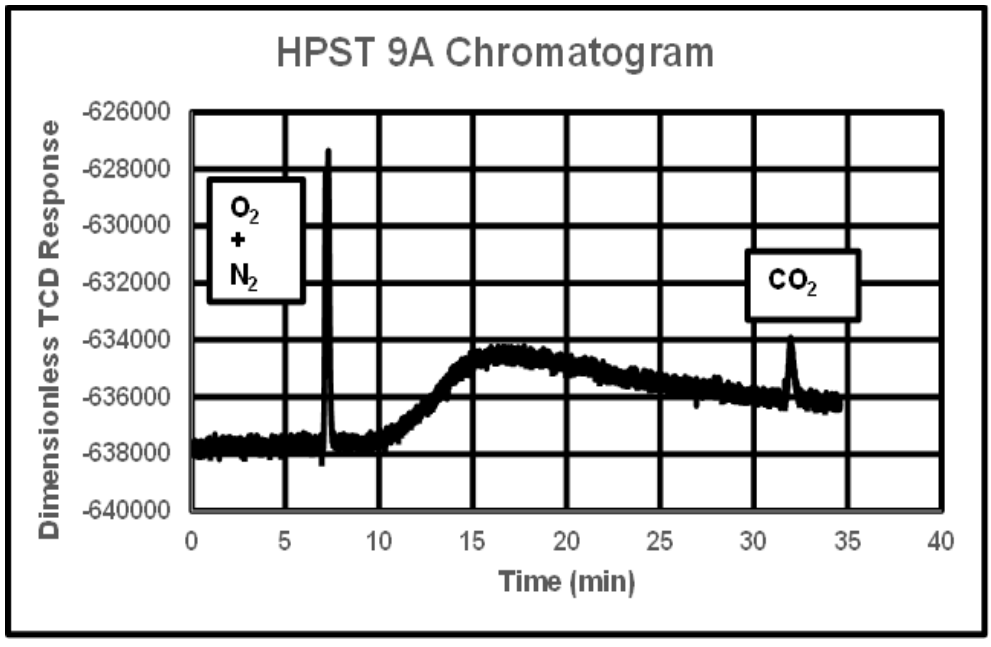

Fig. 22 HPST9A (SB2) GC curve (101.9 Torr total gas pressure measured at GC)

Figure 23 is a chromatographic detail for the second sample bottle (SB2) taken in the HPST9 experiment (Figs. 8 and 20).

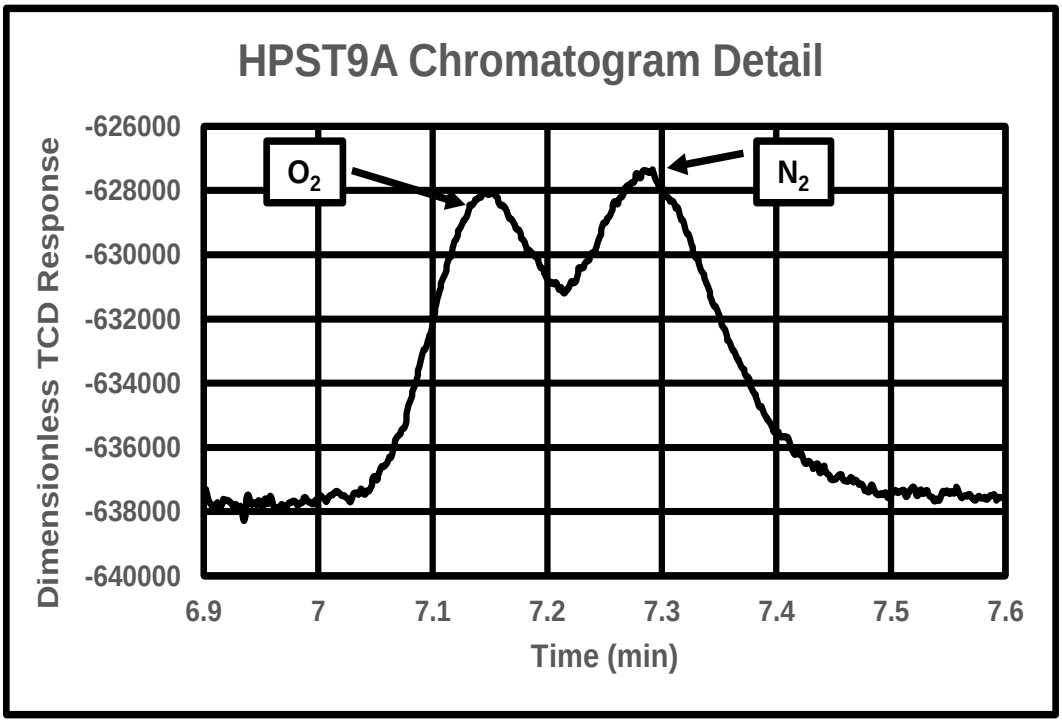

Fig. 23 HPST9A (SB2) GC curve detail (101.9 Torr total gas pressure measured at GC)

According to Table 5 this sample bottle contains 15.95 × 0.2585 = 4.123 std-atm-cc O_2 and 15.95 ×0 .5544 = 8.843 std-atm-cc N_2 along with 15.95 × 0.1871 = 2.984 std-atm-cc CO_2. Note that the HPST9A gas pressure at the GC is higher in Fig. 23 than for HPST8A (Fig. 19) because of the added O_2 that did not react chemically and the ragged curve appearance for HPST8A noted in Fig. 19 is greatly reduced.

7. Summary Results: Possibilities and Observations

Gas evolution experiments combined with mathematical modeling consistently show that many presently required long life munitions thermal reserve battery volumetric energy densities could be increased by factors of 5 or more. Gas control, materials selection, chemical preprocessing, battery construction, and thermal modeling methods are all important considerations. Although the maximally attainable reductions in volume available from optimized gas control might not be immediately available, smaller improvements from improved gas control methods that have not been completely optimized might be of crucial interest to vendor

applications in the Long-Range Precision Fires Modernization Priority. Vendors might be able to use the $BaCrO_4$ and O_2 oxidant methods described in this report to remove H_2 gas from operating thermal batteries in the near future. Materials might be decomposed pyrotechnically when the thermal battery is initiated to form an initial burst of O_2 that could help to remove evolved H_2 gas.

Gas pressures were measured directly during ignition at approximately 0.1-s intervals and showed no sudden spike at the moment of ignition so that much gas had either not yet been evolved or had already been removed by approximately 0.1 s after pyrotechnic initiation. Most evolved gases in this report appear to have been removed within the first 2 s following pyrotechnic ignition while the pyrotechnic powder ash was still at high temperatures. Much interaction between the gases probably occurred in the gas phase at elevated temperatures. Some additional tests of the H_2 gas removal methods such as gas gettering, which has proven effective in atmospheres with high concentrations of H_2 gas[18,32] might be useful while the test fixture, required chemicals, and technical expertise remain immediately available.

Removal of all H_2 gas evolved from LCCMFTHP without any added O_2 using only a higher mass ratio of $BaCrO_4$ per gram of heat paper might be possible. For experiment HPST9, both methods were tried simultaneously and the HPST9 experiment was a complete success in that it removed all evolved H_2 gas measureable by the GC. Additional testing in the absence of O_2 while keeping the $BaCrO_4$/heat paper mass ratio at the HPST9 level or higher seems appropriate. The ash of 22/78 Zr/$BaCrO_4$ is thought to be rich in barium oxide (BaO), and BaO has a known capability to remove H_2O from closed chemical systems.[33] Heat paper using powder mixtures with lower concentrations of Zr powder than 22/78 Zr/$BaCrO_4$ might be tested. The ash retention of evolved water at high temperatures could be checked in preliminary experiments by heating the ash components and analyzing the gases evolved from the ash after the completion of experiments such as HPST8 and HPST9.

The measured amount of total gas evolved from the LCCMFTHP in 2017 for the HPST5 experiment (20.79 std-atm-cc/g of heat paper) was about 50% greater than that evolved in 2012 (13.87 std-atm-cc/g of LCCMFTHP) as shown in Tables 2 and 3 and the amount of H_2 gas evolution increase from 2012 to 2017 (11.43 and 16.07 std-atm-cc/g of heat paper respectively) was about 40% as shown in Table 6. The quantity and chemical composition of gas evolution might vary significantly from sample to sample. Additional testing to verify and distinguish the effects of sample reproducibility and storage conditions is suggested. Experiments (HPST1 through HPST4) done in 2017 showed that H_2 gas evolved from heat paper

pyrotechnic powders containing significant amounts of PbO_2 were not removed effectively using $Zr/BaCrO_4$ pyrotechnic powder mixtures.

Levels of H_2 gas dissolved in either the iron powder of $Fe/KClO_4$ pyrotechnic heat pellets or in the Zr powder of $Zr/BaCrO_4$ pyrotechnic powder mixtures might be reduced to negligibly low levels or eliminated by chemical preprocessing methods. Appropriate levels of carbon could be intentionally dissolved into either the iron of the $Fe/KClO_4$ pyrotechnic heat pellets or the Zr of the $Zr/BaCrO_4$ pyrotechnic powders to react with any H_2 gas evolved on thermal battery initiation and help convert evolved H_2 gas to CH_4, which has a much lower thermal conductivity value.[34] Placement of carbon directly within the pyrotechnic powders either as a separate powder or as a dissolved metal constituent might help to enhance the formation of CH_4 from evolved H_2 gas on pyrotechnic powder ignition.

Non-microporous thermal insulation materials used with opacification agents could effectively replace more expensive microporous thermal insulators for many applications if high thermal conductivity H_2 gas could be sufficiently removed from operating thermal battery gas atmospheres.[35,36] Non-microporous thermal insulators with opacification agents at moderate densities will have thermal conductivity values similar to those of the gases in their porous structures and would become much better thermal insulators if H_2 gas could be removed (Figs. 1 and 2). The ash of the heat paper plus $BaCrO_4$ shown to remove H_2 gas from the operating atmosphere in this report will not be formed until the moment of ignition of the thermal battery and therefore will not need to be chemically protected during the required 10- to 20-year shelf life of the thermal battery.

For a typical LCCM thermal battery version with a total internal volume of 25.2 cc using a typical microporous thermal insulation package, the LCCM battery global void volume was estimated as 12.71 cc based on the weights and theoretical densities of the LCCM component materials.[3,5,6] The void volume percentages in all LCCM thermal batteries are high relative to many munitions reserve thermal batteries because of the large amount of porous thermal insulation required. Operating munitions thermal reserve batteries will normally have much smaller void volume percentages, higher operating battery case temperatures, and correspondingly higher gas pressures than were present during tests done in the RTF for this report. Initial chemical reaction rates between the $Zr/BaCrO_4$ ashes and the operating gas atmospheres including the H_2 gas removal rates for those batteries can therefore be expected to be accelerated relative to those measured in this report. The effective retention of water vapor from H_2 oxidation in operating thermal battery atmospheres at elevated temperatures by heat paper ash and any additional enhancing chemical agents must be demonstrated and confirmed.[33] The amounts of H_2 to be removed and retained are small. For LCCM a nominal total of

50 std-atm-cc of H_2 gas (4.497 mg) were evolved, which increased the thermal conductivity values of the thermal insulation package by a nominal factor of approximately 3.[5,6,19,35]

Ad hoc methods of thermal battery improvement using gas control methods for specific applications and technical demonstrations have consistently been proven effective for many years[17,19,20,35] but have focused largely on the use of battery construction methods and on backfilling certain hermetically sealed thermal batteries by low thermal conductivity value chemically inert gases such as argon, krypton, or xenon. Although these ad hoc gas control improvement methods have been demonstrably effective in both laboratory and field tests, their performance in a specific application with a short time delivery requirement is usually not readily predictable, especially when a 10- or 20-year storage lifetime must be guaranteed. Also, because of the overdesigned nature of most thermal batteries, parameters other than gas control such as chemical preprocessing and battery construction methods can often be changed to meet the desired performance values. In addition, the performance requirements can often be relaxed slightly to allow more space for the thermal battery.

8. Conclusions

Munitions thermal reserve batteries are known for their high performance and reliability at moderate cost. Huge increases in the energy densities are possible for most of these batteries. Simple, easily implemented, and reliable methods of thermal battery improvement will be required to sustain technical and financial interest in the short term.

A short burst of O_2 from an oxygen-rich chemical material or mixture when the thermal battery is initiated might help to remove H_2 gas from the operating thermal battery atmosphere as was shown for HPST9 in this report and might be useful for the Long-Range Precision Fires Modernization Priority in the short term. That removal of H_2 gas could reduce thermal conductivity values (and increase thermal lifetimes) by factors ranging from 1.5 to 3 when starting with the best microporous thermal insulators and by factors ranging from 4 to 6 when starting with less expensive but commonly used thermal insulators.

In the long term, a more comprehensive thermal battery miniaturization method that will be explained in Part 2 of this series is presently under investigation at ARL. That new method has the potential to provide greater thermal battery life extension and volume reduction than all of the gas control methods reported in Part 1. The establishment of that more comprehensive method is expected to require a moderate initial multidisciplinary applied technology effort, but once the groundwork has

been accomplished that method is expected to become a standard technology for future thermal batteries. Most future munitions thermal batteries using that new method are expected to have total volumes reduced by factors of 2 to 3 or more and thermal lifetimes extended by factors of 10 to 20 or more when compared with present munitions thermal batteries.

9. References

1. Krieger F. Heat transfer optimization of high–spin thermal batteries. Adelphi (MD): Army Laboratory Command (US), Harry Diamond Laboratories; 1990 Oct. Report No.: HDL-TR-2174.

2. Krieger F. Miniaturization of high-spin thermal batteries for GPS and LCCM artillery fuzes. Proc. 1997 Sensors and Electron Devices Symposium; 1997; College Park, MD. p. 299.

3. Krieger F, M Ding. Heat transfer in the LCCM thermal reserve battery. Adelphi (MD): Army Research Laboratory (US); 2009 Sep. Report No.: ARL-TR-4843.

4. Krieger F. Development and operating characteristics of the PS 132 thermal battery. Adelphi (MD): Army Laboratory Command (US), Harry Diamond Laboratories; 1986 Jan. Report No.: HDL-TR-2075.

5. Krieger F. Heat transfer in high-current thermal batteries. Proceedings of the 35th International Power Sources Conference; 1992 June; Cherry Hill, NJ. p. 223.

6. Krieger F. Thermal optimization of Li(Al)/FeS2 thermal batteries. Proceedings of the 36th Power Sources Conference; 1994 June; Cherry Hill, NJ. p. 399.

7. Krieger F. Thermal batteries for ordnance fuzing. Adelphi (MD): Army Electronics Research and Development Command (US), Harry Diamond Laboratories; 1982 July. Report No.: HDL-TR-1989.

8. Davis P, Winchester C. Limiting factors to advancing thermal battery technology for Naval applications. Dahlgren (VA): Naval Surface Warfare Center (US); 1991 Oct. Report No.: NAVSWC TR 91-614.

9. Orrson K, Kilroy W, Bowles C, Winchester C, Weinberg M. Advanced power supplies for fuzes. Silver Spring (MD); Dahlgren Division Naval Surface Warfare Center (US); 1995 Mar 15. Report No.: NSWCDD/TR-94/174.

10. McIntyre R. Procedure for determination of gas evolved by thermite mixtures. Washington (DC): Diamond Ordnance Fuze Laboratories; 1960 Feb. Report No.: TR-702.

11. Bachner F, Alexander C. Technique for measuring gas evolved during combustion of pyrotechnic heat powders. Washington (DC): Harry Diamond Laboratories; 1968 Feb. Report No.: TM-68-4.

12. Krieger F. Miniature thermal batteries for low-current applications. 45th Annual NDIA Fuze Conference Presentation; 2001 Apr 17; Long Beach, CA.

13. Piekos E, Grillet A, Streeter N, Showalter S. Assessing the sensitivity of thermal battery performance to material thermal properties via simulation. Proceedings of the 46th Power Sources Conference; 2014 July; Orlando FL. p. 399.

14. Roberts S, Long K, Clausen J, Martinez M, Piekos E, Grillet A. Towards a coupled multiphysics model of molten salt battery mechanics. Proceedings of the 46th Power Sources Conference; 2014 July; Orlando, FL. p. 411.

15. Krieger F, Ding M. Experimental and mathematical confirmation of munitions thermal battery heat transfer using FORTRAN and SIERRA finite element thermal models. Proceedings of the 46th Power Sources Conference; 2014 June; Orlando, FL. p. 403.

16. Hodson S, Piekos E, Sayer R, Roberts S, Roberts C. Thermal characterization of molten salt battery materials. Proceedings of the 47th Power Sources Conference; 2016 June; Orlando, FL. p. 382.

17. Krieger F. Low conductivity thermal insulator for thermal batteries. United States patent 3864170. 1975 Feb 4.

18. Krieger F, Shichtman M. Gas gettering in operating thermal reserve batteries. Proceedings of the 41st Power Sources Conference; 2004 June; Philadelphia, PA. p. 87.

19. Krieger F, Ding M. Thermal battery operating gas atmosphere control and heat transfer optimization. Adelphi (MD): Army Research Laboratory (US); 2012 Sep. Report No.: ARL-TR-6156.

20. Krieger F, Ding M. Gas control and thermal modeling methods for pressed pellet and fast rise thin-film thermal batteries. Adelphi (MD): Army Research Laboratory (US); 2015 Sep. Report No.: ARL-TR-7464.

21. Krieger F, Ding M. Lifetime extension of munitions thermal reserve batteries. Proceedings of the 47th Power Sources Conference; 2016 June; Orlando, FL. p. 429.

22. Krieger F, Ding M. Gas analysis and control methods for thermal batteries. Adelphi (MD): Army Research Laboratory (US); 2013 Sep. Report No.: ARL-TR-6665.

23. Microtherm Inc., 1731 Fred Lawson Drive, Maryville (TN) 37801, info@microtherm.de.

24. Morgan Thermal Ceramics, 2730 Industrial Parkway, Elkhart (IN) 46516 www.morganthermalceramics.com.

25. Lide D, editor. Handbook of chemistry and physics. 89th ed. Boca Raton (FL): CRC Press; 2008. p. 6–37.

26. Tsederberg NV. Thermal conductivity of gases and liquids. Cambridge (MA): MIT Press; 1965.

27. Unifrax, 600 Riverwalk Parkway, Suite 120, Tonawanda NY 14150, www/unifrax.com

28. Aspen Aerogels Inc. Northborough (MA). https://www.aerogel.com.

29. Edington J, Cotton A. Evaluation of aerogel insulation for thermal batteries. Proceedings of the 47th Power Sources Conference; 2016 June; Orlando, FL. p. 386.

30. Headley A, Hileman M, Robbins A, Piekos E, Stirrup, E, Roberts C. Thermal conductivity measurements and modeling of ceramic fiber insulation materials. Int J Heat Mass Transfer. 2019;129:1287–1294. Elsevier, Amsterdam, Netherlands.

31. Krieger F, Mullins J, Poese B, Ding M, Amabile K, Dratler R, Poret J, Janow C. Gas evolution from thermal battery materials. Proceedings of the 44th Power Sources Conference; 2010 June; Las Vegas, NV. p. 517.

32. ASTM F 798-97 (Reapproved 2002). Standard practice for determining gettering rate, sorption capacity, and gas content of nonevaporable getters in the molecular flow region. West Conshohocken (PA): ASTM International; 2003.

33. Baldauf GA, Elkind MJ, inventors; Nokia Bell Labs, assignee. Barium oxide moisture getter preparation. United States patent 3214381A. 1962 Dec 5.

34. Hansen M. Constitution of binary metal alloys. New York (NY): McGraw-Hill Book Company, Inc; 1958.

35. Krieger F, Poese B, Ding M. Gas control experiments and calculations for pressed pellet thermal batteries. Proceedings of the 45th Power Sources Conference; 2012 June; Las Vegas, NV. p. 551.

36. Roberts S, Harris S, Hetzler A, Piekos E, Schroeder B, Trembacki E. Establishing the credibility of the thermally activated battery simulator, full-battery version 4: verification, validation, and uncertainty quantification. Albuquerque (NM): Sandia National Laboratories; 2017 Apr. Report No.: SAND2017-3397. [For Official Use Only. Export Controlled Information]

37. Kelley, K. Contributions to the data on theoretical metallurgy. Bureau of Mines Bulletin 584. Washington (DC): Government Printing Office (US); 1960.

Appendix A. Munitions Thermal Reserve Battery Characteristics

A.1 Munitions Thermal Reserve Battery Characteristics

1) Munitions thermal reserve batteries overview—well characterized—Department of Defense (DOD)/Department of Energy (DOE) mainstay for many years—will remain a mainstay in foreseeable future

    a. Shelf life requirement typically 10 to 20 years

    b. Highly reliable

        - 99.9% at 95% confidence level (munitions applications)
        - 99.999% at 98% confidence level (nuclear applications)

    c. Operating ambient temperature ranges wide and adjustable—typically –40 to +60 °C—can be heat balanced for different ambient temperature ranges as required

    d. High power/energy densities—lifetimes from approximately 1 s (Fast Rise ~20 ms activation time batteries) to approximately 4 h (Sonobuoy batteries)—limited by heat transfer, electrochemical quantities—measured Army Research Laboratory (ARL) Energy/Power Densities for Man Portable Non Line of Sight (MANLOS) battery **thermal cell stack only** 79 Wh/kg, 248 Wh/l, 3.70 kW/kg, 12.5 kW/l, 1.1 V/cell at 4 A/cm^2 (energy/power densities shown are also nominal maximal energy and power densities for most fully built munitions thermal reserve batteries including external cases)

2) Munitions thermal reserve battery thermal cells ordinarily operate at temperatures of 400 to 675 °C

    a. Heat loss usually sets munitions thermal battery lifetime limits

    b. Removal of high thermal conductivity (K) H_2 gas is first step

    c. Low Cost Competent Munition (LCCM) thermal battery produced approximately 50 std-atm-cc (~4.497 mg) H_2 gas total

    d. For LCCM with total internal volume of 25.2 cc estimated internal void volume is 12.71 cc

    e. Control of operating gas atmospheres could increase many munitions thermal reserve battery lifetimes markedly

f. Gas control methods are most effective for long life applications where major problem is heat transfer, not electrochemistry

g. Thermal cell heat generation during operation of present production thermal batteries is significant but not yet controllable

3) Operating thermal battery environment is chemically complex so gas removal is difficult to achieve reliably

a. High K H_2 gas might be removed by gas gettering or by oxidation to water

b. Most or all elemental hydrogen could possibly be removed by appropriate chemical preprocessing of materials before thermal battery construction

c. Water has been experimentally held in place by pyrotechnic zirconium/barium chromate ash in materials tests

d. Lower zirconium (Zr) weight percentage Zr/ barium chromate ($BaCrO_4$) pyrotechnic powder mixtures (22/78 vs. 28/72) are experimentally more effective for removing H_2 gas from operating gas atmospheres

e. Lead dioxide (PbO_2) in heat paper reduces H_2 gas removal from operating gas atmospheres markedly

f. Must guarantee that significant amounts of H_2 gas will not be present during battery operation after approximately 20 years storage

g. Experiments show that global insulation K values can be reduced significantly by H_2 gas removal

i. Remove H_2 gas to reduce K values by factors of approximately 1.5 to 3 for microporous thermal insulators

ii. Remove H_2 gas to reduce K values by factors of approximately 4 to 6 for non-microporous thermal insulators

iii. After H_2 gas is removed significant improvement still remains possible

- Remove other gases—backfill with low K value krypton (Kr) or xenon (Xe) gas—develop new thermal insulators

- Pyrotechnically heat thermal insulation
- Use heat generated from thermal cells (so far not controllable)
- Based on known heat capacities and temperature decreases measured during operation MANLOS thermal cells generated 25,591 calories while cooling to 500 °C—more than 3 times the amount of heat lost from natural cooling of the battery components (7724 calories)[6,37]
- Gas evolution experiments combined with mathematical models consistently show that many presently required long life munitions thermal reserve battery volumetric energy densities could be increased by factors ranging from 5 or more using traditional gas control methods with materials selection, chemical preprocessing, battery construction, and thermal modeling methods

4) A potentially patentable heat transfer improvement method that might by itself extend the thermal lifetimes of many thermal batteries much more than all of the gas control methods described in this report is presently under investigation at ARL and will be discussed in Part 2 of this report
    - Does not require the gas control thermal conductivity reduction methods described in this report but would be more effective when used in combination with those thermal conductivity reduction methods
    - Could reduce required LCCM and similar thermal battery volumes by factors ranging from 2 to 3 even with no electrochemical optimization
    - Could extend thermal lifetimes of operating LCCM and similar thermal batteries by factors of 10 to 20 or much more
    - Could open the door to highly significant miniaturization of future thermal battery electrochemical-heat source stack components

- Might become a standard method for future thermal batteries that are extremely small by present standards

A.2 Typical Vendor and ARL Thermal Battery Gas Evolution

The data shown in Figs. A-1 and A-2 were collected during the discharge of a typical vendor thermal battery. Thermal batteries built by ARL typically show similar results.

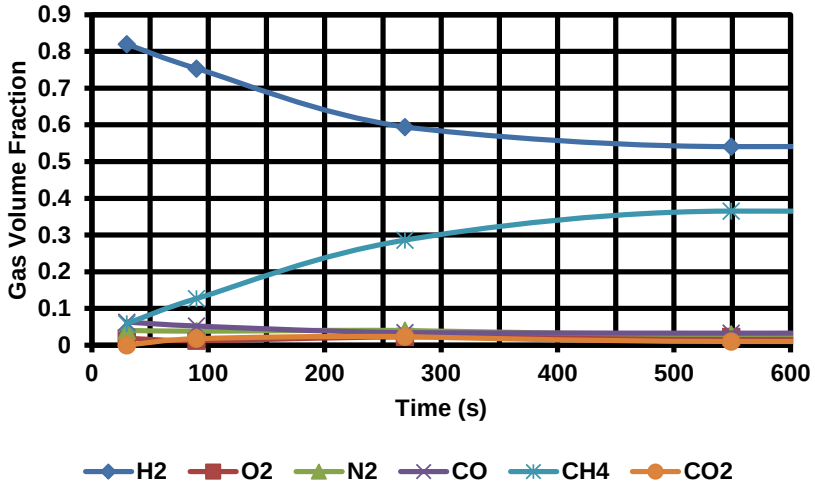

Fig. A-1 Vendor thermal battery operating gas constituents

The six gases shown constitute more than 95 % of the total gas present by volume in this typical operating vendor thermal battery. Similar thermal batteries built at ARL show similar gas evolution results. Note the consistent (and typical) increase of low thermal conductivity methane (CH_4) gas along with the corresponding decrease of high thermal conductivity H_2 gas during thermal battery operation.

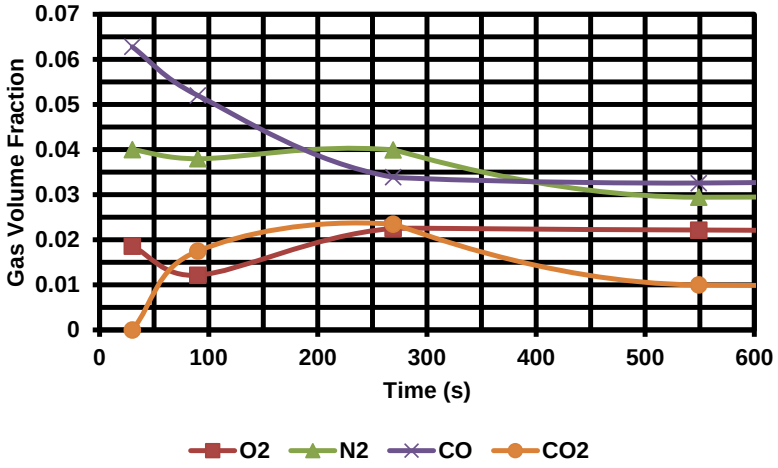

Fig. A-2 Vendor thermal battery operating gas constituents

Fig. A-2 is Fig. A-1 with H_2 and CH_4 removed and an expanded y-axis to help illustrate the chemical composition behavior of the remaining gases during battery operation. Note the consistent decrease of carbon monoxide (CO) and increase of carbon dioxide (CO_2) during approximately the first 300 s of the test.

Appendix B. Gas Handling System (GHS) Test Fixtures and Results (2012)[1]

[1] Krieger F, Ding M. Thermal battery operating gas atmosphere control and heat transfer optimization. Adelphi (MD): Army Research Laboratory (US); 2012 Sep. Report No.: ARL-TR-6156.

The GHS used and the results obtained for the 2012 gas evolution tests are shown in Fig. B-1. Both the GHS hardware volumes and the measured gas volumes originally reported in 2012 were multiplied by 1.294644 as explained in Section 3 and Appendix E of this report.

Gas compositions reported in both 2012 and 2017 were measured using a gas chromatograph (GC) custom built for testing gas evolution properties of munitions thermal batteries. The chromatographs for all tests done in 2012 and 2017 used a PLOT gas capillary chromatographic column with a thermal conductivity detector and an ultra-high purity (UHP) argon carrier gas.

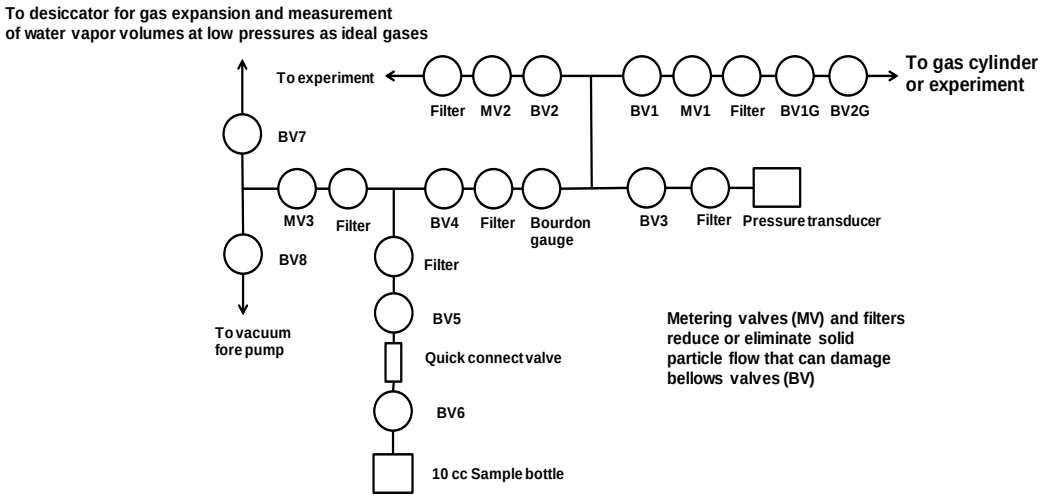

Fig. B-1 GHS system used in 2012

Notes: GHS+RTF without SB = 82.08 cc.
Desiccator+butyl tubing = 2975 cc.
The metering valves were designed to slow but not completely eliminate gas flow (note the low rate of pressure rise from time zero in Figs. B-2 and B-3 when MV2 was closed). The use of the closed metering valves in the 2012 gas evolution experiments permitted partial confinement of the gas to the reusable test fixture (RTF) but precluded the measurement of the instantaneous gas pressures during the first few seconds after ignition that were measured for the 2017 gas evolution experiments.

A baseline gas evolution test of LCCM flight test heat paper (LCCMFTHP) only using the 2012 GHS is shown in Fig. B-2. Note the high maximum gas pressure in the absence of added barium chromate ($BaCrO_4$) when MV2 is opened. Note that the gas pressure curve reported in 2012 is unchanged[1] but the gas quantities reported here are all the gas quantities reported in 2012 multiplied by a nominal correction factor of 1.295 (see Section 3 of the report and Appendix E [Tables E-1 through E-4]).

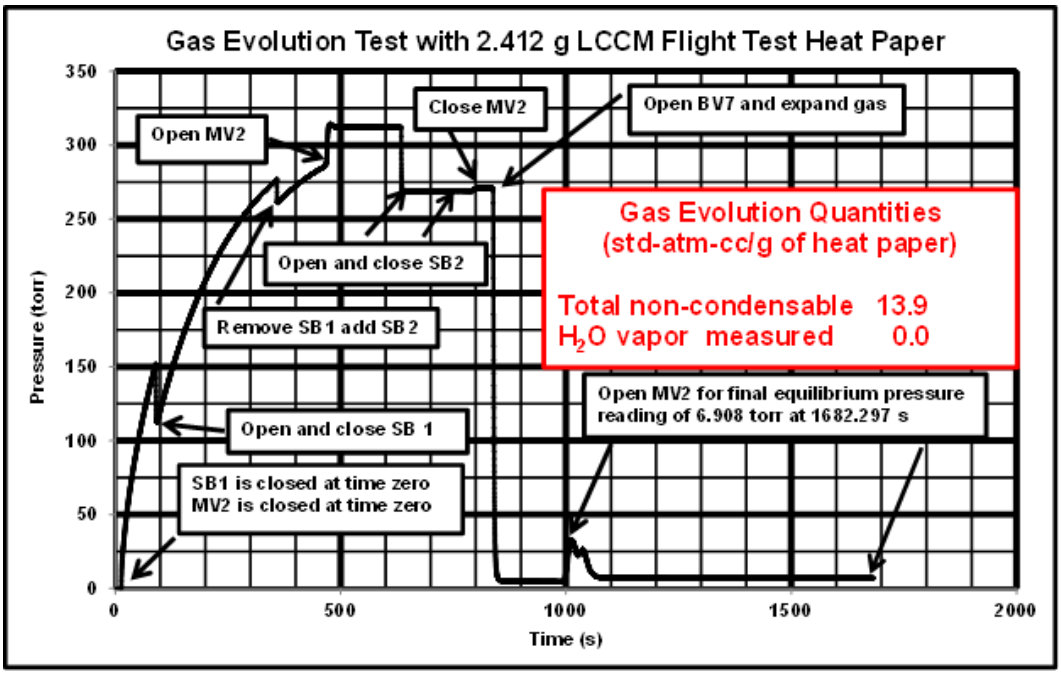

Fig. B-2 2012 Gas evolution test using only LCCMFTHP

[1] Krieger F, Ding M. Thermal battery operating gas atmosphere control and heat transfer optimization. Adelphi (MD): Army Research Laboratory (US); 2012 Sep. Report No.: ARL-TR-6156.

A gas evolution test using LCCMFTHP heat paper with added $BaCrO_4$ powder in the 2012 GHS is shown in Fig. B-3. Note the much lower maximum gas pressure in this figure with the added $BaCrO_4$ when compared with the gas pressure shown in Fig. B–2, which uses essentially the same amount of heat paper.

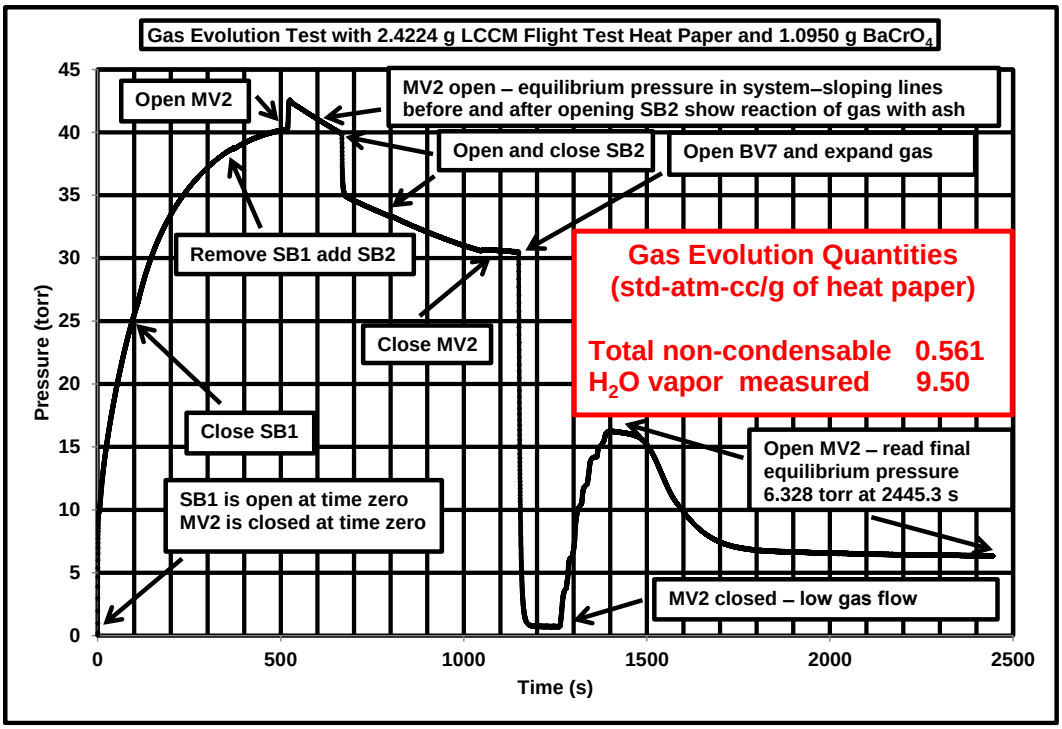

Fig. B-3 2012 Gas evolution test using LCCMFTHP with $BaCrO_4$

Appendix C. Reusable Test Fixture (RTF) Drawings for 2017

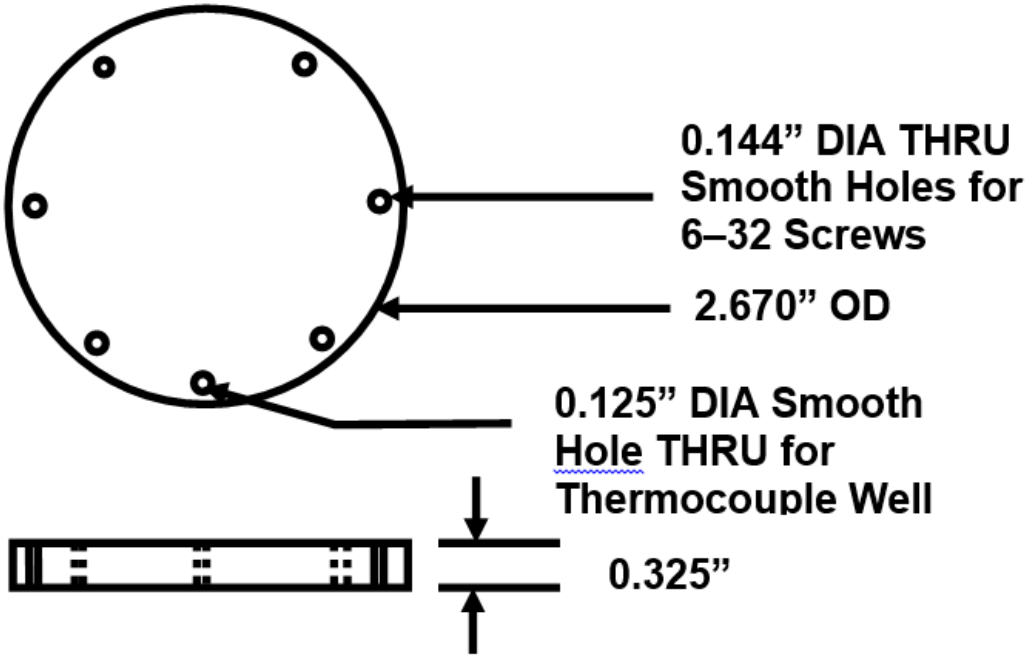

Fig. C-1 RTF header drawing (SS 304)

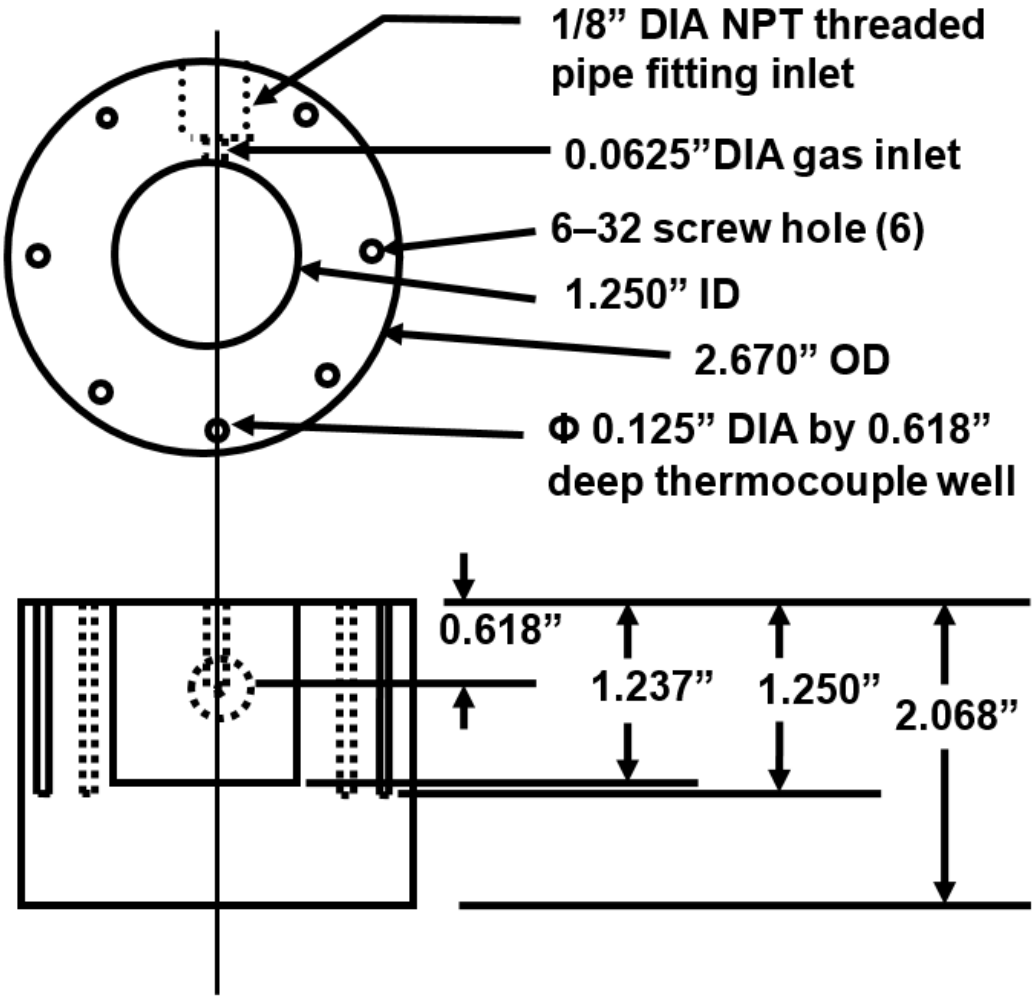

Fig. C-2 RTF case drawing (SS 304)

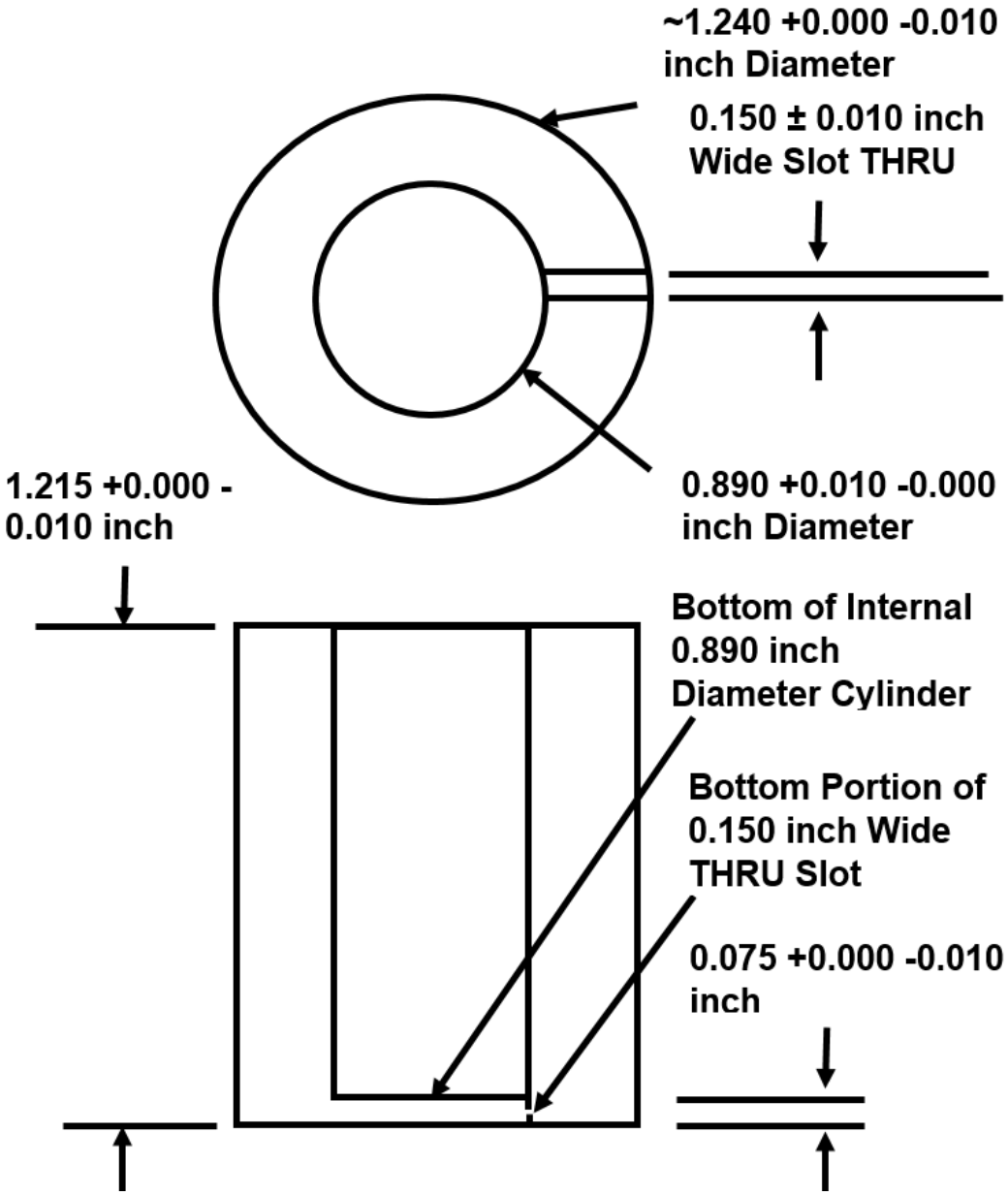

Fig. C-3 RTF cylinder inset drawing (SS 304)

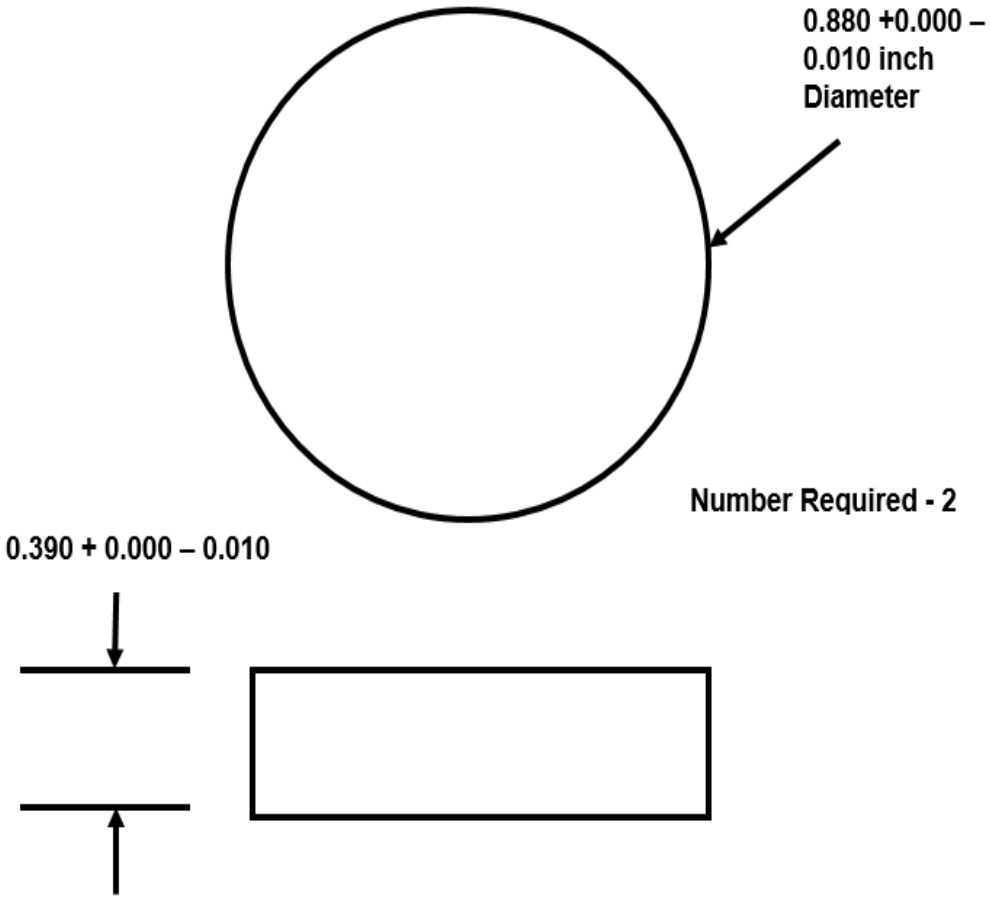

Fig. C-4 RTF inset disk for inset cylinder drawing (SS 304)

Appendix D. Step-by-Step Procedure to Quantify Gas Evolution from Heat Paper with Subsequent Gas Collection and Analysis of the Resulting Gas Atmosphere – Standing Operating Procedure (SOP)

This appendix appears in its original form, without editorial change.

Purpose: To establish safe operating procedures and assign responsibilities for operations pertaining to H_2 gas removal from ambient atmospheres. This Appendix lists and clarifies the physical-technical work to be done along with the required experimental safety procedures. The complete, finalized, and approved SOP for this experiment including additional administrative precautions and administrative personnel with contact information must be posted in the working area and must be read, understood, complied with, and signed by all relevant personnel before work can proceed.

Brief Description of Experiment:

The objective of this experiment is to collect and characterize the gases evolved from $Zr/BaCrO_4$ pyrotechnic powder based heat paper when the heat paper is initiated in an atmosphere of O_2. After taking two gas samples in separate stainless steel (SS) sample bottles, the remaining gas in the gas handling system (GHS) is expanded so that the gas pressure will be below the vapor pressure of water at room temperature and any evolved liquid water can be measured as an ideal gas from the pressure readings before and after gas expansion.

A copy of this SOP will be posted in the working area at all times.

Transportation of Pyrotechnic Chemicals to Lab:

The pyrotechnic powders will be transported in an approved government vehicle by personnel holding a valid US Army driver's license in an acceptable container.

Chemicals in Lab: During work on this SOP no other chemicals will be allowed in the laboratory room.

Approximately 25 cubic centimeters (cc) of pure O_2 at one atmosphere of pressure will be inside the 25 cc internal volume SS RTF and approximately 25 cc of H_2 gas at one atmosphere of pressure will be evolved when a $Zr/BaCrO_4/BaCrO_4$ powder mixture is ignited while inside the hermetically sealed SS RTF. Maximum gas pressure values in the RTF after pyrotechnic ignition have usually been less than 760 torr.

Equipment in Lab: The equipment used includes electrical circuits to initiate the battery, capacitance manometers, gas pressure transducers, power supplies, capacitors, etc., some of which present high voltage (120 V Max) and other electrical hazards. ARL personnel are not permitted to remove covers or panels that expose electrical hazards or work near exposed electrical hazards and must successfully complete formal Electrical Worker training provided by the ARL Safety Office. All electrical equipment must be NRTL approved or approved by an electrical SME.

Electrostatic Ignition Hazard: Thermal burns from electrostatic ignition of the $Zr/BaCrO_4$ based heat paper are a hazard. To mitigate this risk the amount of pyrotechnic material used is small and appropriate further mitigation of burns caused by direct personal contact is avoided through the use of non-sparking scalpels, spatulas, screwdrivers, and forceps along with proper Personal Protective Equipment (PPE) consisting of thermal gloves, electrical gloves, safety glasses with side shields, face shield, flame resistant lab coat, grounding strap, and electrically conductive shoes (see PPE Addendum below).

General Laboratory Orientation:

1. Be sure you understand the experimental procedure and safety issues before starting work in the laboratory—ask questions as required throughout the entire process
2. Read this SOP and the Deliberate Risk Assessment Worksheet (DRAW) for this SOP
3. Read any applicable SOPs for thermal battery work that are available
4. Read SDSs for Zr, $BaCrO_4$, barium oxide (BaO, BaO_2), chromium oxide (CrO, CrO_2, CrO_3, Cr_2O_3), zirconium oxide (ZrO_2), H_2, and O_2
5. Familiarize yourself with building, room, test materials, and equipment required
6. Verify that the laboratory room ground strip and electrically conductive floors are functional and approved by Risk Management—use those ground strips and your electrically conductive shoes as instructed by your supervisor
7. Discuss previous similar experiments and analyses with your supervisor before proceeding
8. Persons should fully understand instruments and equipment before operation
9. Persons must have knowledge of electricity and obtain electrical safety training
10. At least one person working on the experiment must have valid fire extinguisher training
11. Persons must be familiar with the locations of portable eyewash and safety shower, and know how to use these in case of accident
12. All chemicals not actively used must be stored in a flammables cabinet outside the work area during this experiment
13. All chemical containers must be labeled

14. During experiments for this SOP, keep a manual running log of the air temperature accurate to nominally 0.2 °C to use in gas volume calculations—use a regular laboratory thermometer

15. Keep a manual running log of the barometric pressure using the Digital Capacitance Manometer (DCM) when convenient—measure the barometric pressure just before running the experiment as described in the experimental checklist

16. Keep in mind that burns are the major hazard for this SOP—use gloves and forceps to avoid physical contact with the pyrotechnic materials to reduce your risk for burns

17. Keep in mind that risk factors decrease significantly when smaller quantities of pyrotechnic materials are present (see Electrostatic Ignition Hazard section)

General Laboratory Operation:

1. Pyrotechnic powder weighing, mixing, testing, and postmortem HAZMAT disposal for this experiment will all be done in the appropriate designated work area

2. Personnel Protective Equipment Safety Protection—wear as appropriate to the activity all required PPE including grounding strap, conductive shoes, safety glasses with side shields, face shield, flame resistant lab coat, and thermally resistant gloves as outlined in the Electrostatic Ignition Hazard section and in the PPE Addendum

   i. Before handling or mixing pyrotechnic powders test grounding wrist strap

   ii. When handling or mixing pyrotechnic powders wear face shield and grounding wrist strap

3. Do not exceed the quantities of any of the active chemicals in the experiment without first consulting with your supervisor

4. Do not open electrical equipment (avoid exposure to high voltages [120 V nominal maximum])

5. Verify building and room electrical ground acceptability with Risk Management before opening pyrotechnic sample jars—use building and room electrical grounds according to instructions from your supervisor and Risk Management to ground yourself and your tools while working with pyrotechnic powders

6. Buddy system is mandatory when mixing pyrotechnic powders—never cut heat paper with scissors—friction from scissors can ignite heat paper—see Powder Mixing Addendum

7. Avoid inhalation of powder when mixing—previous tests show inhalation hazards are negligible during similar mixing processes

8. The powders in the RTF shall be ignited only when the hermetically sealed RTF is in the steel blue blast chamber (pig)

9. The Erlenmeyer flask (Fig. D–1) is to be evacuated only in the steel blue blast chamber (pig)

10. Gas evolution test step—use of the buddy system is mandatory for this step—walk through this test with your supervisor before actually performing the test and study the written step-by-step instructions in the Test Procedure Checklist Guide Addendum shown in this SOP—ask questions as necessary

11. All chemical spills on benches, desks, and floor must be cleaned immediately

12. Collect chemical waste in the hazardous waste barrel—ensure sufficient water is present in barrel to prevent pyrotechnic ignition and burning of disposable Accuwipes (See Hazardous Waste Addendum)

Procedure For Fire Emergency

A. A person present with valid fire extinguisher training can attempt to suppress a small fire if it can be accomplished safely

B. If the fire cannot be suppressed safely:

1. Pull fire alarm

2. Remove all personnel from the fire area and call the number designated by your supervisor to check that the Fire Department is on the way

Procedure for Power or Ventilation Outage

1. Do not begin any work with hazardous chemicals in any laboratory when there is an electrical power or ventilation outage

2. If an electrical power or ventilation outage occurs while working in a laboratory with hazardous chemicals, immediately store the chemicals as appropriate under the conditions available as closely as possible to those of this SOP, its corresponding Deliberate Risk Assessment Worksheet, and all relevant SDSs until power and ventilation facilities can be restored

Report all accidents (injuries*, spills, fires) to your supervisor in the manner requested by your supervisor or safety officer

For all emergencies during non-business hours, call the Emergency Number supplied by your supervisor or safety officer

(*Report work-related injuries and illnesses as required by your supervisor or safety officer)

RTF TEMPERATURE AND PRESSURE ADDENDUM

The $Zr/BaCrO_4$ pyrotechnic powder burns with momentary high peak temperatures (~2700 °C). Despite the initial high peak temperatures, the RTF body (1299.8 grams) will quickly cool the 1.1 gram of pyrotechnic mix powder ash generated during the process.

The total mass of the $Zr/BaCrO_4$ pyrotechnic powder based heat paper mix will not exceed nominally 1.1 grams, which will deliver 412.5 calories. Calculations show that burning 25 cc of O_2 at standard temperature and pressure (STP) (0 °C and 760 torr) with 25 cc STP of H_2 gas to form water vapor produces 59.05 calories of energy. The combined heat generated in the sealed RTF is 471.55 calories, which can raise the final temperature of the body of the RTF bottom cylinder with a specific heat of 0.1125 cal/(g-°C) to 3.22 °C above the RTF initial ambient temperature (room temperature).

Gas evolution quantity calculations and pressure measurements from previous experiments show that the instantaneous internal hermetically sealed RTF gas pressure on ignition will be less than 3 atmospheres maximum, rapidly declining to less than 1 atmosphere. Negligible gas leakage was found through the silicone rubber gaskets at 100 pounds per square inch gauge (PSIG). All BVs in the GHS are rated at 1000 PSIG.

PPE-ADDENDUM

When mixing pyrotechnic powders and when doing gas evolution testing, the buddy system is mandatory. Wear thermal gloves, safety glasses with side shields, face shield, flame resistant laboratory coat, conductive shoes, cotton clothing and grounding strap to prevent burns. Use non-sparking scalpels, spatulas, screwdriver and forceps, and use plastic lids rather than metal lids on the pyrotechnic jars whenever possible. Be sure that all tools are clean and dry before allowing them to contact the experimental chemicals. Be aware of readily available locations and proper uses of portable eyewash and safety shower. Know location of fire extinguishers. At least one buddy must have currently valid fire extinguisher

training. Wear electrically insulating electrical gloves to protect against exposure to approximately 50 to 120 volts AC and DC.

When leak testing the GHS manifold/system setup wear safety glasses with side shields.

Wear electrical gloves to protect against electrical shock from 120 volts AC and DC as required.

POWDER MIXING ADDENDUM

Powder mixing step – Use of the buddy system is mandatory when mixing pyrotechnic powders. Weigh the pyrotechnic materials inside the Lexan box on a ceramic sheet covering a microporous thermal insulating sheet. The small amount of heat paper used will not burn through the ceramic sheet. Mix the pyrotechnic powders inside the RTF while the RTF is inside the Lexan box. Wear grounding strap, flame resistant laboratory coat, safety glasses with side shields, electrically conductive shoes, and thermal gloves as required. Into the clean and dry RTF weigh out sequentially approximately 1.1 grams of the supplied pyrotechnic heat paper and approximately 0.65 grams of $BaCrO_4$. From the approximately 1.1 grams of pyrotechnic heat paper use a scalpel to cut a rectangle nominally 0.6 inch wide by 0.9 inch long by 0.023 inch thick of mass nominally 0.25 grams for ignition by the nichrome wire. Never cut pyrotechnic heat paper with scissors because the resulting friction can cause ignition. Tear the remaining pyrotechnic heat paper into small pieces using chemical forceps. Mix the small pyrotechnic heat paper pieces with the $BaCrO_4$ powder loosely but thoroughly by hand with a small, clean, dry screwdriver or spatula.

EQUIPMENT ADDENDUM

Equipment used includes a desktop computer with monitor, pressure-time recording software, Data Acquisition Switch Unit (DASU), DCM, Pressure Transducer, Vacuum Fore Pump, GHS and gas sample collection manifold, ignition capacitor, direct current power supply, weighing balance with calibrated weights, spotwelder, portable eyewash, and safety shower.

GHS ADDENDUM

A sketch of the GHS system is shown in Fig. D-1 for reference. The SS BVs all have 1000 PSIG capacity and the sealed RTF was leak tested successfully at 100 PSIG (7.80 atm) internal pressure. The suggested allowable working pressure for the copper tubing is 2700 PSIG. During ignition the Erlenmeyer flask and the RTF must both be inside the steel blue blast chamber (pig). Do not apply a positive gas

pressure to the Erlenmeyer flask. Follow the Test Procedure Checklist Guide Addendum when working with the GHS.

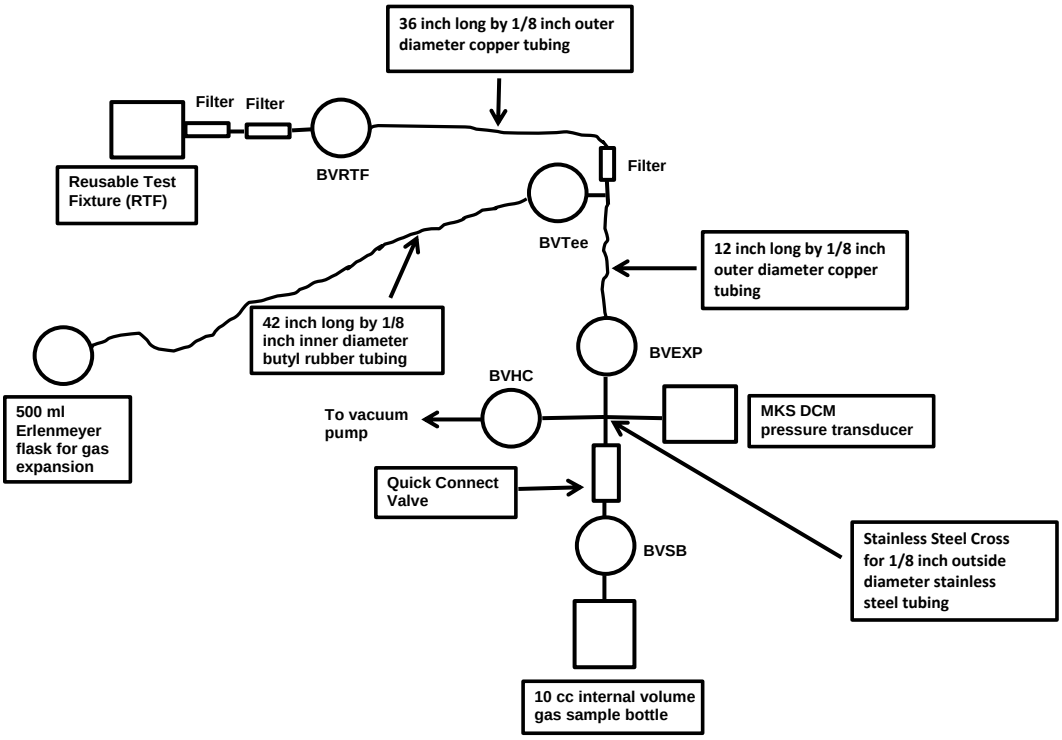

Fig. D-1 Schematic of GHS manifold (not to scale)

Internal Volumes (cc): RTF physical cylinder bottom 24.88; Empty RTF+tubing up to closed BVRTF=26.93 (Gas-ash reaction volume can be completely confined within the RTF+tubing up to closed BVRTF); GHS+RTF+SB=54.44; Erlenmeyer flask+butyl tube=590.0

Total volume of 10 cc SB plus SS tubing to closed BVSB=12.95 ± 5 %

TEST PROCEDURE CHECKLIST GUIDE ADDENDUM

1) A test procedure checklist guide for the experiment is shown for convenience—circumstances may require deviations from following the checklist exactly—consult with your supervisor if you have questions

2) Place the Erlenmeyer flask with the 43 inch long 1/8 inch inside diameter butyl tube attached to the 500 ml Erlenmeyer flask into the steel blue blast chamber pig—thread that butyl tube through the hole in the side of the steel blue blast chamber pig—attach the other end of that butyl tube to the GHS at the BVTee hose connect fitting (Fig. D-1)

- **a.** Detach the RTF from the GHS at the RTF end brass swage fitting attached to the 36 inch long 1/8 inch outer diameter (OD) copper

tube—use two 7/16 inch open end wrenches to avoid causing gas leaks after reassembly (Fig. D-1)

b. Read the air temperature to nominally 0.2 °C using a regular laboratory thermometer and start a manually recorded running log of the air temperature using that thermometer

c. Never apply a gas pressure greater than room pressure to the Erlenmeyer flask (to prevent the Erlenmeyer flask from shattering)

3) Place the detached RTF inside a Lexan box connected to the room exhaust system to protect against inhaling hexavalent chromium ($BaCrO_4$); remove the lid from the RTF and begin preparing the experimental 28/72 weight percent $Zr/BaCrO_4$ pyrotechnic powder based heat paper mixed with added $BaCrO_4$ test sample inside the RTF which is inside the Lexan box

a. Use only clean, dry, non-sparking tools to contact pyrotechnic materials (forceps, scalpels, spatulas, screwdrivers, etc.)

b. Wear all required PPE (see PPE Addendum); heat paper ignition is very sensitive to electrostatic discharge but heat paper quantities are very small

c. Weigh heat paper total quantity at approximately 1.1 grams in glass jar or beaker

d. Cut one heat paper rectangle at approximately 0.6 inch by 0.9 inch by 0.023 inch thick weighing nominally 0.25 to 0.30 grams and set aside for use with nichrome wire match (use scalpel, never scissors to cut heat paper—friction from scissors can ignite heat paper)

e. Tear the rest of the heat paper into small pieces using forceps and add to the pyrotechnic test sample inside the RTF

f. Weigh approximately 0.65 grams extra $BaCrO_4$ and add to RTF

g. Thoroughly mix small heat paper pieces with extra $BaCrO_4$ using a small, clean, dry screwdriver or spatula

h. After powders are mixed add six silicone rubber gaskets (SRGs), each SRG roughly 1/32 inch thick and a nichrome wire electric match to the RTF top (see SRG Addendum)

i. Place nichrome match wire in contact with the heat paper ignition rectangle in the RTF directly underneath the third SRG (see SRG Addendum)

j. Add RTF SS lid to the top rubber gasket and attach RTF SS lid to RTF SS bottom cylinder using six 6-32 SS screws (use a screwdriver with hand force only) and hermetically seal the RTF so that the match leads protrude 3 to 4 inches past the ODs of the SRGs—the bottom of the SS RTF lid should be approximately

0.100 to 0.130 inches from the top of the SS RTF body for a good hermetic seal

k. Place the RTF with lid attached (Fig. D–1) near the steel blue blast chamber (pig) and connect the RTF to the GHS—discuss this operation with your supervisor before proceeding to ensure minimal possibility of damage to the GHS

4) Ensure that the GHS manifold is properly connected and sealed—note that the inline 0.5 micron filters keep powder particles expelled from pyrotechnic ignition from damaging the bellows valves (BVs) (see GHS Addendum Fig. D-1)

a. The RTF, 500-ml Erlenmeyer flask, and BVEXP valves are all connected using a brass Tee (BVTee) and the flexible 36 inch long 1/8 inch OD copper tubing as shown in Fig. D-1 of the GHS Addendum

b. The 10 cubic centimeter (cc) internal volume SS gas sample bottle is sealed using the BVSB valve and then connected to the GHS through a quick connect valve

c. The DCM is connected to the BVHC, BVSB, and BVEXP valves using an SS cross and SS gas fittings

d. The vacuum fore pump is connected to the GHS with 1/8 inch inner diameter (ID) butyl tubing through a hose connect (HC) directly attached to the BVHC valve

5) Ensure that equipment is properly connected to acquire test data and has 120 V AC service

a. General Purpose Interface Bus (GPIB) cable is connected to the computer and to the DASU

b. DASU is connected through the harness to the DCM PDR (Power Supply Digital Readout) and to the DCM Pressure Transducer

6) Turn on test equipment

a. Computer/monitor is turned on

b. DASU is turned on

c. DCM and PDR are both plugged in and operating

d. RTF contains test material with match and is hermetically sealed as in step 4

e. Vacuum fore pump is operating with butyl tubing connected to BVHC (BVHC is closed)

f. Check that the 120 Volt 1 A DC power supply used to supply 85 V DC required to charge the 1000 microfarad capacitor and the 1000 microfarad capacitor itself are both functional (both are required to

ignite the pyrotechnic material in the RTF using the nichrome wire match)

7) Ensure test system operates as expected
- **a.** Double click DASU icon on computer desktop
- **b.** Under Tools select Channel Monitor and download channel 109 to read DCM voltage (A 7.60 voltage reading on the display equals 760 torr equals one atmosphere equals 101325 Pa)
- **c.** Open the BVRTF, BVTee, BVEXP, and BVSB valves
- **d.** Slowly but completely open BVHC valve with the vacuum fore pump operating
- **e.** Read and confirm the DASU and the computer channel monitor voltages
- **f.** Check that the DASU voltage outputs are stable and near zero under vacuum after BVHC has been completely open for at least 10 min—fore pump noise should be nearly inaudible
- **g.** Close the BVHC valve
- **h.** Check that the DASU voltage outputs are stable and near zero under vacuum with BVHC closed for at least 5 min to ensure that the system does not have a gross leak before proceeding with the final evacuation
- **i.** Run an equipment check scan using the DASU software and confirm that the scan is saved as expected
- **j.** Open the BVHC valve and dry the test powders in the fixture for at least 16 h under vacuum (~50 microns mercury or 6.67 Pa) before testing
- **k.** Close BVHC and BVRTF if necessary to pause experiment after drying test powders

8) Evacuate and leak test the entire GHS and the two SS gas sample bottles
- **a.** Open the BVHC valve with the vacuum fore pump running if necessary
- **b.** Ensure that all valves (BVSB, BVEXP, BVTee, and BVRTF) are open
- **c.** Pump system down to about 50 microns of mercury (6.67 Pa) - Check that fore pump is nearly inaudible when pumped down
- **d.** After fore pump nearly inaudible for 10 to 30 min adjust the DASU voltage to zero with a small screwdriver
- **e.** Close BVHC for 30 min and test for gas leaks into the GHS by observing any DASU voltage increase
- **f.** At the end of the 30-min leak test read the DASU voltage and calculate the amount of gas that leaked into the system using the

DASU voltage increase and Leak Test Addendum and the GHS component inner volumes (Fig. D-1) (should be nominally 0.06 cc standard temperature and pressure [STP] total gas leak for a 30-min leak test [STP = 0 °C and 760 torr])—this is the first leak test with BVTee to the Erlenmeyer flask and with BVRTF to the RTF both open

g. Close BVTee and BVRTF

h. Repeat steps a. through f. for the second leak test but with BVTee and BVRTF both closed

i. After the second leak test calculation (should be nominally 0.000213 STP cc total gas leak for a 30-min leak test), open BVHC, allow GHS to evacuate until you confirm slight or zero DCM voltage decline for at least 10 min, zero the DCM with a small screwdriver if necessary, and then close the BVSB valve—the BVSB valve is attached to your second 10 cc internal volume SS gas sample evacuated bottle—label this sample bottle 1B

j. Close BVSB to 1B, remove 1B from the quick connect and replace it with an identical SS 10 cc internal volume gas sample bottle at the quick connect

k. Repeat steps i. through j. for the second identical sample bottle and label the second evacuated SS sample bottle 1A—this is your first 10 cc internal volume SS gas sample evacuated bottle

l. Open BVSB for SS sample bottle 1A and evacuate the system with BVHC open for at least 10 min with negligible change in the reading with the DCM transducer properly zeroed before proceeding

m. Close BVSB for SS sample bottle 1A

n. Close BVHC

9) Fill RTF with O_2—general comments and initial gas pressure reading

a. Familiarize yourself with the small O_2 cylinder—note that the reducing gauge has a completely closable hand valve—attached to that hand valve are two outlets, one for a swage fitting to a 1/8 inch OD copper tube, and one a hose connect for a 3/8 inch ID butyl tube (BVO_2HC)—the 3/8 inch ID HC fitting was chosen to reduce the possibility of gas leaks when used with the 1/8 inch diameter butyl tubing

b. <u>Never</u> allow the DCM pressure to exceed 1000 torr (avoid DCM diaphragm damage)

c. Detach the end of the 36-inch-long copper tube from the GHS at the brass swage fitting attached to the outer end of the filter at

BVTee—use two 7/16-inch open end wrenches to avoid causing permanent gas leaks (see Fig. D-1 above)

d. Note that the 36-inch-long copper tube and the RTF are the only GHS components that will ever be attached to the O_2 cylinder so that excess pressure from the O_2 cylinder can never damage the DCM

e. Check that BVEXP is open—read the DCM barometric pressure and start a manually recorded running log of the room barometric pressure—note that the DCM will begin reading room ambient pressure (nominally 7.6 V on the DASU)

f. The DASU will measure the ambient laboratory room pressure directly when the 36-inch-long copper tube swage fitting is removed from the GHS if BVEXP is open (compare Fig. D-1 above)—this is your initial reading of the room ambient gas pressure

g. Use the O_2 cylinder bellows valve (BVO_2HC) and BVRTF to fill the RTF with O_2 as shown next in step 10—the small gas cylinder contains 12 cubic feet of O_2 at one atmosphere gas pressure and 70 °F

h. When adding O_2 <u>never</u> apply a vacuum directly to the open O_2 cylinder regulator reducing valve—be sure the hand valve to the O_2 cylinder reducing valve is closed before opening BVO_2HC

10) Fill RTF with O_2 at room ambient gas pressure (nominally one atmosphere pressure)

a. Attach the 36-inch-long copper tube swage fitting to the BVO_2HC brass Tee swage fitting so that the O_2 cylinder can be directly attached to the RTF, attach the RTF to the 36-inch-long copper tube swage fitting, and place the RTF inside the steel blue blast chamber pig

b. Ensure that the O_2 cylinder regulator reducing gauge hand valve and the BVO_2HC bellows valve attached to O_2 cylinder regulator brass Tee are both closed

c. Open the main valve to the O_2 cylinder regulator and adjust the O_2 cylinder reducing gauge pressure reading to about 5 PSIG

d. Open the O_2 cylinder reducing gauge hand valve and let O_2 purge the O_2 cylinder regulator through the brass Tee swage fitting for nominally 30 s, then close the reducing gauge hand valve and set the reducing gauge pressure reading to about 15 PSIG

e. Place the butyl tube from the vacuum pump onto the hose connect next to BVO_2HC and begin evacuating the 36-inch-long RTF-attached copper tubing

f. Open BVRTF, evacuate the RTF, and wait 2 to 5 min until pump noise minimal

g. Close BVO_2HC

h. Open the O_2 cylinder regulator reducing gauge hand valve with the reducing gauge reading 15 PSIG and fill the RTF and the RTF-attached copper tubing to 15 PSIG

i. Ensure that the hand valve on the O_2 cylinder reducing gauge and BVO_2HC are both closed

j. Open BVO_2HC and evacuate the 36-inch-long copper tube and the RTF

k. Wait until the vacuum fore pump becomes nearly inaudible for at least 2 min, then close BVO_2HC

l. Repeat h. through k. five times

m. Open the O_2 cylinder regulator reducing gauge hand valve with the reducing gauge reading 15 PSIG and fill the RTF and the RTF-attached copper tubing to 15 PSIG—this is the final fill of the RTF with O_2 after five flushes

n. Remove the swage fitting to the RTF-attached copper tubing from its position on the O_2 cylinder brass Tee swage, read and manually record the DASU voltage (note that the DASU is reading room air pressure with which the O_2 in the RTF will quickly equilibrate) and then close BVRTF—close BVRTF about 10 s after removing the RTF-attached copper tubing from the O_2 cylinder brass Tee swage to minimize leakage of air into the pure O_2 atmosphere of the RTF from the open end of the RTF-attached copper tubing and at the same time allow time for the O_2 pressure in the RTF to equilibrate with the room air pressure—the DCM voltage that you read will be near 7.60 V and will be a reading of the pressure of the O_2 that will be sealed into the RTF—this is your final reading of the room ambient gas pressure reading and of the O_2 pressure in the RTF—compare with your initial reading of the ambient gas pressure from 9.e

o. Place the RTF copper tube swage fitting back onto the GHS BVTee filter (step 10.g)—the RTF now contains thoroughly mixed pyrotechnic powders and a nichrome wire match along with a measured O_2 atmosphere with pressure of nominally 1 atmosphere in a physical volume of nominally 25 cubic centimeters

p. Check that BVRTF, BV1A (bellows valve to sample bottle 1A), and BVTee are all closed and that BVEXP is open

q. Remove the butyl tube from BVO_2HC, replace that butyl tube back onto BVHC, and evacuate the GHS system

r. After the vacuum fore pump has been barely audible for at least 2 min check that the DCM is properly zeroed

s. Leak test and calculate gas entering the system over a 10 to 30 min time frame with BVHC closed and record test leak rate

t. Open BVHC and adjust the DCM to zero voltage with a small screwdriver if necessary (evacuate and recheck zero after leak test)

11) Begin the test—prepare to manually record experimental backup data as explained in the following steps:

a. Keep periodic manual records of times and gas pressures during the scan for backup of the electronic record—keep manual records of the ignition time and of the opening and closing times of the SS sample bottles 1A and 1B

b. Use the DASU to record about 30 min of gas pressure data during the test at a rate of approximately one reading each 0.1 second

c. Wear all required PPE including gloves to protect against electrical shock

d. Any gas escape from the system will be minimal—the initial positive gas pressure spike that develops inside the hermetically sealed RTF immediately after pyrotechnic ignition should be limited to about 3 atmospheres of pressure—that gas pressure should rapidly decline below 1 atmosphere of pressure as the evolved H_2 reacts with the O_2 and the rapidly cooling $Zr/BaCrO_4$ pyrotechnic powder based heat paper ash

e. Turn on the 120 V 1 A Power supply set to 0.0 V

f. Charge the 1000 microfarad 100 V capacitor to 85 V

i. Double check that capacitor polarity is correct

ii. Use charging lead of capacitor

iii. Use power supply 10 volt and 1 volt increment buttons

g. Set up timer application on computer as a reference to manually record backup pressure-time readings and any unexpected events during the electronic scan

h. Check that BVHC and BVEXP are open with DCM properly zeroed and check that BVTee, BVRTF, and BV1A are closed—check that vacuum fore pump noise is nearly inaudible for at least 2 min

i. Check that the SS sample bottle BV1B is both closed and evacuated for sample collection

j. Zero the DCM pressure reading with a small screwdriver if necessary

k. Close BVHC and manually record the time of closing of BVHC

l. Start the scan that will monitor the output voltage on the DASU and manually record the scan start time from the timer application on the computer

m. Ignite the powder in the RTF by discharging the capacitor charged to 85 V across the match leads, preferably within about 20 s after starting the scan

n. The DASU voltage will remain near zero until BVRTF is opened

o. Open BVRTF between approximately 5 to 5.5 min after pyrotechnic ignition—remember to take periodic manual pressure-time readings as backup data during the scan, especially after opening BVRTF

p. After opening BVRTF watch the pressure rise on the DASU—if the pressure is increasing slowly wait as long as 60 s before opening BV1A (bellows valve to sample bottle 1A)—leave BV1A open for 10 to 20 s to allow gas pressures to equilibrate, then close BV1A—make manual notes of the times and gas pressures when BV1A is opened and closed

q. Remove sample bottle 1A and replace with it sample bottle 1B at the quick connect valve sometime before approximately 15 min after pyrotechnic ignition—make a manual note of the time of replacement because momentary small pressure changes from the quick connect valve operations will be present on the DASU time-pressure record to serve as time and pressure backup data

r. Open and close BV1B (bellows valve to sample bottle 1B) about 20 ± 2 min after ignition of the pyrotechnic powders—leave BV1B open for 10 to 20 s to allow gas pressures to equilibrate, then close BV1B—make manual notes of the times and pressures when BV1B is opened and closed

s. Allow the system to run with the BV1B closed for approximately 120 s to check for pressure changes

t. Open BVTee after the pressure increase check to let the gas remaining in the GHS expand into the 500-ml Erlenmeyer flask in order to check for the presence of water vapor

u. Stop the scan about 30 ± 2 min after pyrotechnic powder ignition

v. Continue to take manual gas pressure readings intermittently over the next few hours as appropriate to help monitor and understand unexpected gas pressure changes in the RTF

12) Place the digital data from the electronic scan onto a CD for later analysis

13) Continue the gas analysis and postmortem tests as appropriate—consult with your supervisor if you have questions

HAZARDOUS WASTE ADDENDUM

The hazardous waste barrel labels should list all hazardous materials inside the barrel. The labels on the hazardous waste barrel should include the words "Hazardous Waste", "Toxic", "Hexavalent Chromium", "Heat Paper", 'Zirconium", and "Barium Chromate". Once a month check that the hazardous waste barrel has excess water to ensure that sufficient water is present so that no heat paper (or any other pyrotechnic material) is in contact with combustible materials. Recycle the hazardous waste drum by coordinating with the HAZMAT team at least quarterly (every 3 months). The hazardous waste drum must have a 55 gallon capacity or less.

NICHROME WIRE MATCH ADDENDUM

The spotwelder used to make the matches had intuitive programmable controls to control the amount of electrical power applied to dual spotweld pulses on a percentage basis of the full pulse power available. Instructions in this addendum are for that spotwelder, but can be adapted to other spotwelder models as appropriate.

The nichrome wire match consists of a short length of nichrome wire spotwelded between two nickel ribbons. The match does not use any materials other than nickel and nichrome and delivers only negligible quantities of evolved gas.

The match is best made on a clean SS sheet that serves as an uncontaminated work area using clean SS cylinders that serve as hand rollers. Use one of the SS hand rollers to roll the nickel ribbons flat on the SS sheet before spotwelding. Do not place any electrical insulation on the nickel ribbons until after the match is hermetically sealed within the RTF in order to avoid gas leaks from the RTF. The match uses a 1000 microfarad capacitor that has been charged to 85 volts to ignite the pyrotechnic materials.

NICHROME WIRE MATCH CONSTRUCTION GUIDE CHECKLIST ADDENDUM:

1. Cut two nickel ribbons, each ribbon nominally 4.5 inches long by 0.100 inches wide by 0.003 inches thick and roll both ribbons flat on the clean SS sheet using a dry, clean SS cylindrical roller as described—use gloves, Accuwipes, and/or finger cots to prevent contaminating the SS sheet, SS rollers, and nickel ribbons with oil from your hands
2. The length of bare nichrome wire between the two nickel ribbons in your finished match should be nominally 0.3 to 0.5 inches
3. At one end of one of the nickel ribbons place the end of a nichrome wire of 0.003 inch diameter so that the nichrome wire overlaps the top surface end of the nickel ribbon by approximately 0.3 inches and the nichrome wire protrudes at least 0.6 inches past the end of the top surface of the nickel ribbon
4. The nichrome wire should be roughly centered between the two edges of the nickel ribbon
5. Starting at the nichrome wire end of the nichrome wire-nickel ribbon overlap begin spotwelding using dual spotwelder settings of 1.5% and 4%
6. Spotweld 6 to 10 times at the 1.5% and 4% setting from the end of the nichrome wire for a nominal distance of 0.2 inches down the length of the nichrome wire leaving the last nominal 0.1 inch of the nichrome wire-nickel ribbon overlap free of spotwelds—these are low power setting spot welds designed to tack weld the nichrome wire into place
7. Set the spotwelder to 4% and 10% and spotweld the same nichrome wire 4 to 6 times from the end to the nichrome wire for a distance of about 0.1 inches—at the very end of the nichrome wire these higher settings will be applied to portions of the nichrome wire already partially flattened with the tack spotwelds, which will help provide mechanical strength to the nichrome wire spotwelds without electrically cutting the nichrome wire—for the second nominal 0.1 inch the nichrome wire will remain tackwelded to the nickel ribbon at the lower setting—for the last nominal distance of 0.1 inch to the end of the nickel ribbon there will be no spotwelds
8. If you want the nichrome wire length between the two nickel ribbons in the finished match to be nominally 0.3 inches, cut the nichrome wire you just spotwelded onto the nickel ribbon so that

the nichrome wire protrudes nominally 0.6 inches past the end of the nickel ribbon

9. Grip the spotwelded nickel ribbon at the spotwelded end of the nichrome wire with forceps and bend the long end of the spotwelded nickel ribbon straight back over the top surface of the spotwelded nichrome wire
10. Grip the spotwelded nickel ribbon with forceps at the outer end of the spotwelded nickel ribbon at the fold just made and bend the long end of the spotwelded nickel ribbon straight back over the folded end of the nickel ribbon so that there are three layers of nickel ribbon all nominally 0.3 inches long with the bare 0.003-inch diameter nichrome wire protruding at least 0.6 inches past the triply folded nickel ribbon
11. Clamp the three nickel ribbon layers together with clean, dry pliers or an equivalent clean, dry metal hand crimping tool
12. Spotweld the triply folded nickel ribbon area 6 to 8 times at the ribbon edges and corners using spotweld settings of 11% and 22% —be careful not to spotweld directly on top of the 0.003-inch nichrome wire to avoid electrically cutting the nichrome wire
13. Repeat steps 1 through 12 with the second nickel ribbon starting at the end of the 0.003-inch diameter nichrome wire now protruding 0.6 inches from the triply folded nickel ribbon spotweld area
14. When finished the length of the bare 0.003-inch diameter nichrome wire between the two triply folded nickel ribbon ends should be nominally 0.3 inches
15. Measure the resistance of the finished match at the outer ends of the nickel ribbons (should be nominally 4.5 ohms)
16. Weigh the finished match
17. Check the match resistance immediately after hermetically sealing the test powders inside the RTF to ensure that the nichrome wire is intact and that the match is not touching the RTF case or lid internally—nominal match resistance should remain unchanged
18. The match can be ignited using the supplied 1000 microfarad capacitor that has been charged to 85 V
19. Adjust the spotweld settings as required to accommodate changes in the spotwelder itself over time or in the nickel ribbons and nichrome wires that may occur during any specific spotweld process

SILICONE RUBBER GASKET (SRG) ADDENDUM

There are six SRGs between the SS RTF bottom cylinder and the SS RTF lid. All of the SRGs will be die cut from red silicone rubber sheet nominally 0.03125 inches thick. Starting from the top of the RTF bottom cylinder in sequence:

1. Two gaskets both 2 3/16 inch OD by 31/32 inch ID
2. One gasket 2 3/16 inch OD with two holes nominally 5/32 inch diameter roughly centered and spaced approximately 0.070 inches apart for nichrome wire match leads
3. Match leads through here (third SRG from SS RTF bottom cylinder) —match leads protrude 3 to 4 inches past ODs of SRGs on the top surface of the third SRG—nichrome wire match and heat paper rectangle are directly below the bottom surface of the third SRG
4. Three blank gaskets each 2 3/16 inch OD
5. RTF SS Lid with six holes for 6-32 SS screws (0.325 inch thick)

Appendix E. Gas Quantity Calculations for 2017–2019 (HPST8 and HPST9 Examples)

The HPST8 experiment was the most effective experiment done in 2017. The HPST8 reusable test fixture (RTF) was isolated from the GHS using an SS bellows valve (BVRTF). The HPST8 RTF and gas handling system (GHS) are shown in Fig. 3 of the main report. The HPST8 zirconium (Zr)/barium chromate ($BaCrO_4$) pyrotechnic powder based heat paper was intimately mixed with the added $BaCrO_4$ powder. The HPST8 experiment done in 2017 used 1.134-g Zr/$BaCrO_4$ pyrotechnic powder-based heat paper with 0.6509-g $BaCrO_4$ with an improved GHS for H_2 gas removal. Data calculation quantities and the numbers used for the HPST8 gas evolution and removal experiment are shown in Tables E-1 and E-2.

Table E-1 Gas quantity calculations for HPST8 (numbers used and calculated)

	A	B	C
1	HPST8 Gas Evolution Calculation Details		
2	Measurement accuracies and rounding errors in these calculations were ignored for mathematical convenience and are addressed as required in the report		
3	1.134	g	LCCMFTHP mass
4	0.734832	g	$BaCrO_4$ mass in LCCMFTHP
5	0.285768	g	Zr mass in LCCMFTHP
6	0.1134	g	Glass fiber mass in LCCMFTHP
7	1.134	g	Check of HPST8 LCCMFTHP total mass
8	4.5	g/cc	Density of $BaCrO_4$
9	0.163296	cc	Volume of $BaCrO_4$ in heat paper
10	6.52	g/cc	Density of Zr
11	0.043829448	cc	Volume of Zr in heat paper
12	2.196	g/cc	Density of glass (silicon dioxide [vitreous])
13	0.051639344	cc	Volume of glass fiber in heat paper
14	0.6509	g	Extra mass $BaCrO_4$ added
15	0.144644444	cc	Volume of extra $BaCrO_4$ added
16	0.1	g	Estimated mass of nickel ribbon inside RTF
17	8.90	g/cc	Density of nickel
18	0.011235955	cc	Estimated volume of nickel inside RTF
19	0.414645192	cc	Estimated total solid volume of all ash components + nickel ribbon inside HPST8 RTF
20	10	cc	SS Sample bottle volume – manufacturer's specification ± 10 %
21	. . .	. . .	DCM volumes were all measured relative to a designated 10 cc sample bottle attached to a bellows valve (BVSB) with SS gas fittings and tubing
22	. . .	. . .	The DCM volume values were ultimately confirmed by water weight of the 500-ml Erlenmeyer flask combined with calculated volume of the 42-inch-long butyl rubber connecting tube to the Erlenmeyer flask (590 cc) to an estimated accuracy of ± 5 %
23	. . .	. . .	The DCM measurement for that 590 cc volume was 455.7237 cc
24	. . .	. . .	The correction factor ratio used for all DCM measurements was 590/455.7237 = 1.294644 cc

Table E-1 Gas quantity calculations for HPST8 (numbers used and calculated) (continued)

	A	B	C
25	1.294644101	DCM factor	The internal volume of the 10 cc sample bottle plus the SS tubing up to the closed BVSB used was 12.94644 cc
26	12.94644101	cc	DCM corrected sample bottle plus SS tubing to closed BVRTF volume from ideal gas law and calculations – standard volume used for calculations HPST5 through HPST8 experiments – (estimated accuracy ± 5 %)
27	. . .	. . .	Estimated accuracy of all GHS volumes measured using the DCM factor is ± 5 %
28	. . .	. . .	. . .
29	26.92613748	cc	DCM corrected empty RTF volume plus two 0.5 micron filters plus RTF side of BVRTF volume
30	14.56435775	cc	DCM corrected volume of small GHS plus 36-inch copper tubing for HPST8
31	590	cc	Estimated true volume of Erlenmeyer flask plus butyl tube (water weight and calculation) to ± 5 % accuracy
32	273.15	°K	273.15 °K = 0 °C = standard temperature for ideal gas
33	24.5	°C	Average ambient temperature during HPST8 experiment
34	760	torr	760 torr = 760 mm mercury = one standard atmosphere of pressure for ideal gas
35	108.27949	torr	Gas pressure when sample bottle HPST8 was closed 106.201 s after RTF was opened
36	77.00999	torr	Gas pressure sample bottle when HPST8a was closed 856.201 s after RTF was opened
37	74.89934	torr	Gas pressure at 1149.4 s after the RTF was opened just before opening BVTee
38	13.35784	torr	Gas pressure at end of electronically recorded portion of HPST8 test 1722.4 s after RTF was opened
39			RTF was opened 198.797 s after scan start by electronic record
40			Manually recorded ignition time occurred 10 s after scan start
41	1000	torr	Maximum DCM transducer pressure rating for HPST8 experiment
42	1.315789474	atm	Maximum DCM transducer pressure rating for HPST8 measured in atmospheres
43	22.38934123	torr	Vapor pressure of water at 24 °C torr
44	23.76945472	torr	Vapor pressure of water at 25 °C torr
45	20.7917	std atm cc/g	Total HPST5 gas evolved (one SB + GHS – ash + RTF) measured at 41.8 s/g of heat paper
46	20.4227	std atm cc/g	Total HPST5 gas evolved (both SB + GHS – ash + RTF) before gas expansion measured at 794.8 s/g of heat paper
47	54.02229105	cc	Estimated total volume of GHS + RTF + SB with tubing and all ash+Ni ribbon inside HPST8
48	7.063190596	std atm cc	Total HPST8 gas in GHS+RTF containing ash+SB with tubing to BVRTF Volume 106.201 s after RTF was opened
49	6.228563136	std atm cc/g	Total HPST8 gas in GHS+RTF containing ash+SB with tubing to BVRTF Volume 106.201 s after RTF was opened/g of heat paper
50	1.692693491	std atm cc	Total HPST8 gas in SB1 plus tubing up to BVRTF when BVSB closed at 106.201 s after RTF was opened

Table E-1 Gas quantity calculations for HPST8 (numbers used and calculated) (continued)

	A	B	C
51	5.023446612	std atm cc	Total gas SB2+system when SB2 closed at 856.201 s after RTF opened
52	1.203868884	std atm cc	Total gas in SB2 when closed at 856.201 s
53	6.716140103	std atm cc	Total gas in both SB, GHS and RTF when SB2 closed at 856.201 s after RTF opened
54	5.922522137	std atm cc/g	Total HPST8 gas evolved per gram of heat paper at 856.201 s after RTF opened
55	3.714892716	std atm cc/g	Total gas in GHS and RTF with both sample bottles closed just before opening BVTee at 1149.4 s after RTF opened
56	10.17886897	std atm cc	Total gas in GHS and RTF with both sample bottles closed after opening BVTee at electronic scan end 1722.4 s after RTF opened
57	6.463976253	std atm cc	Total apparent liquid water expressed as vapor at end of electronic scan 1722.4 s after BVRTF was opened from gas that was left in GHS and RTF
58	5.700155426	std atm cc/g	Total apparent liquid water evolved expressed as vapor/g of heat paper
59	54.43693624	cc	Empty GHS+RTF+SB1 (no ash present)
60	0.2513		Fraction of H_2 gas in sample bottle SB1 (Table 3 of main report)
61	0.2612		Fraction of H_2 gas in sample bottle SB2 (Table 3 of main report)
62	1.565237916	std atm cc/g	Total H_2 gas present per gram of heat paper when SB1 was closed at 106.201 s after RTF opened
62	1.532185299	std atm cc/g	Total H_2 gas present per gram of heat paper when SB2 was closed at 856.201 s after RTF opened
64	. . .	. . .	. . .
65	. . .	. . .	HPST8 Water Vapor Details
66	. . .	. . .	Since liquid water was present when the RTF was opened at 856.201 s after ignition the entire volume of the GHS+RTF including the two sample bottles
67	. . .	. . .	must have been saturated with water vapor at the experimental temperature of 24.5 °C
68	66.96873206	cc	Volume of GHS+RTF-ash+2 SB
69	23.07939798	torr	Vapor pressure of water at 24.5 °C
70	1.866286344	std atm cc	Estimated total water vapor present in entire system including both sample bottles before BVTee is opened when liquid water is present
71	8.330262597	cc	Estimated total evolved water (water vapor before BVTee is opened plus apparent liquid water measured at end of electronic scan)
72	0.36079175	std atm cc	Total water vapor possible in 12.94644 cc SB plus tubing to closed BVRTF at 24.5 °C
73	. . .	. . .	. . .
74	. . .	. . .	HPST8 Total Volume of All Gases When SB1 Was Closed (H_2, O_2, N_2, CO, CH_4, CO_2)
75	23.5777878	std atm cc	Total gas that HPST8 heat paper would evolve based on the HPST5 gas evolution rate at time SB1 closed if no added $BaCrO_4$ were present

Table E-1 Gas quantity calculations for HPST8 (numbers used and calculated) (continued)

	A	B	C
76	7.063190596	std atm cc	Total gas that HPST8 heat paper actually did evolve at time SB1 was closed
77	16.5145972	std atm cc	Total gas removed by 0.6509 g $BaCrO_4$
78	25.37194224	std atm cc/g	Total gas removed/g of $BaCrO_4$ when SB1 was closed based on HPST5 gas generation rate

The cell numbers used to calculate the gas quantities in Table E-1 are shown in Table E-2.

Table E-2 Gas quantity calculations for HPST8 (cell numbers and formulas for calculations)

	A	B	C
1	HPST8 Gas Evolution Calculation Details		
2	Measurement accuracies and rounding errors in these calculations were ignored for mathematical convenience and are addressed as required in the report		
3	1.134	g	LCCMFTHP mass
4	=A3*0.72*0.9	g	$BaCrO_4$ mass in LCCMFTHP
5	=A3*0.28*0.9	g	Zr mass in LCCMFTHP
6	=A3*0.1	g	Glass fiber mass in LCCMFTHP
7	=A4+A5+A6	g	Check of HPST8 LCCMFTHP total mass
8	4.5	g/cc	Density of $BaCrO_4$
9	=A4/A8	cc	Volume of $BaCrO_4$ in heat paper
10	6.52	g/cc	Density of Zr
11	=A5/A10	cc	Volume of Zr in heat paper
12	2.196	g/cc	Density of glass (silicon dioxide [vitreous])
13	=A6/A12	cc	Volume of glass fiber in heat paper
14	0.6509	g	Extra mass $BaCrO_4$ added
15	=A14/A8	cc	Volume of extra $BaCrO_4$ added
16	0.1	g	Estimated mass of nickel ribbon inside RTF
17	8.90	g/cc	Density of nickel
18	=A16/A17	cc	Estimated volume of nickel inside RTF
19	=A9+A11+A13+A15+A18	cc	Estimated total solid volume of all ash components + nickel ribbon inside HPST8 RTF
20	=10	cc	SS Sample bottle volume – manufacturer's specification ± 10 %

Table E-2 Gas quantity calculations for HPST8 (cell numbers and formulas for calculations) (continued)

	A	B	C
21	. . .	. . .	DCM volumes were all measured relative to a designated 10 cc sample bottle attached to a bellows valve (BVSB) with SS gas fittings and tubing
22	. . .	. . .	The DCM volume values were ultimately confirmed by water weight of the 500 ml Erlenmeyer flask combined with calculated volume of the 42-inch long butyl rubber connecting tube to the Erlenmeyer flask (590 cc) to an estimated accuracy of ± 5 %
23	. . .	. . .	The DCM measurement for that 590 cc volume was 455.7237 cc
24	. . .	. . .	The correction factor ratio used for all DCM measurements was 590/455.7237 = 1.294644 cc
25	=590/455.7237	DCM Factor	The internal volume of the 10 cc sample bottle plus the SS tubing up to the closed BVSB used was 12.94644 cc
26	=A20*A25	cc	DCM corrected sample bottle plus SS tubing to closed BVRTF volume from ideal gas law and calculations – standard volume used for calculations HPST5 through HPST8 experiments – (estimated accuracy ± 5 %)
27	. . .	. . .	Estimated accuracy of all GHS volumes measured using the DCM factor is ± 5 %
28	. . .	. . .	. . .
29	=20.7981*A25	cc	DCM corrected empty RTF volume plus two 0.5 micron filters plus RTF side of BVRTF volume
30	=11.2947*A25	cc	DCM corrected volume of small GHS plus 36-inch copper tubing for HPST8
31	590	cc	Estimated true volume of Erlenmeyer flask plus butyl tube (water weight and calculation) to ± 5 % accuracy
32	273.15	°K	273.15 °K = 0 °C = standard temperature for ideal gas
33	24.5	°C	Average ambient temperature during HPST8 experiment
34	760	torr	760 torr = 760 mm mercury = one standard atmosphere of pressure for ideal gas
35	108.27949	torr	Gas pressure when sample bottle HPST8 was closed 106.201 s after RTF was opened
36	77.00999	torr	Gas pressure sample bottle when HPST8a was closed 856.201 s after RTF was opened
37	74.89934	torr	Gas pressure at 1149.4 s after the RTF was opened just before opening BVTee
38	13.35784	torr	Gas pressure at end of electronically recorded portion of HPST8 test 1722.4 s after RTF was opened
39	. . .	. . .	RTF was opened 198.797 s after scan start by electronic record
40	. . .	. . .	Manually recorded ignition time occurred 10 s after scan start

Table E-2 Gas quantity calculations for HPST8 (cell numbers and formulas for calculations) (continued)

	A	B	C
41	1000	torr	Maximum DCM transducer pressure rating for HPST8 experiment
42	=A41/A34	atm	Maximum DCM transducer pressure rating for HPST8 measured in atmospheres
43	22.3893412287195	torr	Vapor pressure of water at 24 °C torr
44	23.7694547248951	torr	Vapor pressure of water at 25 °C torr
45	20.7917	std atm cc/g	Total HPST5 gas evolved (one SB + GHS – ash + RTF) measured at 41.8 s/g of heat paper
46	20.4227	std atm cc/g	Total HPST5 gas evolved (both SB + GHS – ash + RTF) before gas expansion measured at 794.8 s/g of heat paper
47	=A29+A30+A26-A19	cc	Estimated total volume of GHS + RTF + SB with tubing and all ash+Ni ribbon inside HPST8
48	=A47*A35*A32/((A32+A33)*A34)	std atm cc	Total HPST8 gas in GHS+RTF containing ash+SB with tubing to BVRTF volume 106.201 s after RTF was opened
49	=A48/A7	std atm cc/g	Total HPST8 gas in GHS+RTF containing ash+SB with tubing to BVRTF volume 106.201 s after RTF was opened/g of heat paper
50	=A26*A35*A32/((A32+A33)*A34)	std atm cc	Total HPST8 gas in SB1 plus tubing up to BVRTF when BVSB closed at 106.201 s after RTF was opened
51	=A47*A36*A32/((A32+A33)*A34)	std atm cc	Total gas SB2+system when SB2 closed at 856.201 s after RTF opened
52	=A26*A36*A32/((A32+A33)*A34)	std atm cc	Total gas in SB2 when closed at 856.201 s
53	=A50+A51	std atm cc	Total gas in both SB, GHS and RTF when SB2 closed at 856.201 s after RTF opened
54	=A53/A7	std atm cc/g	Total HPST8 gas evolved per gram of heat paper at 856.201 s after RTF opened
55	=(A47-A26)*A37*A32/((A32+A33)*A34)	std atm cc/g	Total gas in GHS and RTF with both sample bottles closed just before opening BVTee at 1149.4 s after RTF opened
56	=(A47-A26+A31)*A38*A32/((A32+A33)*A34)	std atm cc	Total gas in GHS and RTF with both sample bottles closed after opening BVTee at electronic scan end 1722.4 s after RTF opened
57	=A56-A55	std atm cc	Total apparent liquid water expressed as vapor at end of electronic scan 1722.4 s after BVRTF was opened from gas that was left in GHS and RTF
58	=A57/A7	std atm cc/g	Total apparent liquid water evolved expressed as vapor/g of heat paper
59	=A47+A19	cc	Empty GHS+RTF+SB1 (no ash present)
60	0.2513	. . .	Fraction of H_2 gas in sample bottle SB1 (Table 3 of main report)
61	0.2612	. . .	Fraction of H_2 gas in sample bottle SB2 (Table 3 of main report)

Table E-2 Gas quantity calculations for HPST8 (cell numbers and formulas for calculations) (continued)

	A	B	C
62	=(A49*A60)	std atm cc/g	Total H_2 gas present per gram of heat paper when SB1 was closed at 106.201 s after RTF opened
62	=(A50*A60+A51*A61)/A7	std atm cc/g	Total H_2 gas present per gram of heat paper when SB2 was closed at 856.201 s after RTF opened
64	. . .	. . .	. . .
65	. . .	. . .	HPST8 Water Vapor Details
66	. . .	. . .	Since liquid water was present when the RTF was opened at 856.201 s after ignition the entire volume of the GHS+RTF including the two sample bottles
67	. . .	. . .	must have been saturated with water vapor at the experimental temperature of 24.5 °C
68	=A47+A26	cc	Volume of GHS+RTF-ash+2 SB
69	=(A43+A44)/2	torr	Vapor pressure of water at 24.5 °C
70	=A68*A69*A32/((A32+A33)*A34)	std atm cc	Estimated total water vapor present in entire system including both sample bottles before BVTee is opened when liquid water is present
71	=A57+A70	cc	Estimated total evolved water (water vapor before BVTee is opened plus apparent liquid water measured at end of electronic scan)
72	=A26*A32*A69/((A32+A33)*A34)	std atm cc	Total water vapor possible in 12.94644 cc SB plus tubing to closed BVRTF at 24.5 °C
73	. . .	. . .	. . .
74	. . .	. . .	HPST8 Total Volume of All Gases When SB1 Was Closed (H_2, O_2, N_2, CO, CH_4, CO_2)
75	=A7*A45	std atm cc	Total gas that HPST8 heat paper would evolve based on the HPST5 gas evolution rate at time SB1 closed if no added $BaCrO_4$ were present
76	=A48	std atm cc	Total gas that HPST8 heat paper actually did evolve at time SB1 was closed
77	=A75-A76	std atm cc	Total gas removed by 0.6509 g $BaCrO_4$
78	=A77/A14	std atm cc/g	Total gas removed/g of $BaCrO_4$ when SB1 was closed based on HPST5 gas generation rate

Data calculation quantities and the numbers used for the HPST9 gas evolution and removal experiment are shown in Tables E-3 and E-4.

The HPST9 experiment done in 2019 was built as identically as possible to the HPST8 experiment, except that 1.134 g of heat paper and 0.756 g of $BaCrO_4$ were used with 26.05 std-atm-cc of O_2 hermetically sealed into the RTF following pyrotechnic ignition until 208 s after the start of the scan. *All* of the evolved H_2 gas as measured by the GC was removed in the HPST9 experiment.

Table E-3 Gas quantity calculations for HPST9 (numbers used and calculated)

	A	B	C
1	HPST9 gas evolution calculation details		
2	Measurement accuracies and rounding errors in these calculations were ignored for mathematical convenience and are addressed as required in the report		
3	0.1	g	Estimated nickel lead mass inside RTF
4	8.9	g/cc	Density of nickel
5	0.011236	cc	Estimated nickel lead volume inside RTF
6	. . .	. . .	. . .
7	1.134	g	Mass of LCCMFTHP
8	0.734832	g	Mass of $BaCrO_4$ in LCCMFTHP
9	0.285768	g	Mass of Zr in LCCMFTHP
10	0.1134	g	Mass of glass fiber in LCCMFTHP
11	1.134	g	Check of LCCMFTHP total mass
12	. . .	. . .	. . .
13	4.5	g/cc	Density of $BaCrO_4$
14	0.163296	cc	Volume of $BaCrO_4$ in heat paper
15	6.52	g/cc	Density of Zr
16	0.043829448	cc	Volume of Zr in heat paper
17	2.196	g/cc	Density of glass fiber in heat paper (silicon dioxide (vitreous))
18	0.051639344	cc	Volume of glass fiber in heat paper in heat paper
19	0.756	g	Mass of extra $BaCrO_4$ added
20	0.168	cc	Volume of extra $BaCrO_4$ added
21	0.438000747	cc	Estimated total solid volume of all ash components and nickel match leads inside HPST9 RTF
22	. . .	. . .	. . .
23	20.7981	cc	RTF DCM volume
24	11.2497	cc	DCM volume of small GHS plus 36-inch copper tubing for HPST8 and HPST9
25	10	cc	Sample bottle volume – manufacturer's value ± 10 %
26	12.94644101	cc	Measured volume of sample bottle + tubing + BVSB
27	273.15	K	273.15 K = 0 C = standard temperature for ideal gas
28	197.27395	torr	Gas pressure when sample bottle HPST9 was closed 270 s after scan start and 62 s after RTF was opened
29	1.65	ratio	Previously measured gas pressure reduction ratio when opening SB to make GC measurement

Table E-3 Gas quantity calculations for HPST9 (numbers used and calculated) (continued)

	A	B	C
30	119.5599697	torr	Expected HPST9 SB gas pressure to be seen at GC
31	111.15	torr	HPST9 gas pressure at GC when run started (decreased from 127 torr originally in about 15 min and then held steady for hours)
32	9.45	°C	Average ambient temperature of HPST9 experiment
33	760	torr	Standard atmospheric pressure
34	184.97143	torr	Gas pressure when sample bottle HPST9a was closed ~1030 s after scan start and ~822 s after RTF opened
35	112.103897	torr	Expected HPST9a SB gas pressure to be seen at GC
36	101.9	torr	HPST9a gas pressure at GC when run started (decreased from 115.3 torr in about 12 min and then held steady for hours)
37	184.76181	torr	Gas pressure just before BVTee opened at 1333.797 s after scan started
38	13.11931	torr	Gas pressure at end of scan 1927.396 s after scan started
39	590	cc	Measured volume of Erlenmeyer flask plus butyl tube
40	. . .	. . .	. . .
41	23.76945472	torr	Vapor pressure of water at 25 ºC
42	8.612208241	torr	Vapor pressure of water at 9 ºC
43	9.211507525	torr	Vapor pressure of water at 10 ºC
44	8.881892919	torr	Vapor pressure of water at 9.45 ºC
45	. . .	. . .	. . .
46	20.79174395	std atm cc/g	Total volume of HPST5 gas per gram of heat paper previously measured at 41.8 s after ignition
47	. . .	. . .	. . .
48	. . .	. . .	. . .
49	0.438000747	cc	Estimated total solid volume of all ash+nickel ribbon inside HPST9 RTF
50	53.99893549	cc	Volume of GHS+RTF-ash+SB1 for HPST9
51	1.294644101	DCM factor inc.	DCM factor increase (590/455.7237 = true volume of Erlenmeyer flask plus butyl tubing divided by DCM measured volume)
52	. . .	. . .	. . .
53	13.54785045	std atm cc	Total HPST9 gas SB1+GHS+RTF when SB1 closed at 62 s after RTF opened (62+208 = 270 s after scan start) – includes some added O_2

Table E-3 Gas quantity calculations for HPST9 (numbers used and calculated) (continued)

	A	B	C
54	11.94695807	std atm cc/g	Total HPST9 gas SB1+GHS+RTF per gram of heat paper when SB1 closed at ~270 s after scan start – includes some added O_2
55	3.248146378	std atm cc	Total HPST9 gas in SB1 + tubing to BVSB when closed at ~270 s after scan start– includes some added O_2
56	12.70297103	std atm cc	Total HPST9 gas SB2+GHS+RTF when SB2 closed at ~1030 s after scan started and ~822 s after RTF opened – includes some added O_2 and some added air
57	3.045583466	std atm cc	Total HPST9 gas in SB2 + tubing to BVSB when SB2 closed at ~822 s after RTF opened – includes some added O_2 and some added air
58	15.95111741	std atm cc	Total HPST9 gas in both SBs and system when SB2 closed ~1030 s after scan started and ~ 822 s after RTF opened – includes some added O_2 and some added air
59	14.0662411	std atm cc/g	Total HPST9 gas evolved per gram of LCCMFTHP at ~ 1030 s after scan started and ~822 s after RTF opened – includes some added O_2 and some added air
60	9.646443269	std atm cc	Total gas in HPST9 GHS and RTF with both sample bottles closed just before opening BVTee at 1333.797 s after scan started – includes some added O_2 and some added air
61	9.657387562	std atm cc	Total gas in HPST9 GHS and RTF with both sample bottles closed just before opening BVTee at 1333.797 s after scan started – alternate calculation method – includes some added O_2 and some added air
62	. . .	. . .	. . .
63	2.403266954	std atm cc	Rough estimate of air quantity that leaked into system when adding SB2 (HPST9a) ~298 s after scan start
64	. . .	. . .	. . .
65	. . .	. . .	Note that the final amount of gas in HPST9 is high because of the added O_2 and because of difficulties with the quick connect valve when HPST9a was attached to the GHS ~298 s after scan started
66	. . .	. . .	Note that no significant amount of gas leaked into or from the GHS until the addition of the second sample bottle at ~298 s after scan start

Table E-3 Gas quantity calculations for HPST9 (numbers used and calculated) (continued)

	A	B	C
67	10.52911665	std atm cc	Total gas in GHS and RTF excluding both sample bottles after opening BVTee at electronic scan end 1927.396 s after scan start – includes some added O_2 and some added air
68	0.882673379	std atm cc	Total apparent liquid water measured at end of electronic scan at 1927.396 s from gas that was left in GHS and RTF expressed as vapor
69	0.778371587	std atm cc/g	Total apparent liquid water measured at end of electronic scan at 1927.396 s from gas that was left in GHS and RTF expressed as vapor/g of heat paper
70	54.43693624	cc	Volume of empty GHS+RTF+SB1 (no ash present)
71	0	std atm cc/g	Total H_2 gas present per gram of heat paper when SB1 was closed ~270 s after scan start
72	0	std atm cc/g	Total H_2 gas present per gram of heat paper when SB2 was closed ~1030 s after scan start
73	. . .	. . .	. . .
74	. . .	. . .	If liquid water were present when the RTF was opened at ~1030 s after scan start the entire volume of the GHS+RTF must have been saturated with water vapor
75	. . .	. . .	at the experimental temperature of 9.45 °C – the two sample bottle gas atmospheres would also have been saturated
76	66.94537651	cc	Physical volume of GHS+RTF-ash+2 SB
77	8.881892919	torr	Vapor pressure of water at 9.45 °C
78	0.756208538	std atm cc	Estimated water vapor present in entire system including both sample bottles just before BVTee was opened at 9.45 °C
79	. . .	. . .	. . .
80	. . .	. . .	HPST9 RTF opening occurred 208 s after scan start
81	. . .	. . .	Manual records show HPST9 heat paper was ignited 3 s after scan start – no electronic records because BVRTF was closed during ignition
82	0.146241753	std atm cc	Total water vapor possible in 12.94644 cc SB+tubing+BV+quick connect valve body at 9.45° C
83	. . .	. . .	. . .
84	23.57783764	std atm cc	Total gas HPST9 heat paper would evolve based on HPST5 gas evolution rate if no added $BaCrO_4$ were present

Table E-3 Gas quantity calculations for HPST9 (numbers used and calculated) (continued)

	A	B	C
85	13.54785045	std atm cc	Total HPST9 gas actually present when SB1 closed at ~270 s after scan start (62 s after RTF opened) – includes some added O_2
86	12.70297	std atm cc	Total HPST9 gas actually present when SB2 closed at ~1030 s after scan start (822 s after RTF opened) – includes some added O_2 and some added air
87	10.87487	std atm cc	Total HPST9 gas removed by 0.756 g $BaCrO_4$ – may include some added O_2 and some added air
88	. . .	. . .	. . .
89	14.38474	std atm cc/g	Total HPST9 gas removed/g of $BaCrO_4$ based on HPST5 gas generation rate (more gas might have been removed but $BaCrO_4$ was present in excess–may include some added O_2 and some added air)

The cell numbers used to calculate the gas quantities in Table E-3 are shown in Table E-4.

Table E-4 Gas quantity calculations for HPST9 (cell numbers and formulas for calculations)

	A	B	C
1	HPST9 Gas Evolution Calculation Details		
2	Measurement accuracies and rounding errors in these calculations were ignored for mathematical convenience and are addressed as required in the report		
3	0.1	g	Estimated nickel lead mass inside RTF
4	8.9	g/cc	Density of nickel
5	=A3/A4	cc	Estimated nickel lead volume inside RTF
6	. . .	. . .	. . .
7	1.134	g	Mass of LCCMFTHP
8	=A7*0.72*0.9	g	Mass of $BaCrO_4$ in LCCMFTHP
9	=A7*0.28*0.9	g	Mass of Zr in LCCMFTHP
10	=A7*0.1	g	Mass of glass fiber in LCCMFTHP
11	=A8+A9+A10	g	Check of LCCMFTHP total mass
12	. . .	. . .	. . .
13	4.5	g/cc	Density of $BaCrO_4$
14	=A8/A13	cc	Volume of $BaCrO_4$ in heat paper
15	6.52	g/cc	Density of Zr
16	=A9/A15	cc	Volume of Zr in heat paper
17	2.196	g/cc	Density of glass fiber in heat paper (silicon dioxide [vitreous])

Table E-4 Gas quantity calculations for HPST9 (cell numbers and formulas for calculations) (continued)

	A	B	C
18	=A10/A17	cc	Volume of glass fiber in heat paper
19	0.756	g	Mass of extra $BaCrO_4$ added
20	=A19/A13	cc	Volume of extra $BaCrO_4$ added
21	=A5+A14+A16+A18+A20	cc	Estimated total solid volume of all ash components and nickel match leads inside HPST9 RTF
22	. . .	. . .	. . .
23	20.7981	cc	RTF DCM volume
24	11.2497	cc	DCM volume of small GHS plus 36-inch copper tubing for HPST8 and HPST9
25	10	cc	Sample bottle volume – manufacturer's value ± 10 %
26	=A25*A51	cc	Measured volume of sample bottle + tubing + BVSB
27	273.15	K	273.15 K = 0 C = standard temperature for ideal gas
28	197.27395	torr	Gas pressure when sample bottle HPST9 was closed 270 s after scan start and 62 s after RTF was opened
29	1.65	ratio	Previously measured gas pressure reduction ratio when opening SB to make GC measurement
30	=A28/A29	torr	Expected HPST9 SB gas pressure to be seen at GC
31	111.15	torr	HPST9 gas pressure at GC when run started (decreased from 127 torr originally in about 15 min and then held steady for hours)
32	9.45	°C	Average ambient temperature of HPST9 experiment
33	760	torr	Standard atmospheric pressure
34	184.97143	torr	Gas pressure when sample bottle HPST9a was closed ~1030 s after scan start and ~822 s after RTF opened
35	=A34/A29	torr	Expected HPST9a SB gas pressure to be seen at GC
36	101.9	torr	HPST9a gas pressure at GC when run started (decreased from 115.3 torr in about 12 min and then held steady for hours)
37	184.76181	torr	Gas pressure just before BVTee opened at 1333.797 s after scan started
38	13.11931	torr	Gas pressure at end of scan 1927.396 s after scan started
39	590	cc	Measured volume of Erlenmeyer flask plus butyl tube
40	. . .	. . .	. . .
41	23.7694547248951	torr	Vapor pressure of water at 25 ºC
42	8.61220824080928	torr	Vapor pressure of water at 9 ºC
43	9.21150752528991	torr	Vapor pressure of water at 10 ºC
44	8.88189291882556	torr	Vapor pressure of water at 9.45 ºC
45	. . .	. . .	. . .
46	20.7917439521277	std atm cc/g	Total volume of HPST5 gas per gram of heat paper previously measured at 41.8 s after ignition

Table E-4 Gas quantity calculations for HPST9 (cell numbers and formulas for calculations) (continued)

	A	B	C
47	. . .	. . .	. . .
48	. . .	. . .	. . .
49	=A21	cc	Estimated total solid volume of all ash+nickel ribbon inside HPST9 RTF
50	=(A23+A24+A25)*A51-A49	cc	Volume of GHS+RTF-ash+SB1 for HPST9
51	1.29464410123941	DCM factor inc.	DCM factor increase (590/455.7237 = true volume of Erlenmeyer flask plus butyl tubing divided by DCM measured volume)
52	. . .	. . .	. . .
53	=A50*A27*A28/((A32+A27)*A33)	std atm cc	Total HPST9 gas SB1+GHS+RTF when SB1 closed at 62 s after RTF opened (62+208 = 270 s after scan start) – includes some added O_2
54	=A53/A7	std atm cc/g	Total HPST9 gas SB1+GHS+RTF per gram of heat paper when SB1 closed at ~270 s after scan start – includes some added O_2
55	=A53*A26/A50	std atm cc	Total HPST9 gas in SB1 + tubing to BVSB when closed at ~270 s after scan start – includes some added O_2
56	=A50*A27*A34/((A32+A27)*A33)	std atm cc	Total HPST9 gas SB2+GHS+RTF when SB2 closed at ~1030 s after scan started and ~822 s after RTF opened – includes some added O_2 and some added air
57	=A56*A26/A50	std atm cc	Total HPST9 gas in SB2 + tubing to BVSB when SB2 closed at ~822 s after RTF opened – includes some added O_2 and some added air
58	=A55+A56	std atm cc	Total HPST9 gas in both SBs and system when SB2 closed ~1030 s after scan started and ~822 s after RTF opened – includes some added O_2 and some added air
59	=A58/A7	std atm cc/g	Total HPST9 gas evolved per gram of LCCMFTHP at ~1030 s after scan started and ~822 s after RTF opened – includes some added O_2 and some added air
60	=(A50-A26)*A27*A37/((A32+A27)*A33)	std atm cc	Total gas in HPST9 GHS and RTF with both sample bottles closed just before opening BVTee at 1333.797 s after scan started – includes some added O_2 and some added air
61	=A58-A55-A57	std atm cc	Total gas in HPST9 GHS and RTF with both sample bottles closed just before opening BVTee at 1333.797 s after scan started – alternate calculation method – includes some added O_2 and some added air
62	. . .	. . .	. . .
63	=A58-A53	std atm cc	Rough estimate of air quantity that leaked into system when adding SB2 (HPST9a) ~298 s after scan start
64	. . .	. . .	. . .

Table E-4 Gas quantity calculations for HPST9 (cell numbers and formulas for calculations) (continued)

	A	B	C
65	. . .	. . .	Note that the final amount of gas in HPST9 is high because of the added O_2 and because of difficulties with the quick connect valve when HPST9a was attached to the GHS ~298 s after scan started
66	. . .	. . .	Note that no significant amount of gas leaked into or from the GHS until the addition of the second sample bottle at ~298 s after scan start
67	=(A50-A26+A39)*A27*A38/((A32+A27)*A33)	std atm cc	Total gas in GHS and RTF excluding both sample bottles after opening BVTee at electronic scan end 1927.396 s after scan start – includes some added O_2 and some added air
68	=A67-A60	std atm cc	Total apparent liquid water measured at end of electronic scan at 1927.396 s from gas that was left in GHS and RTF expressed as vapor
69	=A68/A7	std atm cc/g	Total apparent liquid water measured at end of electronic scan at 1927.396 s from gas that was left in GHS and RTF expressed as vapor/g of heat paper
70	=(A23+A24+A25)*A51	cc	Volume of empty GHS+RTF+SB1 (no ash present)
71	0	std atm cc/g	Total H_2 gas present per gram of heat paper when SB1 was closed ~270 s after scan start
72	0	std atm cc/g	Total H_2 gas present per gram of heat paper when SB2 was closed ~1030 s after scan start
73	. . .	. . .	. . .
74	. . .	. . .	If liquid water were present when the RTF was opened at ~1030 s after scan start the entire volume of the GHS+RTF must have been saturated with water vapor
75	. . .	. . .	at the experimental temperature of 9.45 °C – the two sample bottle gas atmospheres would also have been saturated
76	=A50+A26	cc	Physical volume of GHS+RTF-ash+2 SB
77	=A44	torr	Vapor pressure of water at 9.45 °C
78	=A76*A77*A27/(A27+A32)/A33	std atm cc	Estimated water vapor present in entire system including both sample bottles just before BVTee was opened at 9.45 °C
79	. . .	. . .	. . .
80	. . .	. . .	HPST9 RTF opening occurred 208 s after scan start
81	. . .	. . .	Manual records show HPST9 heat paper was ignited 3 s after scan start – no electronic records because BVRTF was closed during ignition
82	=A26*A27*A44/((A32+A27)*A33)	std atm cc	Total water vapor possible in 12.94644 cc SB+tubing+BV+quick connect valve body at 9.45° C
83	. . .	. . .	. . .
84	=A11*A46	std atm cc	Total gas HPST9 heat paper would evolve based on HPST5 gas evolution rate if no added $BaCrO_4$ were present

Table E-4 Gas quantity calculations for HPST9 (cell numbers and formulas for calculations) (continued)

	A	B	C
85	=A53	std atm cc	Total HPST9 gas actually present when SB1 closed at ~270 s after scan start (62 s after RTF opened) – includes some added O_2
86	=A56	std atm cc	Total HPST9 gas actually present when SB2 closed at ~1030 s after scan start (822 s after RTF opened) – includes some added O_2 and some added air
87	=A84-A86	std atm cc	Total HPST9 gas removed by 0.756 g $BaCrO_4$ – may include some added O_2 and some added air
88	. . .	. . .	. . .
89	=A87/A19	std atm cc/g	Total HPST9 gas removed/g of $BaCrO_4$ based on HPST5 gas generation rate (more gas might have been removed but $BaCrO_4$ was present in excess – may include some added O_2 and some added air)

List of Symbols, Abbreviations, and Acronyms

ARL	Army Research Laboratory
Al	aluminum
atm	atmospheres of pressure
$BaCrO_4$	barium chromate
BaO	barium oxide
BV	bellows valve
BVEXP	bellows valve to experiment
BVRTF	bellows valve at RTF
BVSB	bellows valve for sample bottle
BVTee	bellows valve at TEE to Erlenmeyer flask
CD	compact disk
CO_2	carbon dioxide gas
CO	carbon monoxide gas
cc	cubic centimeters
CH_4	methane gas
DCM	dual capacitance manometer
DOD	Department of Defense
DOE	Department of Energy
GC	gas chromatograph
GHS	gas handling system
GPS	global positioning system
H_2	hydrogen gas
H_2O	water
Hg	mercury
HAZMAT	hazardous materials
Kr	krypton

LCCM	Low Cost Competent Munition
LCCMFTHP	LCCM flight test heat paper
Li	lithium
MANLOS	Man Portable Non Line of Sight
μ–m	1 micro–meter of mercury pressure (760000 μ–m = 1 std atm)
N_2	nitrogen gas
NSWC	Naval Surface Warfare Center
QC valve	Quick Connect valve
Pa	pascal (101325 Pa/atm)
PDR	power supply digital readout
PLOT	porous layer open tubular (gas capillary chromatographic column)
PPE	personal protective equipment
RPS	revolutions per second
RTF	reusable test fixture
SB	sample bottle
Si	silicon
SOP	Standing Operating Procedure
SRG	silicone rubber gasket
SS	stainless steel
TCD	thermal conductivity detector
TEE	“T” shaped metal connection for metal tubing
Torr	pressure exerted by column of Hg (760 Torr = 1 std atm)
UHP	ultra high purity
Xe	xenon
Zr	zirconium
$Zr/BaCrO_4$	zirconium/barium chromate pyrotechnic powder mixture

1 (PDF) DEFENSE TECHNICAL INFORMATION CTR DTIC OCA

1 (PDF) CCDC ARL FCDD RLD CL TECH LIB

1 (PDF) GOVT PRINTG OFC A MALHOTRA

1 (PDF) OMINTEK PARTNERS LLC J RASTEGAR

1 (PDF) USAF AFMC AFLCMC/EBS S RAYMAN

1 (PDF) USN NSWC CRANE ID (USA) S STUART

1 (PDF) USN NSWC CRD BDA MD C WINCHESTER

1 (PDF) DMCA (US) J BREEN

1 (PDF) USARMY JPEO AA V MATRISCIANO

1 (PDF) ACTIVE MATERIALS, LLC R KULLBERG

1 (PDF) USARMY RDECOM AMRDEC P TAYLOR

6 (PDF) US ARMY CCDC AC (USA) K AMABILE B ARMSTRONG G DE BENEDETTO R DRATLER C MCMULLAN A PERGOLIZZI

3 (PDF) OSD OUSD ATL (US) C CROSS C MICHIENZI J JOUET

4 (PDF) ADVANCED THERMAL BATTERIES INC D BRISCOE L BULL G CHAGNON B JANTSON

5 (PDF) EAGLE PICHER TECHNOLOGIES LLC D BHAKTA J FERRARO G KIRK E RAUB T SMITH

5 (PDF) ENERSYS ADVANCED SYSTEMS J BENNETT P SCHISSELBAUER N SHUSTER M TELLO B WIGHTMAN

2 (PDF) MAXPOWER SPECIAL PURPOSE BATTERIES L DU I KOWALCZYK

4 (PDF) SANDIA NATIONAL LABORATORIES E ALLCORN E PIEKOS C ROBERTS S ROBERTS

11 (PDF) US ARMY CCDC ARL (USA) FCDD RLD
6 (HC) A KOTT FCDD RLS M WRABACK FCDD RLS D E SHAFFER J CARROLL FCDD RLS DC C LUNDGREN FCDD RLS DP M BERMAN B GEIL F KRIEGER (1 PDF AND 6 HC) J SWANK FCDD RLS RL W CHURAMAN P GUERIERI